

---

Contemporary and future stresses on estuaries:  
Examples from the Yellow River Delta, the Vietnamese  
Mekong Delta, and the German Bight

---

Von der Fakultät für Bauingenieurwesen und Geodäsie  
der Gottfried Wilhelm Leibniz Universität Hannover

zur Erlangung des Grades  
Doktor-Ingenieur (Dr.-Ing.)

genehmigte Dissertation

von

Dipl.-Ing. Christian Jordan

2022

---

Referent:

Prof. Dr.-Ing. habil. Torsten Schlurmann

Korreferent:

Prof. Dr. rer. nat. habil. Hans Burchard

Tag der Promotion:

01. Februar 2022

---



## Danksagung

Die vorliegende Arbeit entstand während meiner Zeit als wissenschaftlicher Mitarbeiter am Ludwig-Franzius-Institut für Wasserbau, Ästuar- und Küsteningenieurwesen. Bereits während meines Studiums bekam ich die Möglichkeit mich mit dem Einfluss des Klimawandels auf die Tidedynamik in der Deutschen Bucht und den angrenzenden Ästuaren auseinanderzusetzen. Im Anschluss hatte ich das Privileg verschiedene Forschungsprojekte zu bearbeiten, um den Einfluss des Klimawandels sowie direkter menschlicher Eingriffe auf Ästuar tiefgreifend zu studieren. So wurden im Rahmen der Projekte „DELIGHT“ und „Catch-Mekong“ die Auswirkungen verschiedener Einflussfaktoren auf das Gelbflussdelta (China) und das Mekongdelta (Vietnam) untersucht. Die Eindrücke, die ich während Feldmesskampagnen im Zuge dieser Projekte sammeln durfte, haben mich nachhaltig geprägt. Besonderer Dank gilt daher meinem Doktorvater Herrn Prof. Dr.-Ing. habil. Torsten Schlurmann, der mir die Mitarbeit an diesen spannenden Projekten ermöglichte. Weiterhin möchte ich mich bei ihm für die Förderung, den Freiraum zur Entwicklung eigener Ideen sowie für hilfreiche Anregungen in Bezug auf diese Arbeit bedanken.

Weiterer Dank gebührt Herrn Prof. Dr. rer. nat. habil. Hans Burchard für die Übernahme des Korreferates und das Anfertigen eines schriftlichen Gutachtens. Herrn Prof. Dr.-Ing. Vincent Oettel und Herrn Prof. Dr. Thomas Graf danke ich für die Übernahme des Kommissionsvorsitzes beziehungsweise für den Einsatz als weiteres Kommissionsmitglied.

Die wesentlichen Ergebnisse dieser kumulativen Dissertation wurden in internationalen Fachjournalen veröffentlicht. Dies wäre ohne die Mitarbeit meiner Koautoren nicht möglich gewesen, bei denen ich mich ausdrücklich für ihre Beiträge zu den verschiedenen Manuskripten bedanken möchte. Auch möchte ich mich beim gesamten Kollegium des Ludwig-Franzius-Instituts für die herzliche Arbeitsatmosphäre und die exzellente Zusammenarbeit bedanken. Besonderer Dank gilt hierbei Oliver Lojek und Jan Tiede, die mit ihrem großartigen Einsatz maßgeblich zum Gelingen von Feldmesskampagnen beigetragen haben. Mein Dankeschön gilt auch allen weiteren Kolleginnen und Kollegen, HiWis und Studierenden, die mich bei Feldmesskampagnen oder bei der Durchführung von numerischen Simulationen unterstützt haben.

Mein größter Dank gilt jedoch meiner Familie. Danke für eure uneingeschränkte Unterstützung während des Studiums und der Promotion und für die Aufmunterung, wenn die Dinge mal nicht nach Plan verliefen.

Christian Jordan



## Abstract

Formed where the water from rivers meets the sea, processes in estuaries are driven by the mixing between freshwater and seawater. Being home to diverse plant and animal communities, which have adapted to this unique environment, estuaries are one of the most productive ecosystems in the world. Providing a multitude of ecosystem services, estuaries are also of high economic value and contribute to human well-being. Besides providing habitats to aquatic species, estuaries are a source of food and raw materials while also cycling nutrients and contributing to coastal protection by damping the damaging effects of extreme events (e.g., storm surges). In addition, estuaries ensure safe navigation to and from ports and are used for recreational activities. However, with many of the world's largest cities located on estuaries, they are directly exposed to impacts from human activity, such as overexploitation of resources or pollution. Being located in low-lying coastal areas, estuaries are also vulnerable to sea-level rise while simultaneously being impacted by climate change-induced alterations in hydrology. The combination of human-driven and climate-induced changes may lead to the degradation or loss of estuarine ecosystems and the services they provide. In order to minimize negative impacts and to promote a sustainable management of estuaries, it is thus important to investigate how estuarine environments respond to drivers of contemporary and future changes.

Since no two estuaries are alike, examples from the Yellow River Delta (China), the Mekong Delta (Vietnam), and the German Bight are presented in this thesis. Major drivers, which impact these focus regions, include: sand mining/dredging, damming, climate change-induced alterations in hydrology, and sea-level rise. The aim of this thesis is to improve the understanding of how the selected estuaries are impacted by predominant contemporary and projected future drivers. This is accomplished by addressing different research questions with a focus on: (i) improving methods for assessing the present-day impact of selected drivers, (ii) improving projections by addressing less visible impacts and by integrating recently identified relevant processes, and (iii) applying different scenarios of plausible future developments in estuarine environments.

(i) In a first study focusing on the Vietnamese Mekong Delta, improved methods were used to gain new insights into the intensity of regional sand mining activity. It was shown that the regional extraction of sand from the Mekong riverbed, which is driven by socio-economic developments in the region, is significantly higher than the river's natural supply of sand. These findings have strong implications for the stability of the Vietnamese Mekong Delta, which is already subject to riverbank and coastal erosion under present-day conditions.

(ii) Projections of future developments in estuaries were improved by addressing less visible impacts in numerical models and by integrating previously unaddressed processes. A second study concentrating on the Vietnamese Mekong Delta was used to project, for



the first time, the morphodynamic evolution of the Mekong in response to a combination of major drivers, including sand mining, damming, climate change-induced alterations in hydrology, and sea-level rise. In a third study, which focuses on the North Sea, it could also be shown that the morphological evolution of intertidal flats in the Wadden Sea has a significant impact on the tidal dynamics in the region when considering future sea-level rise.

(iii) By applying numerous plausible scenarios of future developments, the second study concentrating on the Mekong was able to identify the operation of hydropower dams as the major driver for future morphodynamic changes in the region, followed by sand extraction. Furthermore, this approach enabled to investigate the local interactions between different drivers. By combining different rates of sea-level rise with various rates of vertical accretion in the intertidal flats of the Wadden Sea, several plausible scenarios were also addressed in the study focusing on North Sea tides. If no vertical accretion is assumed in the intertidal flats, sea-level rise will lead to enhanced tidal asymmetry in the German estuaries Elbe, Weser, and Ems, potentially leading to increased sediment import. In contrast, tidal asymmetries resemble present-day conditions if intertidal flats are able to keep up with sea-level rise.

**Keywords:**

Estuarine dynamics, sand mining, damming, climate change, sea-level rise, Yellow River Delta, Vietnamese Mekong Delta, German Bight



## Kurzfassung

Ästuare bezeichnen die Mündungsbereiche von Flüssen am Übergang zum Meer, wobei ästuarine Prozesse durch die Durchmischung von Süß- und Salzwasser angetrieben werden. Ästuare werden von einer Vielzahl von Pflanzen und Tieren besiedelt, die sich diesen besonderen Bedingungen angepasst haben, und zählen zu den produktivsten Ökosystemen der Welt. Aufgrund erbrachter Ökosystemdienstleistungen sind Ästuare auch aus ökonomischer Sicht von hoher Bedeutung und tragen zum Wohlergehen der Menschen bei. Neben einem Lebensraum für aquatische Arten dienen Ästuare als Quelle für Nahrung und Rohstoffe, helfen bei der Regulierung von Nährstoffen und leisten einen erheblichen Beitrag zum Küstenschutz durch die Dämpfung von Extremereignissen (z.B. Sturmfluten). Außerdem ermöglichen Ästuare als schiffbare Wasserstraßen den Zugang zu Häfen und dienen dem Tourismus. Da viele Megastädte an Ästuaren liegen, werden sie jedoch zunehmend durch direkte menschliche Eingriffe, wie z.B. intensiven Abbau von Ressourcen oder Verschmutzung, geprägt. Durch ihre Lage in flachen Küstengebieten sind sie zudem anfällig gegenüber einem Anstieg des Meeresspiegels und werden zusätzlich von klimainduzierten Veränderungen des hydrologischen Regimes beeinflusst. Die Kombination aus direkten menschlichen Eingriffen und Klimawandel kann zu einer Schädigung ästuariner Ökosysteme und somit auch zu einem Verlust von Ökosystemdienstleistungen führen. Um negative Auswirkungen einer intensiven Nutzung zu minimieren und ein nachhaltiges Management zu gewährleisten, ist es daher von besonderem Interesse die wesentlichen Einflussfaktoren derzeitiger und zukünftiger Entwicklungen in Ästuaren zu untersuchen.

Da keine zwei Ästuare identisch sind, werden in dieser Arbeit Beispiele aus dem Gelbflusdelta (China), dem Mekongdelta (Vietnam) und aus der Deutschen Bucht präsentiert. Diese Fokusregionen werden maßgeblich durch die Auswirkungen von Sandabbau/Unterhaltungsbaggerungen, Staudämmen, klimainduzierten Veränderungen des hydrologischen Regimes und dem Anstieg des Meeresspiegels geprägt. Es ist das Ziel dieser Arbeit das Verständnis zu verbessern, inwiefern die ausgewählten Ästuare durch bereits vorherrschende und projizierte zukünftige Veränderungen beeinflusst werden. Dies wird durch die Untersuchung wissenschaftlicher Fragestellungen mit folgenden Schwerpunkten erreicht: (i) Verbesserung von Messmethoden zur Abschätzung des heutigen Ausmaßes ausgewählter Einflussfaktoren, (ii) Verbesserung von Projektionen durch Untersuchung weniger sichtbarer Auswirkungen sowie durch Integration neuer relevanter Prozesse und (iii) Anwendung unterschiedlicher Szenarien in Projektionen.

(i) In einer ersten Studie mit Fokus auf das Mekongdelta konnten anhand der Anwendung verbesserter Messmethoden neue Erkenntnisse hinsichtlich des heutigen Ausmaßes des regionalen Sandabbaus gewonnen werden. Es wurde nachgewiesen, dass die Entnahme von Sand aus der Gewässersohle des Mekongs, welche durch sozio-ökonomische



Entwicklungen in der Region angetrieben wird, den natürlichen Nachschub erheblich übertrifft. Diese Erkenntnisse haben u.a. weitreichende Implikationen für die Stabilität des Mekongdeltas, das bereits heutzutage von Ufer- und Küstenerosion betroffen ist.

(ii) Projektionen zu zukünftigen Veränderungen in Ästuaren wurden verbessert, indem bisher vernachlässigte Auswirkungen im numerischen Modell untersucht und zusätzliche Prozesse integriert wurden. In einer zweiten Studie mit Fokus auf das Mekongdelta wurde beispielsweise erstmalig projiziert, welche Auswirkungen sich für die morphodynamische Entwicklung des Mekongs aus einer Kombination aus Sandabbau, Staudämmen, klimainduzierten hydrologischen Änderungen und dem Anstieg des Meeresspiegels ergeben werden. In einer dritten Studie mit Fokus auf die Nordsee konnte außerdem aufgezeigt werden, dass das Wachstum von Wattflächen einen erheblichen Einfluss auf die zukünftige Gezeitendynamik der Region vor dem Hintergrund eines Meeresspiegelanstiegs hat.

(iii) Durch die Anwendung einer Vielzahl von plausiblen Szenarien konnte in der zweiten Studie zum Mekong die Errichtung von Staudämmen als dominanter Treiber zukünftiger morphologischer Veränderungen identifiziert werden, gefolgt vom Sandabbau. Außerdem war es möglich die Wechselwirkung unterschiedlicher Einflussfaktoren zu untersuchen. In der Studie mit Fokus auf die Tidedynamik in der Nordsee wurden ebenfalls unterschiedliche Szenarien betrachtet, indem ausgewählte Raten des Meeresspiegelanstiegs mit verschiedenen Raten für das Wachstum von Wattflächen kombiniert wurden. Wachsen die Wattflächen bei einem erhöhten Meeresspiegel nicht mit, so werden sich in den Ästuaren von Elbe, Weser und Ems beispielsweise Tideasymmetrien verstärken, welche zu einem stärkeren Sedimenteintrag führen können. Wachsen die Wattflächen hingegen mit dem Meeresspiegel an, so werden sich die Tideasymmetrien in den Ästuaren nur geringfügig im Vergleich zu heutigen Mustern verändern.

**Schlüsselwörter:**

Ästuardynamik, Sandabbau, Staudämme, Klimawandel, Meeresspiegelanstieg, Gelbflussdelta, Mekongdelta, Deutsche Bucht



## Statement of candidate contribution

The main results of this thesis are published in peer-reviewed journals. Publications considered for this thesis are (in chronological order of their acceptance for publication):

1. **Jordan, C.**, Tiede, J., Lojek, O., Visscher, J., Apel, H., Nguyen, H. Q., et al. (2019b). Sand mining in the Mekong Delta revisited – current scales of local sediment deficits. *Scientific Reports* 9:17823. doi: 10.1038/s41598-019-53804-z
2. **Jordan, C.**, Visscher, J., Dung, N. V., Apel, H., and Schlurmann, T. (2020). Impacts of Human Activity and Global Changes on Future Morphodynamics within the Tien River, Vietnamese Mekong Delta. *Water* 12:2204. doi: 10.3390/w12082204
3. **Jordan, C.**, Visscher, J., and Schlurmann, T. (2021). Projected Responses of Tidal Dynamics in the North Sea to Sea-Level Rise and Morphological Changes in the Wadden Sea. *Frontiers in Marine Science* 8:685758. doi: 10.3389/fmars.2021.685758

As the main author of publication 1, I helped with the design of the research framework and planned/conducted the field surveys. Furthermore, I was responsible for the processing of several hydro-, morpho-, and sedimentological datasets and the analysis of all measured datasets. Finally, I was responsible for visualizing the data and the manuscript draft. Jan Tiede conducted the field surveys, processed the bathymetric datasets, and gave critical input regarding the manuscript. Oliver Lojek planned/conducted the field surveys and gave critical input regarding the manuscript. Hong Quan Nguyen and Chau Nguyen Xuan Quang supported the field surveys, collected datasets from local authorities, and gave critical input regarding the manuscript. Heiko Apel and Jan Visscher designed the research framework, planned the surveys, and gave critical input regarding the manuscript. Torsten Schlurmann designed the research framework and gave critical input regarding the manuscript. Jan Visscher and Torsten Schlurmann also contributed to many technical discussions.

As the main author of publication 2, I helped with the design of the research framework and planned the field surveys. Furthermore, I was responsible for the design of numerical experiments, performed the simulations, and analyzed the measured data and simulation results. Finally, I was responsible for visualizing the data and the manuscript draft. Nguyen Viet Dung helped with the design of numerical experiments, performed simulations, which were needed for the generation of boundary conditions, and gave critical input regarding the manuscript. Heiko Apel and Jan Visscher designed the research framework, planned the surveys, and gave critical input regarding the manuscript. Torsten Schlurmann designed the research framework and gave critical input regarding the manuscript. Jan Visscher and Torsten Schlurmann also contributed to many technical discussions.





As the main author of publication 3, I set up and validated the numerical model, developed the numerical experiments, and performed the simulations. Furthermore, I was responsible for the analysis of simulation results, the visualization of data, and the manuscript draft. Jan Visscher and Torsten Schlurmann contributed to many technical discussions, helped shaping the core idea of the manuscript, and gave critical input.



## Contents

<b>Abstract</b>	<b>ii</b>
<b>Kurzfassung</b>	<b>iv</b>
<b>List of Figures</b>	<b>x</b>
<b>List of Tables</b>	<b>xi</b>
<b>Symbols</b>	<b>xii</b>
<b>Acronyms</b>	<b>xiv</b>
<b>1 Introduction</b>	<b>1</b>
1.1 Motivation . . . . .	1
1.2 Objectives . . . . .	2
1.3 Outline . . . . .	5
<b>2 Definitions and classifications of estuaries</b>	<b>6</b>
<b>3 Study areas</b>	<b>14</b>
3.1 Yellow River Delta . . . . .	14
3.2 Vietnamese Mekong Delta . . . . .	17
3.3 North Sea basin and adjacent estuaries in the German Bight . . . . .	20
<b>4 Drivers of contemporary and future changes in estuaries</b>	<b>27</b>
4.1 Sand mining/dredging . . . . .	27
4.2 Damming . . . . .	31
4.3 Climate change-induced alterations in hydrology . . . . .	34
4.4 Sea-level rise . . . . .	38
4.4.1 Response of tides to rising sea-level . . . . .	41
4.4.2 Response of Wadden Sea tidal basins to rising sea-level . . . . .	44
<b>5 Applied methods</b>	<b>51</b>
5.1 Bottom mapping . . . . .	51
5.2 Hydro-morphodynamic modeling . . . . .	52
<b>6 Publications</b>	<b>57</b>
6.1 Sand mining in the Vietnamese Mekong Delta . . . . .	58
6.1.1 Abstract . . . . .	58
6.1.2 Conclusion and Outlook . . . . .	58



---

6.2	Projections of future morphodynamics in the Vietnamese Mekong Delta . . .	63
6.2.1	Abstract . . . . .	63
6.2.2	Conclusions and Outlook . . . . .	63
6.3	Projections of future North Sea tidal dynamics . . . . .	67
6.3.1	Abstract . . . . .	67
6.3.2	Summary and Outlook . . . . .	67
<b>7</b>	<b>Summary and Outlook</b>	<b>73</b>
7.1	Summary . . . . .	73
7.2	Outlook . . . . .	77
7.2.1	Future research regarding numerical models . . . . .	77
7.2.2	Potential adaptation strategies . . . . .	78
	<b>References</b>	<b>81</b>
<b>A</b>	<b>Appendix</b>	<b>I</b>
A.1	Curriculum Vitae . . . . .	I



## List of Figures

2.1	Classification of estuaries based on ratio of convergence to friction effects . . .	7
2.2	Model of flood-dominant, ebb-dominant, and symmetric tide . . . . .	8
2.3	Classification of estuaries on the basis of their geomorphology . . . . .	9
2.4	Classification of estuaries on the basis of their vertical structure of salinity	10
2.5	Evolutionary classification of coastal environments . . . . .	11
2.6	Classification of estuaries based on parameterizations of selected variables	13
3.1	Map of the Yellow River Basin and the Yellow River Delta . . . . .	15
3.2	Map of the Mekong River Basin and the Vietnamese Mekong Delta . . . . .	19
3.3	Map of Germany and the German Bight . . . . .	22
4.1	Projected global material extraction . . . . .	28
4.2	Construction of large dams by decade . . . . .	32
4.3	Population affected and expected damage caused by future river floods . . .	36
4.4	Twentieth century and projected global mean sea-level rise . . . . .	40
5.1	Conceptual flow chart of Delft3D-FLOW and Delft3D-MOR . . . . .	54
6.1	Bathymetric changes and associated bed load transport rates . . . . .	60
6.2	Map of sand mining sites and associated extraction volumes . . . . .	61
6.3	Changes in riverbank positions . . . . .	62
6.4	Cumulative erosion and deposition for the baseline scenario . . . . .	64
6.5	Mean bed level changes in relation to the baseline scenario . . . . .	65
6.6	Erosion and deposition in relation to the baseline scenario . . . . .	66
6.7	Projected changes in M2 amplitudes along the North Sea coastlines . . . . .	70
6.8	Projected changes in M2 amplitudes for the Wadden Sea . . . . .	71
6.9	Projected changes in flood and ebb dominance for the German Bight . . . . .	72



## List of Tables

6.2.1 Notations used by Jordan et al. (2020) for single drivers . . . . .	66
6.3.1 Notations of selected scenarios investigated by Jordan et al. (2021) . . . . .	70



## Symbols

$A_0$	mean water level (m)
$A_n$	amplitude of a tidal constituent $n$ (m)
$\beta$	coefficient of saline contraction (1/PSU)
$C_D$	bottom drag coefficient (–)
$CFL$	Courant-Friedrichs-Lewy number (–)
$\delta S$	top-to-bottom salinity difference (PSU)
$\Delta t$	time step (s)
$\Delta x$	grid spacing in horizontal x-direction (m)
$\Delta y$	grid spacing in horizontal y-direction (m)
$\eta$	tidal water level (m)
$f_{MORFAC}$	morphological acceleration factor (–)
$Fr_f$	freshwater Froude number (–)
$g$	gravitational acceleration ( $\text{m/s}^2$ )
$H$	total water depth (m)
$M$	mixing parameter (–)
$N_0$	buoyancy frequency (1/s)
$\nu$	diffusive fraction of the total upstream salt flux (–)
$\omega_n$	angular speed of a tidal constituent $n$ (1/s)
$\omega$	tidal frequency (1/s)
$Q_{BC}$	discharge at model boundary ( $\text{m}^3/\text{s}$ )
$R_{erol/dep,DM+S}$	ratio of erosion volume to deposition volume for scenario $DM+S$ (–)
$S_0$	cross-sectional average of salinity (PSU)
$\sigma_m$	standard error of the mean (–)
$\sigma$	standard deviation (–)
$S_{in}$	incoming supply of sand ( $\text{Mt}/\text{yr}$ )
$s_{ocean}$	ocean salinity (PSU)
$S_{res}$	available sand resource (Mt)
$SSC_{sBC}$	suspended sediment concentrations at model boundary ( $\text{kg}/\text{m}^3$ )
$S_{store}$	available sand in storage (Mt)
$S_{xt}$	rate of sand extraction ( $\text{Mt}/\text{yr}$ )
$\theta_{M2}$	phase lag of the surface elevation of the tidal constituent M2 on the Equilibrium Tide at Greenwich ( $^\circ$ )
$\theta_{M4}$	phase lag of the surface elevation of the tidal constituent M4 on the Equilibrium Tide at Greenwich ( $^\circ$ )



$\theta_n$	phase lag of the surface elevation of a tidal constituent $n$ on the Equilibrium Tide at Greenwich (°)
$t$	time period (e.g., s or yr)
$U_f$	cross-sectional average of current velocity (m/s)
$U_R$	cross-sectional average of freshwater velocity (m/s)
$u_s$	near-surface current velocity (m/s)
$U_T$	cross-sectional average of tidal velocity (m/s)
$V_{Extr.}$	sand extraction volume ( $Mm^3/yr$ )



## Acronyms

ADCP	acoustic Doppler current profiler
AMSL	absolute mean sea-level
AR6	Sixth Assessment Report
BfG	German Federal Institute of Hydrology ( <i>German: Bundesanstalt für Gewässerkunde</i> )
BMBF	Federal Ministry of Education and Research ( <i>German: Bundesministerium für Bildung und Forschung</i> )
BP	before present
CFL	Courant-Friedrichs-Lewy
CWSS	Common Wadden Sea Secretariat
DELIGHT	Delta Information System for Geoenvironmental and Human Habitat Transition
DEM	digital elevation model
DOI	digital object identifier
ENSO	El Niño-Southern Oscillation
EROS	Earth Resources Observation and Science
ESA	European Space Agency
ETM	estuarine turbidity maximum
GCM	global climate model
GEBCO	Global Bathymetry Chart of the Oceans
GHG	greenhouse gas
GMSLR	global mean sea-level rise
GNSS	global navigation satellite system
GSO	General Statistics Office of Vietnam
HPA	Hamburg Port Authority
HSAP	Hydropower Sustainability Assessment Protocol
ICES	International Council for the Exploration of the Sea
ICOLD	International Commission on Large Dams
IHA	International Hydropower Association





IIED	International Institute for Environment and Development
IKI	International Climate Initiative ( <i>German: Internationale Klimaschutzinitiative</i> )
IPCC	Intergovernmental Panel on Climate Change
LLUR	State Agency for Agriculture, the Environment and Rural Areas ( <i>German: Landesamt für Landwirtschaft, Umwelt und ländliche Räume</i> )
MBES	multibeam echosounder
MHW	mean high water
MLW	mean low water
MNDWI	modified normalized difference water index
MRC	Mekong River Commission
MTR	mean tidal range
NLWKN	Lower Saxony Water Management, Coastal Protection and Nature Conservation Agency ( <i>German: Niedersächsischer Landesbetrieb für Wasserwirtschaft, Küsten- und Naturschutz</i> )
NWES	northwest European shelf seas
OECD	Organisation for Economic Co-operation and Development
ORS	optimal robust separator
PSU	practical salinity units
RCP	Representative Concentration Pathway
RKM	river kilometer marker
RSLR	relative sea-level rise
SBES	singlebeam echosounder
SDGs	Sustainable Development Goals
SLR	sea-level rise
SROCC	Special Report on the Ocean and Cryosphere in a Changing Climate
SSC	suspended sediment concentration



---

SSP	Shared Socioeconomic Pathway
SVP	sound velocity probe
UBA	German Environment Agency ( <i>German: Umweltbundesamt</i> )
UN	United Nations
UNEP	United Nations Environment Programme
UNESCO	United Nations Educational, Scientific and Cultural Organization
UNSD	United Nations Statistics Division
USA	United States of America
USGS	United States Geological Survey
VMD	Vietnamese Mekong Delta
WCD	World Commission on Dams
WCRP	World Climate Research Programme
WSRS	water-sediment regulation scheme
WSV	Federal Waterways and Shipping Administration ( <i>German: Wasserstraßen- und Schifffahrtsverwaltung des Bundes</i> )
WWF	World Wide Fund for Nature
YRD	Yellow River Delta

# 1 Introduction

## 1.1 Motivation

Estuaries are formed at the mouth of rivers and are continuously changing, driven by variability in river flow, tidal influence, and sediment distribution (Dyer, 1997). Due to the interaction of river discharge and ocean tides, estuaries exhibit unique features, such as the estuarine circulation. The estuarine circulation describes the tidally-averaged along-channel currents through a cross-section, with residual currents being directed seaward at the surface and landward at the bottom. Hence, freshwater is transported toward the sea in the upper portion of the water column, while seawater is transported landward in the bottom portion of the water column. Since early studies assumed that the estuarine circulation was mainly driven by longitudinal density gradients (e.g., Hansen and Rattray Jr., 1965), it is oftentimes also called gravitational circulation. However, the contribution of gravitational circulation to the total estuarine circulation may be exceeded by the so-called tidal straining circulation (Burchard and Hetland, 2010). Tidal straining describes a feedback of the vertical salinity structure on the tidal currents that leads to an asymmetry between ebb and flood velocity profiles (Jay and Musiak, 1994). Other processes were also shown to contribute to the estuarine circulation, e.g., lateral advection (Lerczak and Geyer, 2004) or atmospheric forcing (e.g., Geyer, 1997). The estuarine circulation is also an important driver in the formation of the estuarine turbidity maximum (ETM) (Burchard and Baumert, 1998; Burchard et al., 2018), which is also a common feature of many estuaries. The ETM denotes the part of an estuary, where the suspended sediment concentration (SSC) is considerably higher than elsewhere in the same estuary. Accordingly, the ETM is oftentimes a location of long-term sediment deposition (e.g., de Jonge et al., 2014). In addition, ETM dynamics also impact the functioning of estuarine ecosystems (e.g., Kausch and Michaelis, 1996). Even though the estuarine circulation and the ETM dynamics are not the primary focus of this thesis, these features are undoubtedly impacted by contemporary and future changes in estuaries that will be highlighted hereinafter.

In general, estuaries are one of the most valuable ecosystems in the world, with an estimated annual value of around 23,000 \$/ha (Costanza et al., 1997). They help to regulate disturbances (e.g., by buffering damaging effects of extreme events), are hotspots for global nutrient cycling, provide suitable habitats for a multitude of species, and are a source for the production of food and raw materials (e.g., sand) (Costanza et al., 1997). Furthermore, they provide opportunities for recreational activities, ensure safe navigation to and from major ports, and serve as living laboratories for scientists and students (Costanza et al., 1997). When managed properly, estuarine ecosystem services may play a vital role in achieving the United Nations (UN) Sustainable Development Goals (SDGs),

which provide a global blueprint for the sustainable development of the economic, social, and environmental sectors until the year 2030 (UN, 2015). However, with around 71% of the world's population living at a distance of less than 50 km from an estuary and 21 of the world's 30 largest cities being located on estuaries (Agardy et al., 2005; Ashworth et al., 2015), they are directly impacted by human activity. In general, anthropogenic interventions, such as overexploitation of resources, pollution, and unsustainable hydropower development, may lead to the degradation of estuarine ecosystems (Barbier et al., 2011), hence directly conflicting with many of the UN SDGs. Due to socio-economic growth and the associated increase in demand for electricity and other resources (e.g., sand) (e.g., Frei et al., 2013; OECD, 2018), particularly in underdeveloped and developing countries, human-induced impacts will likely only worsen in the future. Furthermore, estuaries are also vulnerable to climate change-induced alterations in hydrological regimes and sea-level rise (SLR) (e.g., Wong et al., 2014). According to the most recent Sixth Assessment Report (AR6) by the Intergovernmental Panel on Climate Change (IPCC), global surface temperature will continue to rise until at least the middle of this century (Lee et al., 2021). Unless greenhouse gas (GHG) emissions are significantly reduced during the next decades, global warming will exceed 1.5 °C and 2 °C during the 21st century (Lee et al., 2021). As a result, the variability in the water cycle and extreme events are projected to intensify, while even high-end SLR scenarios cannot be ruled out (Douville et al., 2021; Fox-Kemper et al., 2021). To ensure the sustainable development of estuarine environments, it is of utmost importance to understand the response of estuaries to contemporary and future drivers of changes, which may result from global warming and direct human activity.

## 1.2 Objectives

Being special branches of civil engineering, coastal and estuarine engineering normally deal with the planning, design, construction, and maintenance of structures/infrastructure along estuaries. Typical engineering works along estuaries include: structures, such as revetments and groins, or the stabilisation and deepening of channels. While estuarine systems may respond to such interventions that significantly alter their geometry, they are likewise impacted by human-driven and climate-induced changes that originate from the landward and seaward direction. Accordingly, it is also an integral part of coastal and estuarine engineering to critically assess relevant drivers of changes in estuaries, to quantify their impacts, and to develop adaptation strategies to minimize potentially negative impacts.

In general, since no two estuaries are alike, they might differ considerably in terms of dominant processes and drivers of contemporary and future changes. In order to address how different estuaries respond to these drivers, three study sites are investigated in this

thesis: (i) the Yellow River Delta (YRD), (ii) the Vietnamese Mekong Delta (VMD), and (iii) the estuaries in the German Bight. Undoubtedly, these low-lying focus regions will be impacted by climate change, and SLR in particular. In addition, the YRD, which is the location of two nature reserves and home to more than 6 million people, is already heavily impacted by the operation of large hydropower dams and the production of China's second-largest oil field (Kuenzer et al., 2014). Against this background, the Delta Information System for Geoenvironmental and Human Habitat Transition (DELIGHT) project was funded by the Federal Ministry of Education and Research (*German: Bundesministerium für Bildung und Forschung*) (BMBF) (grant number: 02WCL1249B, <https://delight.eoc.dlr.de/en.html>) in order to project regional impacts of human activity and climate change (e.g., Kuenzer et al., 2020). The main objective of the project was the provision of information needed to support the efforts of local stakeholders to implement a plan for future delta development. Even though the DELIGHT project did not yield any peer-reviewed publications that are part of this thesis, the YRD is used as an example of a heavily regulated region.

Similar to the YRD, the VMD is also impacted by the construction and operation of large hydropower dams to meet the increasing regional demand for electricity (e.g., Kondolf et al., 2014; Manh et al., 2015). Home to around 17 million inhabitants (GSO, 2021), the VMD is not only essential for food production in Southeast Asia, but also a major hotspot of sand mining activity (e.g., Jordan et al., 2019b). The growing demand for sand is driven by population growth, urbanization, and economic development (e.g., Peduzzi, 2014). In recent years, numerous international research projects, such as the International Climate Initiative (*German: Internationale Klimaschutzinitiative*) (IKI) Sand Mining Project<sup>1</sup> or the RAMESES project<sup>2</sup>, have focused on these developments in the VMD. Similarly, the project Catch-Mekong (grant number: 02WM1338D, <https://catchmekong.eoc.dlr.de>) was funded by the BMBF to focus on the most pressing topics in the VMD and to support sustainable and transboundary management of regional resources. This project also yielded two publications that are at the center of this thesis and focus on the intensity of present sand mining activity in the VMD (Jordan et al., 2019b) and the projected morphological evolution of the Tien River branch in response to the major drivers of future regional changes (Jordan et al., 2020).

Concentrating on the estuaries of the German rivers Elbe, Weser, and Ems, these estuaries discharge directly into the Wadden Sea, which is the largest intertidal flat system in the world (CWSS, 2021b). Accordingly, these estuaries will be impacted by future feedbacks between SLR, bathymetric changes in the Wadden Sea, and regional tidal dynamics. These feedbacks were addressed in a third paper (Jordan et al., 2021), which is also part

<sup>1</sup>see: <https://www.wwf.de/themen-projekte/projektregionen/mekong-region/dem-mekong-geht-der-sand-aus>

<sup>2</sup>see: <https://www.hull.ac.uk/work-with-us/research/institutes/energy-and-environment-institute/our-work/ramesses>



of this thesis and originates from a 2013 diploma thesis. With major German ports and shipyards being located on the Elbe, Weser, and Ems estuaries, they are also subject to continuous channel deepening to follow the rapid development in maritime traffic. More detailed descriptions of the three focus areas as well as the major drivers of contemporary and future changes in these estuaries are given in chapters 3 and 4, respectively.

Knowledge gaps that were identified and addressed in the outlined publications led to the definition of the following main objectives/research questions of this thesis:

i) How to improve methods for the monitoring/assessment of present-day conditions in estuarine environments?

- In some countries, estuaries are regularly monitored and an abundance of high-quality datasets of parameters, such as bathymetry, water levels, discharges, and SSCs, are readily available. In other countries, however, it is difficult to get access to such datasets or they simply do not exist. This lack of data may hamper a reliable assessment of present-day impacts of human interventions or climate-driven changes on estuaries. To address this, in-situ measurements must focus on suitable methods that provide high-quality datasets to overcome persistent knowledge gaps.

ii) How to improve projections of the impacts of climate change and human activity on estuarine environments?

- When dealing with the response of selected estuaries to climate change and anthropogenic interventions, the focus is regularly shifted toward the most prominent impacts, such as future water and sediment fluxes (e.g., Lauri et al., 2012; Kondolf et al., 2014) or mixing processes (e.g., Smajgl et al., 2015). Less prominent (less visible) impacts, e.g., projected responses of estuarine morphodynamics, are only seldom addressed. In order to improve projections, more focus thus must be given to less prominent impacts of climate change and human activity on estuaries. Furthermore, new insights might render existing projections imprecise. In order to get robust results, it is hence also necessary to integrate recently identified relevant processes, which were not considered in previous projections.

iii) How to address/quantify uncertainties that are inherent to projections of future developments in estuarine environments?

- Due to high computational demands of numerical models, it is sometimes only possible to perform calculations for a limited number of scenarios, particularly when numerous processes, such as flows, sediment transport, and morphodynamics, are involved and high spatial resolution is needed. Whenever possible, however, multiple scenarios for each involved driver should be investigated in order to address uncertainties that are inherent to projections of future developments in estuaries. In this way, one is able to cover the likely range of plausible responses to each in-



involved driver. Additionally, this approach helps to gain valuable insights into the main drivers of future changes and the interactions between multiple drivers.

### 1.3 Outline

The following chapter 2 gives an overview of the most common definitions and classifications that are used to describe estuaries. In chapter 3, the three study areas (i.e., YRD, VMD, and North Sea with adjacent estuaries in the German Bight) are presented. In chapter 4, the major drivers of contemporary and future changes in estuarine environments are introduced. In particular, this thesis focuses on the impacts of sand mining/dredging, damming, climate change-induced alterations in hydrology, and SLR. The impact of these drivers is exemplified by studies of the YRD, the VMD, and the German Bight. In this chapter, the potential responses of tidal dynamics and Wadden Sea morphodynamics to SLR are also described in detail. The main methods that were applied in this thesis (i.e., bottom mapping via multibeam echosounder (MBES) and hydro-morphodynamic modeling) are presented in chapter 5. Insights and main results of this thesis can be found in three peer-reviewed papers, which were published in renowned journals. Chapter 6 outlines the links between the papers while also presenting the abstracts and conclusions, thus giving a summary of the main findings of the three papers. Finally, chapter 7 summarizes the overall findings of this thesis and gives an outlook.

#### Summary of chapter 1:

Estuaries are unique, highly dynamic, and ecologically rich coastal environments. Providing a multitude of ecosystem services, estuaries are of high value, but also increasingly impacted by changes that are driven by climate change and human activity. Focusing on the YRD, the VMD, and the estuaries in the German Bight, this thesis aims to gain new insights into the response of these estuaries to the main drivers of contemporary and future changes. This is done by addressing three research questions with a focus on: (i) improving methods for assessing the present-day impacts of selected drivers on estuarine environments, (ii) improving projections by addressing less visible impacts and by integrating newly identified relevant processes, and (iii) applying different scenarios of plausible future developments in estuaries.

## 2 Definitions and classifications of estuaries

The most widely used definition of an estuary, which is based on the salinity intrusion, is given by Cameron and Pritchard (1963):

*"An estuary is a semi-enclosed coastal body of water having a free connection with the open sea and within which sea-water is measurably diluted with fresh water deriving from land drainage."*

However, defining an estuary simply as the part of a river, where salinities range from approximately 0.1 to 30-35‰, the freshwater tidal zone would be placed in the fluvial environment (Dalrymple et al., 1992). In fact, as pointed out by Guilcher (1958), the term estuary originates from the Latin word *aesthus*, meaning tide. Accordingly, there are also definitions of estuaries that explicitly emphasize the importance of tides. One such definition is given by Fairbridge (1980):

*"An estuary is an inlet of the sea reaching into a river valley as far as the upper limit of tidal rise, usually being divisible into three sectors: (a) a marine lower estuary, in free connection with the open sea; (b) a middle estuary, subject to strong salt and fresh water mixing; and (c) an upper or fluvial estuary, characterized by fresh water but subject to daily tidal action. The limits between these sectors are variable, and subject to constant changes in river discharge."*

Dalrymple et al. (1992) also proposed to distinguish between estuaries and delta distributaries. Arguing that estuaries are characterized by a net landward transport of sediment originating from the estuary mouth, while delta distributaries exhibit a net sediment transport toward the sea, Dalrymple et al. (1992) proposed the following definition:

*"[An estuary is] the seaward portion of a drowned valley system which receives sediment from both fluvial and marine sources and which contains facies influenced by tide, wave and fluvial processes. The estuary is considered to extend from the landward limit of tidal facies at its head to the seaward limit of coastal facies at its mouth."*

Similar to the definition of estuaries, a multitude of classifications exist that distinguish between different types of estuaries. The following paragraphs give an overview of the most common classifications, as summarized in reviews by Dyer (1997) and Valle-Levinson (2010). In terms of tides, estuaries can be classified as (i) microtidal, (ii) mesotidal, and (iii) macrotidal (Davies, 1964). Microtidal estuaries have a tidal range smaller than 2 m, while the tidal range of macrotidal estuaries is greater than 4 m. Estuaries in between those categories are called mesotidal. Sometimes, the term hypertidal is also applied to estuaries with a tidal range greater than 6 m (e.g., Dyer, 1997). While frictional



damping can cause a decrease of tidal amplitudes in landward direction, the convergence of an estuary and the associated concentration of energy may force an increase in tidal amplitudes. Based on the balance/imbalance of friction and convergence, an estuary can thus be classified as (i) hypersynchronous, (ii) synchronous, or (iii) hyposynchronous (Nichols and Biggs, 1985) (see Figure 2.1). In hypersynchronous estuaries, the convergence exceeds friction. As a result, the tidal amplitude increases landward before finally decreasing in the riverine section, where the convergence diminishes and frictional damping dominates. In synchronous estuaries, the friction and convergence are in balance. Accordingly, the tidal range is constant along the estuary until reaching the riverine section. In hyposynchronous estuaries, the effects of convergence are exceeded by frictional damping. In this case, the tidal range decreases throughout the whole estuary. Considering tidal asymmetries, an estuary or parts thereof may also be classified as flood-dominant or ebb-dominant (e.g., Friedrichs and Aubrey, 1988) (see Figure 2.2). Flood dominance is associated with a shorter flood than ebb duration, stronger peak flood currents, and net sediment transport in landward direction. In contrast, ebb dominance results in shorter ebb than flood duration, stronger ebb peak currents, and a net sediment transport in seaward direction.

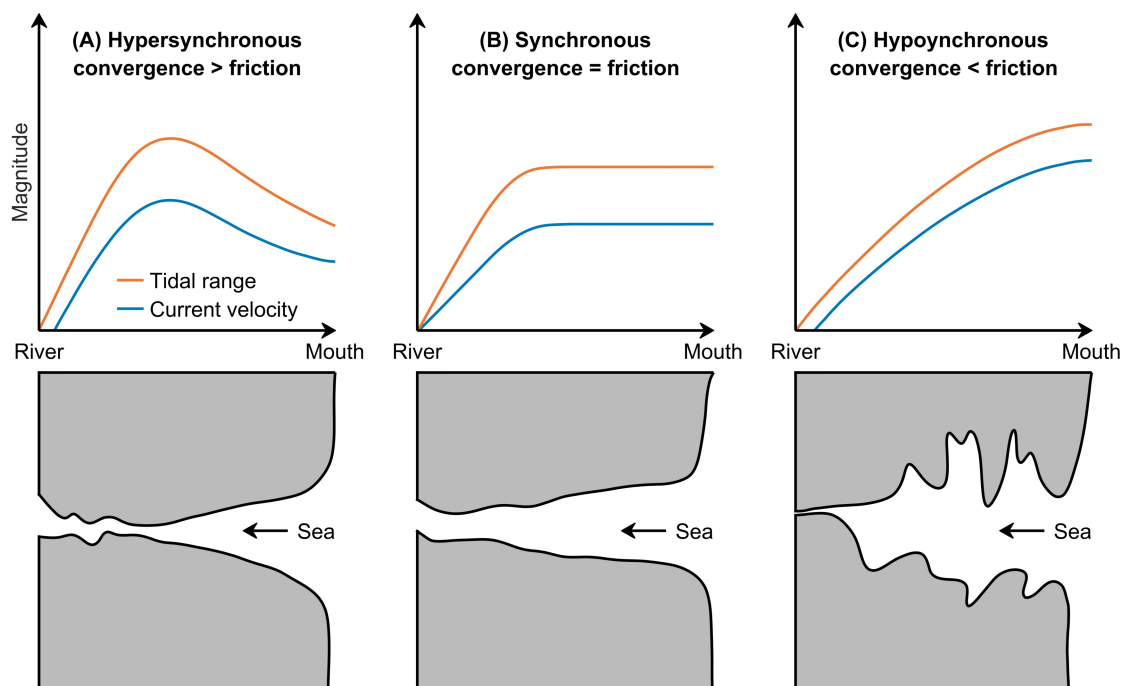


Figure 2.1: Modification of tidal range and current velocity in estuaries with varying ratios of convergence to friction effects. **(A)** Hypersynchronous estuary. **(B)** Synchronous estuary. **(C)** Hyposynchronous estuary. Adapted by permission of Springer Nature Service Center GmbH from Nichols and Biggs (1985).

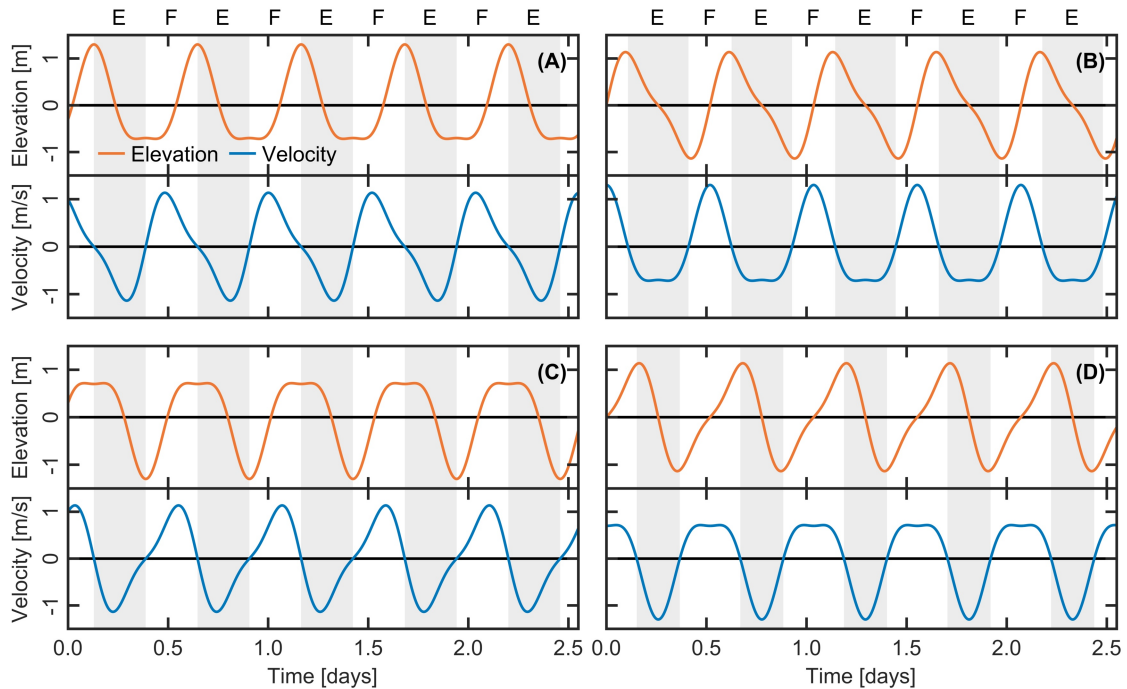


Figure 2.2: Model of flood-dominant, ebb-dominant, and symmetric tide based on the relationship between relative phase and tidal distortion for an amplitude ratio of  $M_4/M_2 = 0.3$ . (A) Symmetric tide ( $2\theta_{M_2} - \theta_{M_4} = 0^\circ$ ). (B) Flood-dominant tide ( $2\theta_{M_2} - \theta_{M_4} = 90^\circ$ ). (C) Symmetric tide ( $2\theta_{M_2} - \theta_{M_4} = 180^\circ$ ). (D) Ebb-dominant tide ( $2\theta_{M_2} - \theta_{M_4} = 270^\circ$ ).  $\theta_{M_2}$  and  $\theta_{M_4}$  are the phase lags of the sea-surface elevation for the tidal constituents  $M_2$  and  $M_4$ , respectively. Letters E and F denote the ebb and flood duration, respectively.

According to their topography, estuaries may also be divided into following groups<sup>3</sup>: (i) coastal plain estuaries, (ii) deltaic estuaries, (iii) lagoons (or bar-built estuaries), (iv) fjords, or (v) tectonic estuaries (Pritchard, 1952; Fairbridge, 1980) (see Figure 2.3). Coastal plain estuaries, which are usually wide and shallow, were formed by the flooding of former river valleys due to rising sea-level over several millennia. In contrast, deltaic estuaries were formed when fluvial sediment was deposited at a river mouth and the redistribution of sediments by tides and waves led to seaward progradation of the coastline. Deltaic estuaries oftentimes have multiple distributaries. Lagoons (or bar-built estuaries) are former embayments that became semi-enclosed when littoral drift led to the formation of sand bars, spits, or barrier islands, partially isolating the coast from the ocean. Fjords are usually located at high latitudes, where U-shaped valleys were eroded by glacial movements. Fjords are characterized by narrow, deep channels with a sill. Tectonic estuaries were once formed by tectonic movements (e.g., due to earthquakes) that resulted in the subsidence of sections of the Earth's crust, which were subsequently filled by ocean water.

<sup>3</sup>Fjärds, rias, and blind estuaries may also be used as additional categories, but were neglected here.

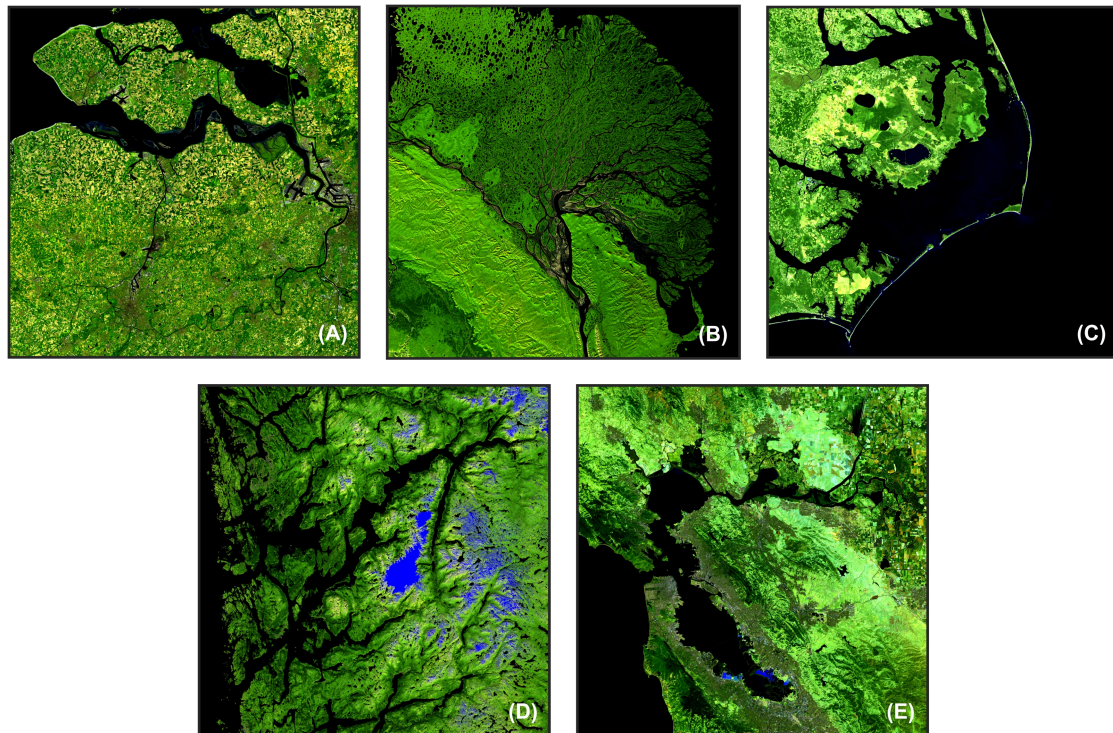


Figure 2.3: Different types of estuaries on the basis of their geomorphology. **(A)** Coastal plain estuary, as exemplified by the Western Scheldt (Belgium, the Netherlands). **(B)** Deltaic estuary, as exemplified by the Lena Delta (Russia). **(C)** Bar-built estuary, as exemplified by the Outer Banks (United States of America (USA)). **(D)** Fjord, as exemplified by the Hardangerfjord (Norway). **(E)** Tectonic estuary, as exemplified by the San Francisco Bay (USA). False color composites were generated based on Landsat-8 and Sentinel-2 imagery. Landsat-8 and Sentinel-2 images courtesy of the United States Geological Survey (USGS), downloaded from the USGS Earth Resources Observation and Science (EROS) Center (<https://earthexplorer.usgs.gov/>). Copernicus Sentinel data, processed by the European Space Agency (ESA).

Estuaries may also be classified in terms of their vertical structure of salinity. According to Pritchard (1955) and Cameron and Pritchard (1963), estuaries can be divided into following groups: (i) salt-wedge estuaries, (ii) strongly stratified estuaries, (iii) weakly stratified estuaries, or (iv) well-mixed estuaries (see Figure 2.4). Salt-wedge estuaries are caused by large river discharge and weak tidal forcing. As a result, outflow dominates throughout most of the water column, while near-bottom inflow is weak. The tidally-averaged vertical salinity profile exhibits a strong so-called pycnocline, with freshwater on top of a wedge of saltwater. Hardly any mixing occurs at the transition between the two water masses. Strongly stratified estuaries are formed by moderate to large river discharge and weak to moderate tidal forcing. These estuaries exhibit a similar stratification to salt-wedge estuaries caused by weak inflow and weak mixing between fluvial and

marine water. The tidally-averaged vertical salinity profile shows a well-developed pycnocline with only slight variations above and below it. Weakly stratified (or partially-mixed) estuaries result from weak to moderate river discharge and moderate to strong tidal forcing. Mixing of fluvial and marine water, which is induced by the stronger tidal currents, is most vigorous for this type of estuary and occurs at all depths. However, the salinity in near-bottom layers typically remains larger than in upper layers. Well-mixed estuaries are formed by strong tidal forcing and weak river discharge. Caused by the strong tidal mixing, the tidally-averaged vertical salinity profile is practically uniform from the surface to the bottom of these estuaries. However, it must be noted that temporal variations in river discharge and tidal forcing may lead to estuaries shifting from one type to another (Valle-Levinson, 2010). Furthermore, different locations within one estuary might be associated with different kinds of vertical salinity structure (Valle-Levinson, 2010).

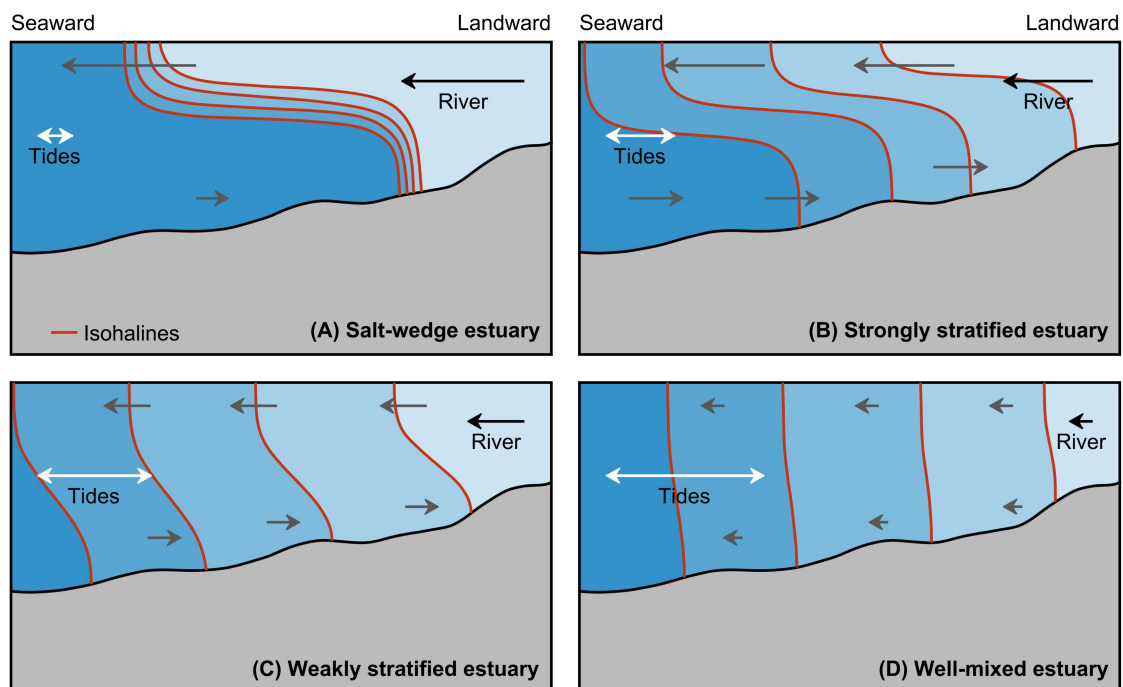


Figure 2.4: Different types of estuaries on the basis of their vertical structure of salinity. (A) Salt-wedge estuary. (B) Strongly stratified estuary. (C) Weakly stratified estuary. (D) Well-mixed estuary. Adapted by permission of Cambridge University Press from Valle-Levinson (2010).

A morphological classification of estuaries was suggested by Dalrymple et al. (1992). This classification by Dalrymple et al. (1992) is based on three categories: (i) river-dominated, (ii) wave-dominated, and (iii) tide-dominated estuaries (see Figure 2.5). Following Galloway (1975), a conceptual triangular diagram is at the center of this classification, which uses the relative magnitudes of river discharge, waves, and tides. The upper part in the diagram (river-dominated zone) is occupied by deltas, where sediment supply of the river

is able to keep up with SLR. In situations without river discharge (lower part in the diagram), strand plains or intertidal flats will be formed. Since they depend on all influences, estuaries occupy the remainder of the diagram (central part in the diagram). The term wave-dominated is applied to estuaries, where tidal influence is small and wave energy at the mouth is relatively high. In contrast, tide-dominated estuaries exhibit large tidal currents in relation to the wave effects and are usually associated with macrotidal conditions. For more details about characteristic morphological features of these types of estuaries, the reader is referred to Dalrymple et al. (1992). It should also be noted, that this diagram was used by Dalrymple et al. (1992) to distinguish estuaries from deltas.

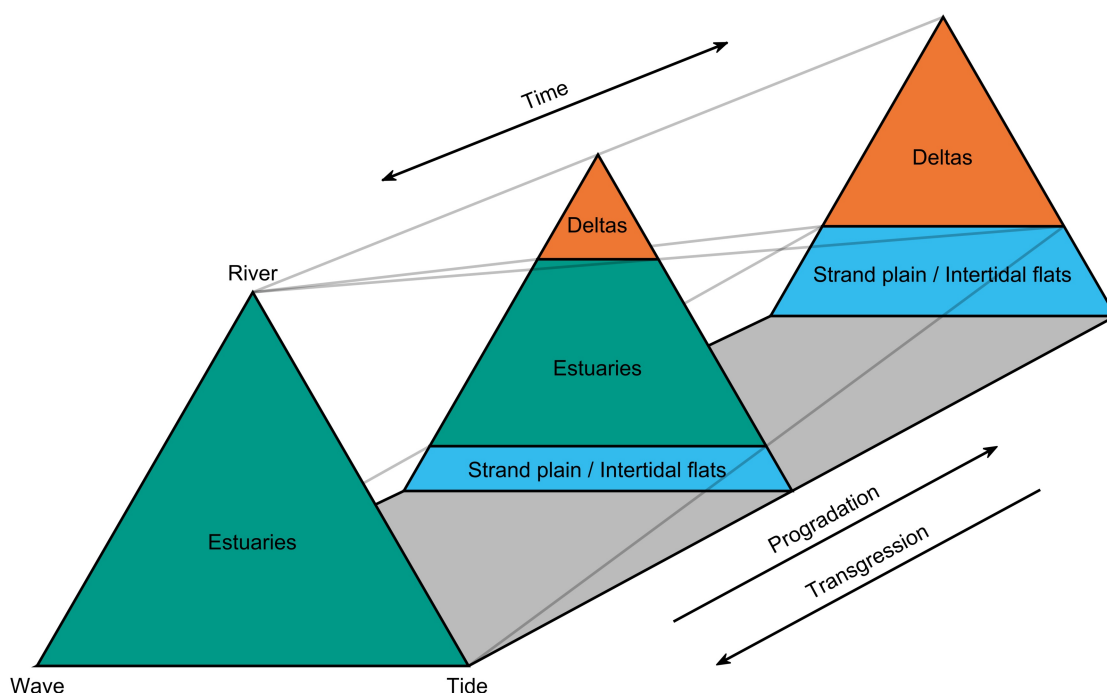


Figure 2.5: Evolutionary classification of coastal environments. The edges of the prism correspond to river-dominated, wave-dominated, and tide-dominated conditions. Deltas occupy the upper part of the diagram, while non-deltaic prograding coasts occupy the lower part. The central part of the diagram is occupied by all estuaries. Dependent on the rate of SLR and sedimentation rate, a coastal area may exhibit transgression or progradation. Adapted by permission of the Society for Sedimentary Geology from Dalrymple et al. (1992).

While most of the outlined classifications are rather qualitative, several authors have also used parameterizations of selected variables to classify estuaries. For example, the classification by Hansen and Rattray Jr. (1966) uses two non-dimensional parameters, which are tidally- and cross-sectionally-averaged: (i) the circulation parameter and (ii) the stratification parameter (see Figure 2.6A). The circulation parameter is the ratio of the near-surface current velocity  $u_s$  to the cross-sectionally-averaged current velocity  $U_f$ .

The stratification parameter is the ratio of the top-to-bottom salinity difference  $\delta S$  to the cross-sectionally-averaged salinity  $S_0$ . Applying the parameters  $u_s/U_f$  and  $\delta S/S_0$ , the diffusive fraction of the total upstream salt flux  $\nu$  can be determined. In the case of strongly stratified estuaries, where mixing is weak and upstream-directed salt transport is dominated by advection, the parameter  $\nu$  is close to 0. For well-mixed estuaries,  $\nu$  approaches 1 and the salt transport is dominated by diffusive processes (i.e., tidal mixing). A more recent estuarine classification scheme, which was proposed by Geyer and MacCready (2014), is based on (i) the freshwater Froude number  $Fr_f$  and (ii) the mixing parameter  $M$  (see Figure 2.6B). Whereas  $Fr_f$  compares the net velocity due to river flow to the maximum propagation speed of the front between fresh and saline water,  $M$  quantifies the effectiveness of the tidal mixing. In detail, the freshwater Froude number is defined by:

$$Fr_f = \frac{U_R}{\sqrt{\beta g s_{ocean} H}} \quad (2.0.1)$$

where  $U_R$  is the cross-sectional average of the freshwater velocity,  $\beta$  is the coefficient of saline contraction,  $g$  is the gravitational acceleration,  $s_{ocean}$  is the ocean salinity, and  $H$  is the water depth. The mixing parameter is defined by:

$$M = \sqrt{\frac{C_D U_T^2}{\omega N_0 H^2}} \quad (2.0.2)$$

where  $C_D$  is the bottom drag coefficient,  $U_T$  is the cross-sectional average of the tidal velocity,  $\omega$  is the tidal frequency, and  $N_0$  is the buoyancy frequency, which is defined by:

$$N_0 = \sqrt{\frac{\beta g s_{ocean}}{H}} \quad (2.0.3)$$

When the term estuary is used in this thesis, it usually refers to the definition by Fairbridge (1980), which emphasizes the importance of tides. Accordingly, the distributaries of the YRD and VMD are also referred to as estuaries. Detailed descriptions of the YRD, the VMD, and the North Sea basin with adjacent estuaries in the German Bight are given in the following chapter 3.

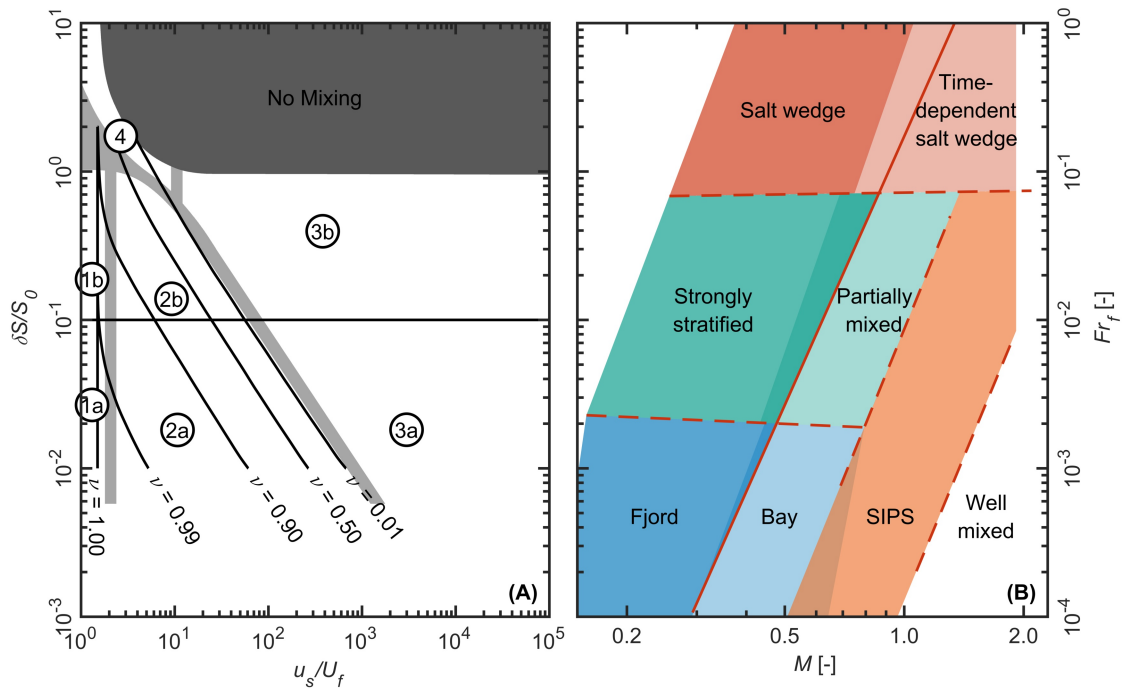


Figure 2.6: Classification of estuaries based on parameterizations of selected variables. **(A)** Estuarine classification diagram, according to the stratification parameter  $\delta S/S_0$  and circulation parameter  $u_s/U_f$ . Type 1 estuaries are well-mixed and show no vertical structure in net flows, while net flows reverse with depth in type 2 estuaries. Type 3 estuaries are characterized by strong gravitational circulation, while type 4 estuaries can be classified as salt-wedge estuaries. Adapted by permission of John Wiley and Sons from Hansen and Rattray Jr. (1966). **(B)** Estuarine parameter space based on the freshwater Froude number  $Fr_f$  and the mixing parameter  $M$ . Adapted by permission of Annual Reviews from Geyer and MacCready (2014).

### Summary of chapter 2:

In the past, several definitions/classifications were formulated to describe the distinctive nature of estuaries. One may classify different types of estuaries on the basis of tides, topography, vertical salinity structure, morphology, or by quantifying a selection of estuarine variables. In this thesis, the term estuary refers to the definition by Fairbridge (1980), hence also including delta distributaries.

## 3 Study areas

In this chapter, the general characteristics of the three focus regions: (i) the YRD, (ii) the VMD, and (iii) the North Sea basin with adjacent estuaries in the German Bight are described. While recent alterations in the hydro-, morpho-, and sedimentological regimes of these regions are presented here, chapter 4 addresses contemporary and (projected) future drivers of regional changes in detail.

### 3.1 Yellow River Delta

The Yellow River (Huang He) has a length of almost 5,800 km and is the second-longest river in China (Liu et al., 2009). Originating from the Qinghai-Tibet Plateau, the river is divided into the upper, middle, and lower reaches on its way from the source to the river mouth at the Bohai Sea (see Figure 3.1B). Around 60 % of the river's discharge originates from its upper reaches (e.g., Yu et al., 2013). In the middle reaches, the Yellow River crosses the Loess Plateau, where nearly 90 % of the river's sediment is picked up (e.g., Yu et al., 2013). Much of the Yellow River's sediments are deposited in the lower reaches, thus raising the riverbed up to a height of 10 m above the surrounding floodplains, making it prone to devastating floods (Chen et al., 2012). Generally, the water and sediment fluxes of the Yellow River show a distinct seasonal variability. More than 60 % of the water and sediment discharge occur during July to October caused by monsoon rains in summer (Wang et al., 2007, 2010a). However, recent observations indicate that the seasonal variability in the river's hydrology has been altered to a large extent (Wang et al., 2010a; Yu et al., 2013). In addition, the mean water discharge of the Yellow River, which was around 1,520 m<sup>3</sup>/s during the 1950s, has decreased to around 460 m<sup>3</sup>/s during the period 2000 to 2010 (Yu et al., 2013). Flood peaks with a daily discharge > 6,000 m<sup>3</sup>/s, which were commonly observed at the Lijin gauge station (see location in Figure 3.1B) before 1969, have not occurred since 1986 (Yu et al., 2013). Also with regard to the sediment load, a substantial reduction was observed in recent years. Based on an estimation of 1,080 Mt/yr, the Yellow River was long considered the world's second-largest river in terms of sediment flux to the ocean (Milliman and Meade, 1983). However, according to estimates for the period 2000 to 2010, the sediment load has decreased to around 143 Mt/yr (Yu et al., 2013). Caused by the huge sediment load, hypopycnal plumes were regularly observed at the mouth of the Yellow River in the past (Wright et al., 1986). Such hypopycnal plumes are formed when river water becomes denser than seawater, and hence the river water flows beneath the seawater. However, daily-averaged SSCs > 35 kg/m<sup>3</sup>, which are needed for the formation of hypopycnal plumes (Wang et al., 2011), were only seldom measured since the beginning of this century (Yu et al., 2013). The mean SSCs have decreased from 25.5 kg/m<sup>3</sup> (1950 to 1999) to 8.8 kg/m<sup>3</sup> (2000 to 2010) (Yu et al., 2013). At the same time,



the grain size of suspended sediments has increased from 18  $\mu\text{m}$  (1950 to 1999) to 25  $\mu\text{m}$  (2000 to 2010) (Yu et al., 2013). Notwithstanding these changes, the sediment transport in the Yellow River is still dominated by cohesive sediments.

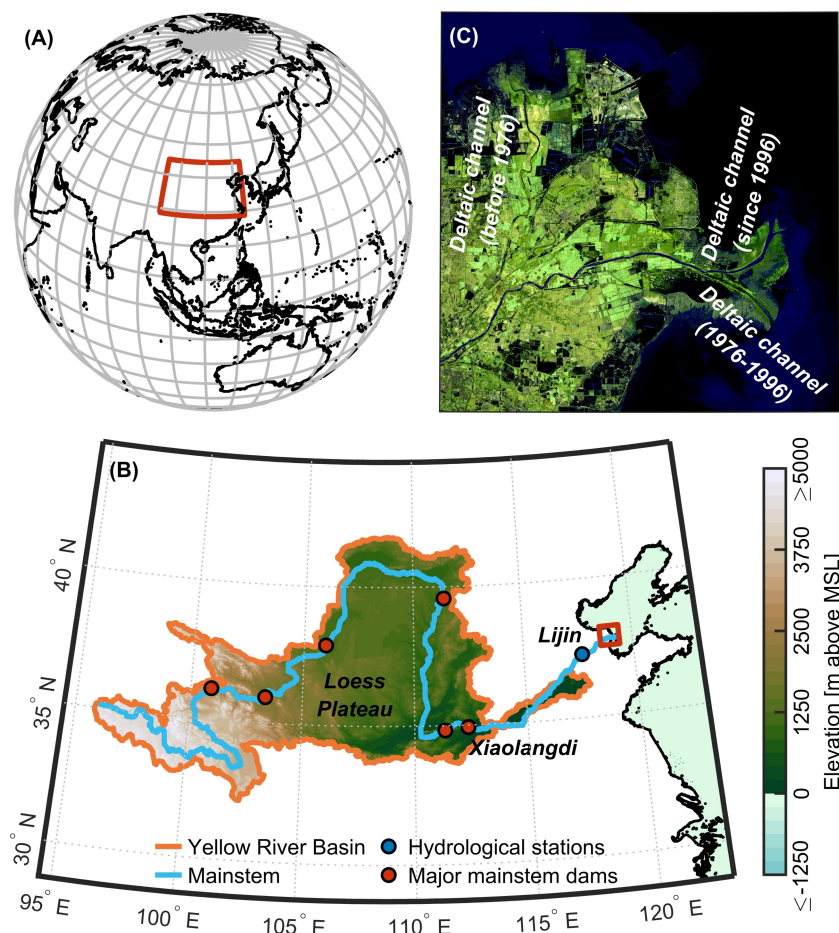


Figure 3.1: Map of the Yellow River Basin and the YRD. (A) Global coastlines with location of the Yellow River Basin. Red rectangle indicates area shown in panel (B). (B) Map of the Yellow River Basin, including locations of major mainstem dams and selected hydrological stations. Red rectangle indicates area shown in panel (C). (C) False color composite of the YRD based on Sentinel-2 image for March 17, 2020. Labels indicate historical evolution of the deltaic channel. Shapefiles in (A, B) copyrighted OpenStreetMap contributors (<https://www.openstreetmap.org>). GEBCO 2021 Grid (GEBCO Compilation Group, 2021) was used for topography and bathymetry data in (B). Sentinel-2 image in (C) courtesy of the USGS, downloaded from the USGS EROS Center (<https://earthexplorer.usgs.gov/>). Copernicus Sentinel data, processed by the ESA.

Throughout the last millennia, the lower Yellow River has shifted its course numerous times. Between 1128 and 1855, the Yellow River discharged directly into the South Yellow Sea (Zhou et al., 2014). During an extreme flood event in 1855, which led to the breaching

of dikes, the Yellow River abandoned its former course and started to discharge into the Bohai Sea (Zhou et al., 2014), where the modern YRD is located (see Figure 3.1C). The modern YRD has an area of around 10,000 km<sup>2</sup> and is home to more than 6 million people, including the city of Dongying with a population that exceeds 2 million inhabitants (Kuenzer et al., 2014). While two nature reserves with rich biodiversity are located in the YRD, it also hosts the Shengli oil field, which is China's second-largest oil field (Kuenzer et al., 2014). Following the classifications of Galloway (1975) and Dalrymple et al. (1992), the YRD may be classified as a wave-dominated delta (Hori et al., 2002). Off the mouth of the Yellow River, waves show seasonal variations that are associated with monsoon activity (Wang et al., 2010b). Maximum significant wave heights during winter can be as large as 5.2 m (Chen et al., 2008). Located in the vicinity of an amphidromic point, the tides at the mouth are microtidal and of irregular semi-diurnal character, with a mean tidal range between 0.6 to 0.8 m (Zhang et al., 1990). Tidal influence varies with discharge, but only reaches up to 10 km from the mouth (Wang et al., 2010b). Accordingly, the Yellow River Estuary may be classified as hyposynchronous. Even when the discharge is low during winter, salinities > 1 practical salinity units (PSU) are usually only observed in the lowermost 4 to 5 km of the estuary (Jordan et al., 2016). With high gradients between near-surface and near-bottom salinity, which can exceed 20 PSU, the Yellow River Estuary can also be classified as a salt-wedge estuary (Jordan et al., 2016). In front of the river mouth, massive amounts of sediment are deposited in summer, which are subsequently resuspended and transported to the offshore area by waves in winter (Yang et al., 2011). While water depths in the active deltaic channel are typically < 1.5 m (Jordan et al., 2016), more than 50 % of the low-lying delta is elevated less than 4 m above the mean sea-level (Liu and Drost, 1997). Driven by recent changes in the sediment load and grain sizes, the progradation rate for the whole delta decreased from 67.9 km<sup>2</sup>/yr (1976 to 1981) to 7.6 km<sup>2</sup>/yr (since 2003) (Wu et al., 2017). From 1997 to 2002, the delta even experienced a slow erosional stage (-6.4 km<sup>2</sup>/yr) (Wu et al., 2017). These developments are partly associated with artificial diversions of the deltaic channel in 1976 and 1996 (see Figure 3.1C) in order to facilitate the operation of the Shengli oil field (Kuenzer et al., 2014). Accordingly, patterns of erosion and accretion show a landward retreat of the abandoned channel and a progradation of the active channel (Kuenzer et al., 2014). Furthermore, dikes were built in 1984 to fix the coastline near existing oil fields, while groins were constructed after 2005 to trap sediments for an expansion of onshore oil production (Bi et al., 2014; Wu et al., 2017). While some of the outlined alterations in the Yellow River's regime can be directly connected to global El Niño-Southern Oscillation (ENSO) events (Wang et al., 2006), the river evidently was also heavily regulated by human activity, which will be highlighted in more detail in chapter 4.

## 3.2 Vietnamese Mekong Delta

The Mekong River has a length of around 4,900 km (Liu et al., 2009). On the way from its source on the Tibetan Plateau to the mouth at the South China Sea, the Mekong River flows through China, Myanmar, Thailand, Laos, Cambodia, and Vietnam. The upper half of the river, which is located in China, is oftentimes referred to as Lancang River. The basin of the Mekong River is also commonly divided into the Upper and Lower Mekong Basin (see Figure 3.2B). The Chinese and Burmese portions of the river basin form the Upper Mekong Basin, while the Lower Mekong Basin covers the basin areas in Thailand, Laos, Cambodia, and Vietnam. The hydrological regime of the Mekong is mainly driven by the Western North-Pacific and Indian monsoon, leading to a distinct dry season (November to May) and wet season (June to October), respectively. Additionally, around 29 % of the annual runoff and 32 % of the suspended sediment to the sea is associated with tropical cyclone activity (Darby et al., 2016). The ENSO is also known to cause inter-annual variations in the river's hydrology, particularly in the Lower Mekong Basin (Räsänen and Kummu, 2013). According to estimates of discharge and sediment load by Milliman and Farnsworth (2011), which have likely become obsolete, the Mekong River was ranked seventh and eleventh, respectively, among the world's greatest rivers. The mean annual flow at Kratie (Cambodia) (see location in Figure 3.2B) is around 13,200 m<sup>3</sup>/s, while the average monthly discharges vary between 1,600 and 37,000 m<sup>3</sup>/s (MRC, 2010). However, recent findings indicate that dry season discharges at Kratie are increasing by up to 68 %, while wet season discharges are declining by as much as 6 % (Räsänen et al., 2017). Considering the sediment loads at Kratie, historical levels were of the order of 160 Mt/yr (Milliman and Meade, 1983), but have seen a substantial reduction in recent years to around 87 Mt/yr (Darby et al., 2016). Nowacki et al. (2015) even argue that the present sediment load could be as low as 40 Mt/yr. Most of the sediment transport is associated with cohesive sediment fractions, while annual sand flux entering the delta is around  $6.2 \pm 2.0$  Mt/yr (Hackney et al., 2020). The contribution of bed load transport to the total sediment load is < 1 % (Jordan et al., 2019b; Hackney et al., 2020).

The delta of the Mekong River (see Figure 3.2C), which covers much of southern Vietnam and parts of Cambodia, is one of the largest river deltas worldwide. During the last 6,000 to 7,000 years, the VMD has prograded more than 200 km from the border to Cambodia to its present coastline in Vietnam (Ta et al., 2002). The VMD is home to around 17 million inhabitants, has an area of around 41,000 km<sup>2</sup>, and includes 13 provinces (GSO, 2021). Being Vietnam's principal rice-producing region, the delta also is a major producer of fruits and vegetables as well as aquaculture products, thus providing food security across the region (Renaud and Kuenzer, 2012). The VMD is also known for being a rich biodiversity location, particularly for birds and fish (Campbell, 2012). North of the delta, near Phnom Penh, the Mekong splits into two main branches: the Tien River ('Mekong

proper') and the Hau River ('Bassac') (see locations in Figure 3.2C). On their way to the coast, the Tien and Hau River are divided into a total of eight distributary channels. According to Wright (1985), the VMD can be classified as a wave-influenced, tide-dominated delta. At the mouth, wave processes are strongly dependent on the monsoonal regime, with monthly mean significant wave heights being of the order of 0.8 to 1.2 m during the winter and 0.5 to 0.6 m during the summer (Dee et al., 2011). Tides at the mouth are mesotidal and of irregular semi-diurnal character (Gugliotta et al., 2017). The average tidal range is around  $2.5 \pm 0.1$  m, while the maximum tidal range can be as high as 3.8 m (Gugliotta et al., 2017). Tidal variations in water levels can still be observed beyond the border to Cambodia (Gugliotta et al., 2017). However, with the tidal range diminishing in landward direction, the Mekong's channels can be classified as hyposynchronous (Eslami et al., 2021). Measurements, which were carried out by Gugliotta et al. (2017), indicate that the salinity intrusion extends up to 50 km from the river mouth during the dry season and around 15 km during the wet season (using the 0.5 PSU isohaline as a proxy). During low flow, the channels of the Mekong River can be classified as partially-mixed estuaries, while a salt-wedge forms during high flow (Nowacki et al., 2015). Furthermore, the distributary channels usually show flood-dominant behavior during low flow that reverses to ebb dominance during high flow (Nowacki et al., 2015). The sediment transport in the distributary channels is directed landward during periods of low discharge, whereas sediment is exported seaward during periods of high discharge (Nowacki et al., 2015). Since the sediment export is larger than the import, the system is prograding (Gugliotta et al., 2017). A particularly large amount of sediment is deposited at the mouth during the wet season (e.g., Xue et al., 2012). As observed by Wolanski et al. (1996) during a high flow period, a small amount of this sediment returns to the estuaries with the salt-wedge, leading to the formation of an ETM. Sediment, which was deposited at the mouth during previous periods of high discharge, is also entrained and transported landward to an ETM during the dry season, when maximum near-bottom SSCs can be as high as  $1.4 \text{ kg/m}^3$  (Wolanski et al., 1998). Another portion of the offshore deposits is resuspended and transported southeastward during the dry season by alongshore currents (Xue et al., 2012). At present, the mean elevation of the VMD is just 0.8 m above the sea-level (Minderhoud et al., 2019), while water depths in the deltaic channels vary considerably, but can locally exceed 50 m (Jordan et al., 2019b). Typically, mud contents are highly variable (5 to 90 %) in the lower 100 km of all distributary channels, while sand dominates in the upstream parts of the Tien and Hau River (Gugliotta et al., 2017). The average thickness of alluvial deposits is of the order of 28 m (Hackney et al., 2020). Recently, large-scale erosion processes were observed in the deltaic channels and along the coasts of the VMD. Measurements indicate that mean channel incision in the Tien River is presently of the order of up to  $-0.5 \text{ m/yr}$  (Binh et al., 2020), while several studies indicate that more than half of the delta shoreline is subject to erosion (e.g., Anthony et al., 2015; Li et al., 2017).

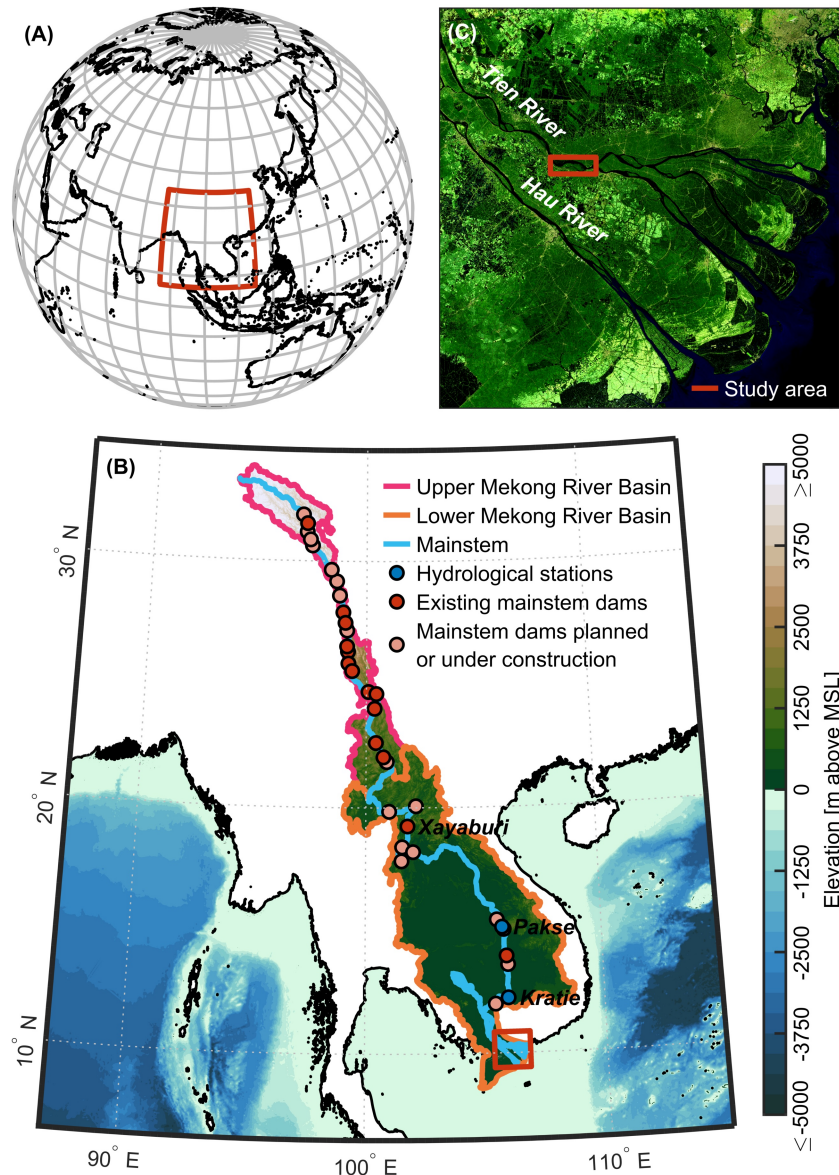


Figure 3.2: Map of the Mekong River Basin and the VMD. (A) Global coastlines with location of the Mekong River Basin. Red rectangle indicates area shown in panel (B). (B) Map of the Mekong River Basin, including locations of existing mainstem dams, dams planned or under construction, and selected hydrological stations. Red rectangle indicates area shown in panel (C). (C) False color composite of the VMD based on Landsat-8 image for August 22, 2020. Red rectangle indicates study area by Jordan et al. (2019b, 2020). Shapefiles in (A, B) copyrighted OpenStreetMap contributors (<https://www.openstreetmap.org>). GEBCO 2021 Grid (GEBCO Compilation Group, 2021) was used for topography and bathymetry data in (B). Landsat-8 image in (C) courtesy of the USGS, downloaded from the USGS EROS Center (<https://earthexplorer.usgs.gov/>).

### 3.3 North Sea basin and adjacent estuaries in the German Bight

During the Early Holocene, sea-level rose by around 60 m between approx. 11,700 and 7,050 before present (BP) (e.g., Smith et al., 2011). During this period, inundation of the North Sea started in the north (Sturt et al., 2013), while the southern North Sea basin was flooded around 9,000 to 8,000 BP (Eisma et al., 1981). With the flooding of the Doggerbank around 7,500 BP (Fitch et al., 2005), the North Sea almost had its present-day geometry. With ongoing SLR, fluvial valleys were flooded, hence creating estuaries along the coasts of the region. Furthermore, tidal basins were formed by the inundation of low-lying parts of the coastal landscape (van der Spek, 1994). A shift from coastline retreat to progradation occurred around 6,600 BP, when sediment supply was sufficient to keep pace with a decelerating SLR (Bungenstock and Schäfer, 2009). With a SLR of around 0.11 m/century (Behre, 2003), the Wadden Sea was formed over the last 3,000 years (Schwarzer et al., 2008). With first dikes being constructed around 900 years ago, the development of the North Sea coastlines is also strongly influenced by anthropogenic activity since the Middle Ages (Bungenstock and Schäfer, 2009). At present, the coastlines of the North Sea are fixed and fortified by coastal protection measures.

Today, the North Sea basin has a surface area of around 575,000 km<sup>2</sup> (including the Skagerrak) (ICES, 1983). The basin width varies considerably, from over 500 km in the North to less than 40 km in the Strait of Dover (Roos et al., 2011). The mean water depth of the North Sea is around 94 m (Schwarzer et al., 2008), while maximum water depths of over 700 m can be found in the Norwegian Trench (Roos et al., 2011). Tidal waves, which enter the basin through an open boundary east of Scotland and through the Strait of Dover (Roos et al., 2011), travel in a counterclockwise direction. Even though diurnal inequalities and tidal asymmetries may play an important role locally, the tides in the North Sea show predominantly semi-diurnal character, with spring tidal ranges surpassing 3.5 m along the coasts of eastern England and in parts of the German Bight (Huthnance, 1991). However, tidal ranges are small in the vicinity of amphidromes in the central part of the Southern Bight and west of Denmark (Huthnance, 1991). In addition, a degenerate amphidromic point can be found at the southern tip of Norway (Howarth, 1990). Located in the southeastern North Sea, the Wadden Sea extends from Den Helder (the Netherlands) to Skallingen (Denmark). Characterized by a chain of barrier islands, tidal inlets, channels, and intertidal flats, the Wadden Sea has a unique ecosystem with highly specialized habitats, flora, and fauna and was declared a United Nations Educational, Scientific and Cultural Organization (UNESCO) World Heritage site in 2009<sup>4</sup> (CWSS, 2021a). At the same time, the Wadden Sea has high socio-economic value and

---

<sup>4</sup>Initially only the Dutch Wadden Sea and parts of the German Wadden Sea were declared a UNESCO World Heritage Site in 2009. Remaining parts of the German and Danish Wadden Sea were added in 2011 and 2014.

has been impacted by human activity for many centuries (Lotze et al., 2005). The coastal plain estuaries of the rivers Elbe, Weser, and Ems directly flow into the Wadden Sea.

With a length of 1,094 km, the Elbe is the fourth-largest river in central Europe (Boehlich and Strotmann, 2008). The estuary of the Elbe River extends around 160 km from the weir at Geesthacht (see location in Figure 3.3B) to the North Sea at Cuxhaven (Kappenberg and Grabemann, 2001). The mean discharge at Neu Darchau, which is located upstream from the weir, is around  $710 \text{ m}^3/\text{s}$  (HPA, 2015). Over the period from 1926 to 2013, the averages of the annual minimum and maximum discharge are around 280 and  $1,970 \text{ m}^3/\text{s}$ , respectively (HPA, 2015). Based on observations for the period 1994 to 2013 (at Hitzacker), the mean fluvial sediment input is around 740,000 t/yr (HPA, 2015). The section between Geesthacht to Cuxhaven denotes the Lower Elbe Estuary, while the Outer Elbe Estuary is located seaward from Cuxhaven. Being an important shipping route, the Elbe Estuary provides entrance to the ports of Cuxhaven, Brunsbüttel, Glückstadt, Bützfleth, and Hamburg. Within the city limits of Hamburg, the Elbe is divided into the Northern and Southern Elbe for around 17 km. From Blankenese to Glückstadt, several islands divide the estuary into main and secondary channels. Downstream from Brunsbüttel, the Elbe Estuary widens and has a funnel-shape geometry. The mouth is characterized by multiple channels and extended intertidal flats. In the navigation channel, water depths can locally be as high as 25 m below chart datum, while a minimum water depth of 14.5 m is guaranteed for shipping (Rolinski and Eichweber, 2000; Boehlich and Strotmann, 2008). Bed material in the navigation channel usually consists of fine to medium sands, which can locally be mixed with 5 to 30 % of silt (BfG, 2008). At the measuring station Elbe, which is located seaward from the mouth of the estuary, annual means for the significant wave height range from 0.9 to 1.2 m (1996 to 2015) (Hagen et al., 2021). At the mouth, the tidal range is around 3.0 m at the gauge station Scharhörn (see location in Figure 3.3C) (HPA, 2015). In landward direction, the tidal range decreases to around 2.8 m at Brokdorf before rising to 3.7 m at St. Pauli (HPA, 2015). Upstream from St. Pauli, the tidal range decreases again to around 2.5 m at the gauge station Zollenspieker (HPA, 2015). The irregular behavior of tidal ranges is likely associated with changes in the convergence of the estuary (Winterwerp et al., 2013). Based on observed tidal ranges, the Elbe Estuary can be classified as mesotidal and hypersynchronous. Moreover, it can be classified as tide-dominated, even though the Elbe Estuary is also influenced by waves. Furthermore, the inner estuary is flood-dominant, while the considerable amount of intertidal flats favors ebb dominance in the outer estuary (Winterwerp et al., 2013). Finally, the Elbe Estuary can be classified as a partially-mixed to well-mixed estuary (Kappenberg and Fanger, 2007). At the landward end of the mixing zone, the ETM of the Elbe Estuary can be observed. The ETM, where SSCs exceed riverine values of around  $0.035 \text{ kg}/\text{m}^3$  by a factor of 10 to 30, is roughly located 40 km landward from the mouth and has a length of 30 km (Kappenberg and Grabemann, 2001).

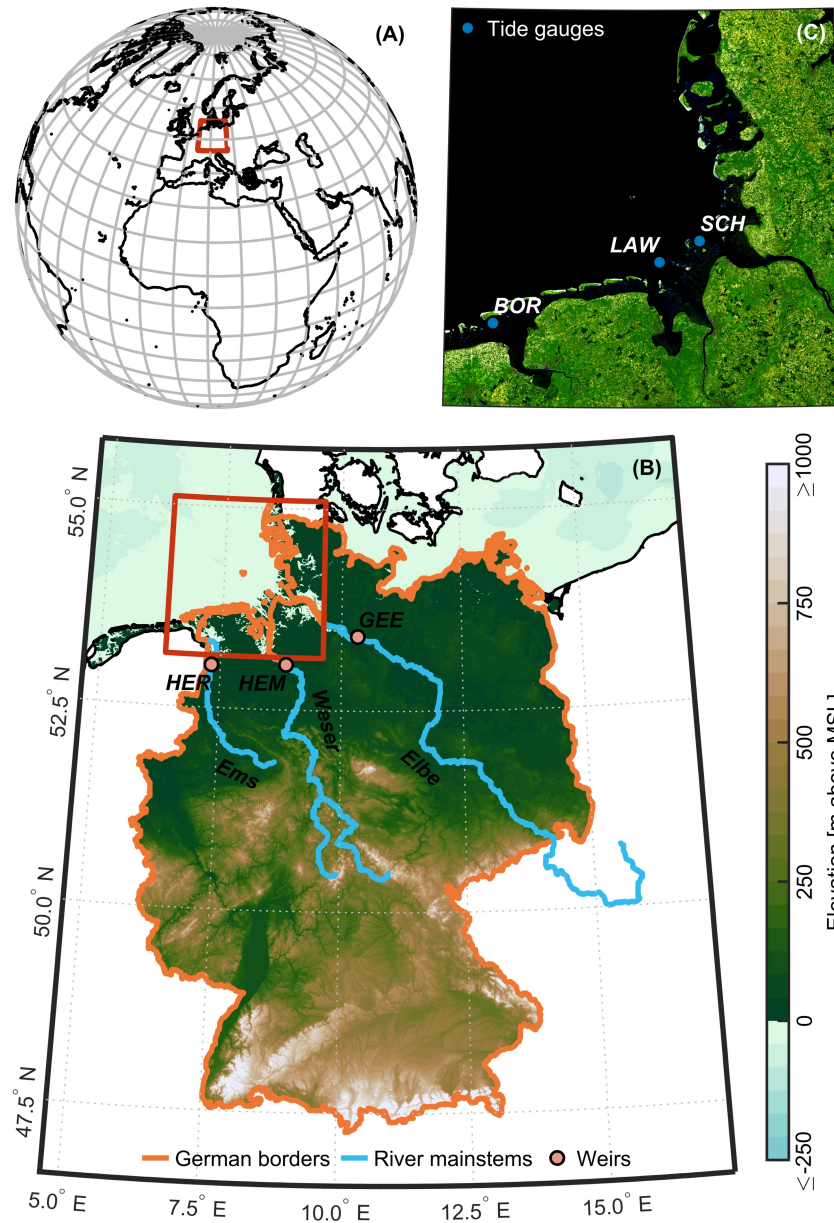


Figure 3.3: Map of Germany and the German Bight. **(A)** Global coastlines with location of Germany. Red rectangle indicates area shown in panel **(B)**. **(B)** Map of Germany, including mainstems of the rivers Elbe, Weser, and Ems. GEE, HEM, and HER indicate the locations of the weirs at Geesthacht, Hemelingen, and Herbrum, respectively. Red rectangle indicates area shown in panel **(C)**. **(C)** False color composite of the German Bight based on Sentinel-2 image for May 8, 2018. SCH, LAW, and BOR indicate the locations of the tide gauges Scharhörn, Leuchtturm Alte Weser, and Borkum Fischerbalje, respectively. Shapefiles in **(A, B)** copyrighted OpenStreetMap contributors (<https://www.openstreetmap.org>). GEBCO 2021 Grid (GEBCO Compilation Group, 2021) was used for topography and bathymetry data in **(B)**. Sentinel-2 image in **(C)** courtesy of the USGS, downloaded from the USGS EROS Center (<https://earthexplorer.usgs.gov/>). Copernicus Sentinel data, processed by the ESA.



The Weser, which has a length of 477 km, is Germany's second-largest river discharging into the North Sea (Seedorf and Meyer, 1992). The tidal boundary of the Weser is defined by the weir in Bremen-Hemelingen (see location in Figure 3.3B). The mean discharge, which is measured at Intschede approx. 30 km upstream from the weir, is around  $320 \text{ m}^3/\text{s}$  (NLWKN, 2015). Long-term averages (1941 to 2013) of the annual minimum and maximum runoff are around 120 and  $1,200 \text{ m}^3/\text{s}$ , respectively (NLWKN, 2015). The long-term average (1970 to 2013) of riverine sediment input is around  $490,000 \text{ t/yr}$  (NLWKN, 2015). The distance from the weir to the seaward boundary at the North Sea, where intratidal and interannual differences in salinity are small, is around 120 km (Grabemann and Krause, 2001). The estuary, which can be divided into the Lower Weser (from Bremen to Bremerhaven) and Outer Weser (seaward of Bremerhaven), marks the entrance to the ports of Bremerhaven, Nordenham, Brake, and Bremen. The Lower Weser Estuary has a channel-like character, whereas the Outer Weser Estuary has a funnel shape. In addition, the Outer Weser is characterized by a two-channel system (Gundlach et al., 2021). Water depths in the navigation channel are around 15 m below chart datum in the Outer Weser and about 9 m in the Lower Weser (Grabemann and Krause, 2001). Except for the ETM, the bed material in the channels mainly consists of fine to medium sands (Grabemann and Krause, 2001). The tidal range is around 2.9 m at the tide gauge Leuchtturm Alte Weser (see location in Figure 3.3C) in the Outer Weser (LLUR, 2014) and increases up to 4.2 m at the tide gauge Große Weserbrücke (NLWKN, 2015). From the location Große Weserbrücke to the weir at Bremen-Hemelingen, the tidal range slightly decreases (WSV, 2021). Accordingly, the Weser Estuary can be classified as meso- to macrotidal, hypersynchronous, as well as tide-dominated. In addition, with peak ebb currents usually being stronger than peak flood currents, most of the Weser Estuary shows ebb dominance (Schrottke et al., 2006). Based on the vertical structure of salinity, the estuary can also be classified as partially-mixed (Grabemann et al., 1997). At the lower salinity reaches of the mixing zone, the ETM in the Weser Estuary has a length of around 15 to 20 km and is roughly located between Brake and Bremerhaven (e.g., Grabemann and Krause, 2001; Schrottke et al., 2006). Maximum SSCs in the ETM can surpass  $2 \text{ kg/m}^3$  (Lange et al., 2008). Fluid mud may occur in the ETM of the Weser Estuary, although no continuous fluid mud layer can be found (Schrottke et al., 2006).

Located at the border between the Netherlands and Germany, the Ems has a length of around 370 km (Seedorf and Meyer, 1992). Extending from the weir at Herbrum (see location in Figure 3.3B) to the island Borkum, the Ems Estuary has a length of approx. 100 km (de Jonge et al., 2014). Upstream from the weir, the mean runoff at Versen measures around  $80 \text{ m}^3/\text{s}$  (NLWKN, 2015). Long term averages (1941 to 2013) of the annual minimum and maximum discharge are around 20 and  $360 \text{ m}^3/\text{s}$ , respectively (NLWKN, 2015). Based on the period from 1965 to 2013, the long-term average of annual riverine sediment input into the estuary, which is measured at Lathen, amounts to around

55,000 t/yr (NLWKN, 2015). Located along the Ems Estuary, there are a major shipyard in Papenburg as well as the ports of Eemshaven, Delfzijl, Emden, and Leer. The Lower Ems Estuary from Herbrum to Emden has a channel-like shape, while the Outer Ems Estuary from Emden to Borkum is characterized by a funnel-shaped geometry. The navigation channel downstream from Emden has a minimum water depth of 8.5 m below chart datum, while the Lower Ems was temporarily deepened to 7.3 m (below mean high water (MHW)) (Krebs and Weilbeer, 2008). Nowadays, the current maintenance depth in the Lower Ems is 6.3 m, since water depths can be temporarily increased by the closure of the storm surge barrier at Gandersum (Oberrecht, 2020). In the Lower Ems, bed sediments upstream from Papenburg are mainly sandy, while bed material between Papenburg and Emden largely consists of cohesive sediments (Oberrecht, 2020). The tidal range in the estuary increases from around 2.4 m at the tide gauge station Borkum Fischerbalje (see location in Figure 3.3C) to 3.7 m at Papenburg (LLUR, 2014; NLWKN, 2015). From Papenburg to the weir at Herbrum, a reduction in tidal range can be measured (Oberrecht, 2020). Based on these observations, the Ems Estuary can be classified as a mesotidal, hypersynchronous, and tide-dominated estuary. Except for the vicinity of the Dollart Bay, the Ems Estuary also shows a distinct dominance of flood currents (Pein et al., 2014). Finally, the estuary can be classified as partially-mixed (Papenmeier et al., 2013). Presently, the ETM of the Ems Estuary is located roughly between Terborg and the weir at Herbrum, extending over a length of around 30 km (Oberrecht, 2020). Between 1954 and 2005, the ETM has moved upstream by around 25 km and has broadened significantly (de Jonge et al., 2014). With SSCs in some parts of the estuary increasing by a factor of up to 10 during this period (de Jonge et al., 2014), the Ems Estuary has shifted to a hyper-turbid state (Winterwerp and Wang, 2013). When discharge is low, maximum SSCs in the ETM can nowadays be as high as  $40 \text{ kg/m}^3$  during flood (Oberrecht, 2020). A characteristic feature of the ETM in the Ems Estuary is the presence of thick fluid mud deposits, which have developed since the early 1990s (de Jonge et al., 2014). These mud deposits, which occur throughout the whole ETM, can reach concentrations of up to  $500 \text{ kg/m}^3$  while remaining mobile at concentrations below around  $200 \text{ kg/m}^3$  (Papenmeier et al., 2013).

### Summary of chapter 3:

- **Yellow River Delta**

The Yellow River was long considered the world's second-largest river in terms of sediment load to the ocean. While crossing the Loess Plateau, nearly 90 % of the river's huge amount of sediment is picked up. However, the Yellow River has seen substantial decreases in water and sediment fluxes in recent decades. Additionally,

- **Yellow River Delta (continued)**

a reduction in SSCs was observed, accompanied by an increase in the grain size of suspended sediments. Nowadays, characteristic hyperpycnal plumes at the mouth of the Yellow River occur only infrequently. Being located at the transition to the Bohai Sea, the YRD is home to around 6 million inhabitants while also hosting two nature reserves. In addition, China's second-largest oil field is located in the delta. To facilitate oil production, the delta has become subject to multiple engineering works (e.g., river diversions, construction of dikes and groins) in the past 50 years. Being classified as a wave-dominated delta, waves at the river mouth show seasonal variations that are associated with monsoon activity, while tides are microtidal. Since tidal range diminishes landwards, the estuary of the Yellow River can also be classified as hyposynchronous. Due to high salinity gradients between near-surface and near-bottom layers, the Yellow River also shows the characteristics of a salt-wedge estuary. Following a stage of rapid accretion (1976 to 1981), the YRD has only experienced stages of slow accretion or even erosion after 1982.

- **Vietnamese Mekong Delta**

In general, the hydrology of the Mekong River is driven by monsoonal climate, while tropical cyclones and the ENSO also contribute to variations in the river's water and sediment fluxes. However, recent observations indicate that dry season discharges are increasing, while wet season discharges are decreasing. Furthermore, the Mekong River has seen a substantial decline in sediment loads over the past decades, as suggested by recent estimates. Being home to around 17 million inhabitants and a diversity of species, the low-lying VMD also provides food security across Southeast Asia. Within the delta, the Mekong River is divided into two major branches (Tien and Hau River), which split into a total of eight distributary channels on their way to the coast. The delta itself can be classified as a wave-influenced, tide-dominated delta. According to predominant tidal dynamics, distributary channels may also be classified as mesotidal and hyposynchronous estuaries. Additionally, the estuarine channels are partially-mixed and show flood dominance during low discharge. In contrast, a salt-wedge is formed during periods of high discharge, when the channels also become ebb-dominant. The formation of an ETM in the distributary channels also shows seasonal variations. During the last 6,000 to 7,000 years, when it was formed by river flows, waves, and tides, the delta prograded more than 200 km from the border between Cambodia and Vietnam to its present-day coastline. However, observations of erosion processes indicate that the delta is starting to shrink.

- **North Sea basin and adjacent estuaries in the German Bight**

SLR during the Early Holocene led to the flooding of large areas of the North Sea basin while also creating estuaries and tidal basins along the region's coastlines. Caused by a deceleration in SLR, the Wadden Sea was formed in the southeastern North Sea during the last 3,000 years. While exhibiting a unique ecosystem, the Wadden Sea is characterized by barrier islands, tidal inlets, channels, and intertidal flats. Furthermore, the coastal plain estuaries of the German rivers Elbe, Weser, and Ems directly flow into the Wadden Sea. Besides SLR, human interventions have shaped the geometry of the North Sea basin. Nowadays, the coastlines of the region are fixed and fortified by coastal protection measures. The tides in the North Sea region are predominantly semi-diurnal and can locally exceed spring tidal ranges of 3.5 m. Concentrating on the estuaries of the rivers Elbe, Weser, and Ems, these estuaries are of high economic value by providing entrance to major ports and shipyards. All of these estuaries may be classified as coastal plain, hypersynchronous, and tide-dominated estuaries. Based on their tidal ranges, the Ems Estuary and Elbe Estuary can also be classified as mesotidal, while the Weser Estuary is meso- to macrotidal. According to tidal asymmetries, the estuaries Ems and Elbe are generally denoted as flood-dominant, while the Weser Estuary is rather ebb-dominant. Considering the vertical structure of salinity, the Ems and Weser are partially-mixed estuaries, while the Elbe Estuary is partially-mixed to well-mixed. Furthermore, the formation of an ETM can be observed in the lower salinity reaches of the mixing zone of all of these estuaries. However, measured SSCs in the ETMs of the three estuaries are distinctly different. Additionally, fluid mud is not present in the Elbe Estuary and can only be found locally in the Weser Estuary, whereas thick deposits occur throughout the whole ETM of the Ems Estuary.

## 4 Drivers of contemporary and future changes in estuaries

As shown in this chapter, estuaries are coastal environments that are increasingly exposed to climate change and human exploitation. This thesis concentrates on contemporary and future changes in estuaries, which are driven by sand mining/dredging, damming, climate change-induced alterations in hydrology, and SLR. However, other drivers can undoubtedly also have significant impacts on estuaries. Originating from regions of agriculture, industry, or from urban areas, pollutants may significantly impact the biodiversity in estuaries (Best, 2019). Over-enrichment of nutrients, for example, may lead to algal blooms, increased turbidity, and a decrease in dissolved oxygen (UNEP-DHI and UNEP, 2016). In addition, between around 1.15 and 2.41 Mt of plastic waste are transported annually by rivers to the coastal oceans (Lebreton et al., 2017), impacting the health of aquatic species and humans. The delivery of plastic waste to the oceans is mainly dominated by Asian rivers, with the Yellow River and Mekong River also being among the 10 top-ranked rivers with regard to their contribution to the total global plastic load (Schmidt et al., 2017). Besides pollutants, overfishing and the introduction of non-native species also pose major threats to the biodiversity in estuaries. In many countries, the growing demand for seafood has led to the overexploitation of many important species in estuarine waters, hence impacting the function of the ecosystem (e.g., Kennish, 2017). At the same time, the spread of non-native species may also lead to a decline or even complete disappearance of native species (e.g., Bernauer and Jansen, 2006). Concentrating on the drivers that are addressed in detail in the following subchapters, their global-scale impacts are presented first, before focusing on impacts on the scale of individual study sites, where applicable.

### 4.1 Sand mining/dredging

Nonmetallic minerals account for almost 50% of the global extraction of materials, thus even exceeding fossil fuels and biomass (Miatto et al., 2017). In 2010, a total of 35 Gt of nonmetallic minerals were extracted globally, showcasing a 3.5-fold growth since 1970 (Miatto et al., 2017). With contributions of around 14.3 and 10.9 Gt, gravel and sand are the main nonmetallic materials being extracted (Miatto et al., 2017). Since reliable data on their extraction is scarce, cement production is oftentimes used to estimate global use of these aggregates (Peduzzi, 2014). Presently, the global extraction of aggregates substantially exceeds the yearly amount of sediment carried by all of the world's rivers (Peduzzi, 2014). In general, aggregates are consumed by a wide range of sectors, with sand being a key ingredient of concrete, asphalt, glass, and electronics (Torres et al., 2021). However, most notably driven by the economic growth and urbanization in Asian developing countries, gravel and sand are mainly used by the construction industry and for land

reclamation projects (Miatto et al., 2017; Bisht, 2021). According to the Organisation for Economic Co-operation and Development (OECD), the projected demand for sand, gravel, and crushed rock will rise to 55 Gt/yr by the year 2060, hence almost doubling the recent scale of extraction (OECD, 2018) (see Figure 4.1). This growing demand has the potential to trigger social conflicts and fuel concerns over aggregate scarcity (Torres et al., 2021).

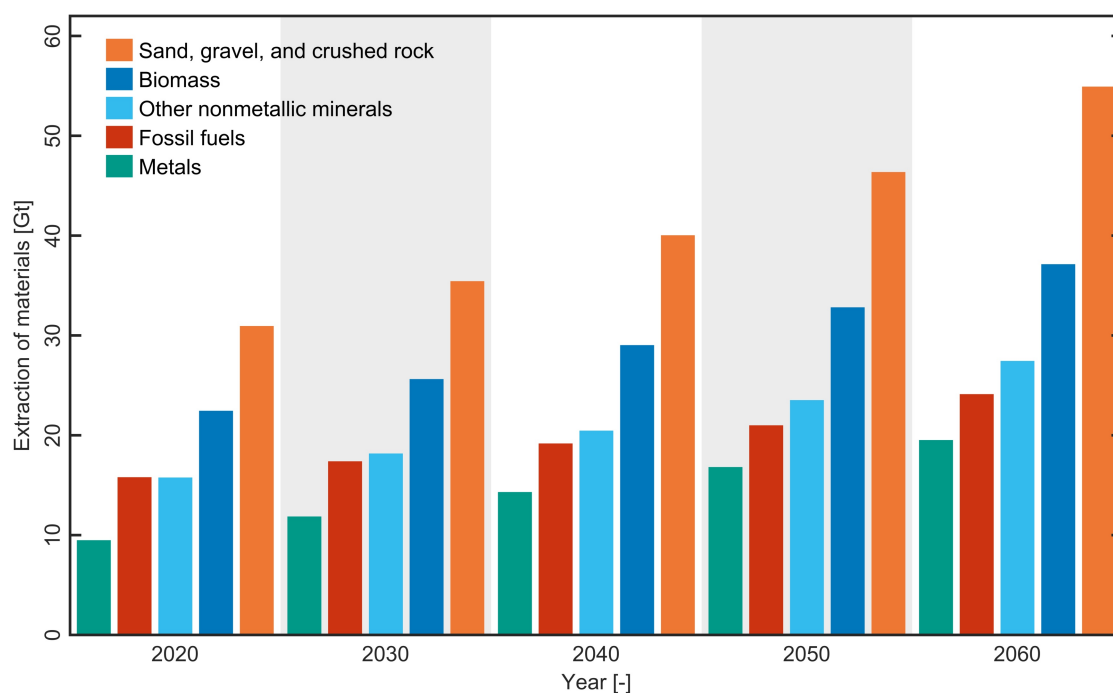


Figure 4.1: Projected global material extraction. Based on data from OECD (2018).

Focusing on the extraction of sand, one can differentiate between five major sources, depending on its geographical availability: (i) riverine sand, (ii) sand originating from beaches and coastal regions, (iii) sand originating from lakes and creeks, (iv) marine sand, and (v) sand originating from crushed rock (Bisht, 2021). Due to the spherical shape of grains, desert sand is usually not suitable for use in the construction sector, although available in large quantities (Bisht, 2021). Even though around 90 % of the global consumption of sand originates from terrestrial quarries and pits, riverine and coastal sources are increasingly exploited to cope with the demand for sand (UNEP, 2019). In contrast to marine aggregates, which need to be thoroughly washed before being used for concrete, riverine aggregates require significantly less processing (Peduzzi, 2014). Additionally, riverine sand is particularly well-suited for use in the construction sector due to a rather angular shape of individual grains (Bisht, 2021). Furthermore, urban areas are oftentimes located in close proximity to riverine systems, making riverine sand easily accessible (Bisht, 2021). Throughout the last decades, large amounts of sand were extracted

from many of the world's big rivers. Prominent examples include: the Mississippi River (USA) (Yuill et al., 2016), the Loire River (France) (Latapie et al., 2014), and the Pearl River (China) (Lu et al., 2007). Whereas sand mining has been prohibited or at least heavily regulated in many rivers in North America and Europe, the lack of regulations in many underdeveloped and developing countries has caused unsustainable or even illegal mining of riverine sediments (Gavriletea, 2017). Many large river basins also span several countries, complicating the monitoring of sand mining activity or the implementation and enforcement of laws (Bendixen et al., 2019a). As a result, estimates of sand extraction are lacking for many of the world's large river systems (Hackney et al., 2021).

Compared to most river basins, sand mining in the Mekong River is relatively well-documented, as indicated by the number of studies that were published in the past decade. Based on questionnaires, Bravard et al. (2013) estimated that  $34.5 \text{ Mm}^3/\text{yr}$  of sand were extracted from the Mekong River's channels in 2011, with Cambodia being the largest extractor ( $20.8 \text{ Mm}^3/\text{yr}$ ), followed by Vietnam ( $7.8 \text{ Mm}^3/\text{yr}$ ). Using high-resolution bathymetric maps, Jordan et al. (2019b) estimated a sand extraction of  $4.64 \pm 0.31 \text{ Mm}^3/\text{yr}$  for only a 20 km section of the Tien River branch (see location in Figure 3.2C), which was surveyed during two in-situ campaigns in 2018. According to local authorities, the sand mining volume for the whole VMD was 28 and  $17.8 \text{ Mm}^3/\text{yr}$  for the years 2015 and 2018, respectively (Eslami et al., 2019; Jordan et al., 2019b). Newest estimates based on remote sensing indicate that sand extraction volumes could still be substantially underestimated. For example, Hackney et al. (2021) estimate that sand mining activity in the Lower Mekong River in Cambodia increased to around  $36.9 \text{ Mm}^3/\text{yr}$  in 2020, hence almost doubling the reported value by Bravard et al. (2013). Recent findings by Gruel et al. (Preprint) for the VMD indicate that sand mining volumes in 2015 were of the order of  $38 \text{ Mm}^3/\text{yr}$  and increased to around  $47 \text{ Mm}^3/\text{yr}$  in 2020, with an average of  $42 \text{ Mm}^3/\text{yr}$  during the observed 6-year period. This would represent more than a 5-fold increase in comparison to the estimate by Bravard et al. (2013) and a 1.5-fold increase in relation to official statistics from local authorities. As observed by Jordan et al. (2019b), the discrepancies between official statistics and actual extraction volumes likely result from illegal extraction of sand, i.e., dredging without valid licenses or a violation of license regulations. Even though Vietnam and Cambodia banned sand exports in 2009 and 2017 (Koehnken and Rintoul, 2018), respectively, sand is likely still exported to neighboring countries, such as Singapore. This is also highlighted by discrepancies between sand imports/exports, which are documented by the UN Comtrade Database. For the period 2007 to 2016, for example, the reported sand exports from Vietnam to Singapore (123 million US\$) do not match the reported sand imports of Singapore from Vietnam (878 million US\$) (UNSD, 2021).

Assuming a sand density of  $1,600 \text{ kg/m}^3$ , the total sand flux entering the delta, which is of the order of  $6.2 \pm 2.0 \text{ Mt/yr}$  (Hackney et al., 2020), is presently significantly smaller

than the combined sand extraction in the Lower Mekong River (Cambodia) and the VMD ( $\approx 134$  Mt/yr) (Hackney et al., 2021; Gruel et al., Preprint). To ensure the sustainability of a river's sand resource, Hackney et al. (2020) suggested the following formula, which establishes a mass balance between the natural supply/storage of sand and the rate of sand extraction that is given by:

$$S_{res} = S_{store} + ((S_{in} - S_{xt}) \times t) \quad (4.1.1)$$

where  $S_{res}$  is the available sand resource,  $S_{store}$  is the available sand in storage in the riverbed,  $S_{in}$  is the incoming supply of sand,  $S_{xt}$  is the rate of sand extraction, and  $t$  is a given time period. If the rate of sand extraction is significantly higher than the natural supply of sand, negative impacts are to be expected until the sand storage will finally be exhausted. Presently, estimates of annual channel incision already range between  $-0.13$  and  $-0.50$  m/yr (Brunier et al., 2014; Binh et al., 2020). Focusing on the Tien River, at least 14.8% of the channel incision can be attributed to sand mining (Binh et al., 2020). As projected by Jordan et al. (2020), a further increase in sand extraction rates will only amplify such erosion processes in the Tien River, while a complete prohibition of sand mining activity may help to counterbalance the impacts of other drivers, such as hydropower expansion (see subchapter 4.2). Besides channel incision, impacts on the morphology of the VMD may include: scour around in-channel infrastructure (Lu et al., 2007), bank erosion (Jordan et al., 2019b; Hackney et al., 2020), and receding coastlines (Anthony et al., 2015; Luijendijk et al., 2018). Additional impacts on the environment, such as changes in river habitats, coarsening of bed material, lowering of water tables, reduced flood peaks, tidal amplification, and enhanced saltwater intrusion, can also be triggered by sand mining (e.g., Kondolf, 1997; Best, 2019; Eslami et al., 2019). The outlined impacts on the environment, which might cause the loss of houses and food sources, are critical to the lives and livelihoods of local residents (Torres et al., 2021; Bendixen et al., 2019a).

Even though sand mining for industrial use is not an issue in the estuaries of the German rivers Elbe, Weser, and Ems, they may be used as examples how channel deepening can generally impact estuarine systems. These estuaries were continuously altered by river engineering works, which started as early as the 19th century (Boehlich and Strotmann, 2008; Lange et al., 2008; Krebs and Weilbeer, 2008). Following the rapid development in maritime traffic, several campaigns were carried out to ensure the safe navigation to and from ports/shipyards that are located along these estuaries. As a result of the deepening, the tidal range was substantially amplified, leading to a change from hypo- to hypersynchronous character (e.g., Kappenberg and Fanger, 2007). As described by Winterwerp and Wang (2013), a significant amplification in tidal range may shift an estuary to a hyper-turbid system. If a tipping point is passed, a positive feedback loop is established between tidal amplification, flood dominance, import of fine sediments, and reduction in hydraulic



drag (Winterwerp and Wang, 2013). Whereas the Elbe Estuary and Weser Estuary have not passed this tipping point, the Ems Estuary is a prime example of a hyper-turbid estuary, as shown by a 10-fold increase of SSCs in the ETM and the formation of thick fluid mud layers (de Jonge et al., 2014). In such a hyper-turbid estuary, the environmental quality is deteriorated, which may have significant impacts on local species and the estuarine ecosystem services (de Jonge et al., 2014).

## 4.2 Damming

According to the International Commission on Large Dams (ICOLD), a dam is defined as large if it surpasses a height of 15 m or if a dam higher than 5 m has a storage volume in excess of 3 million m<sup>3</sup> (ICOLD, 2021a). Based on this definition, the global number of large dams is estimated to be around 59,000, with the overwhelming majority being located in Asia (ICOLD, 2021a,b). Globally, the construction of large dams has decreased since the 1970s (Magilligan et al., 2017) (see Figure 4.2). In Germany, for example, around two-thirds of the existing large dams were constructed before 1970, while only five large dams were constructed since the beginning of this century (Speckhann et al., 2021). In recent decades, however, socio-economic growth, climate change, and the increasing electricity demand have led to new hydropower development and the resurgence of large dams, particularly in underdeveloped and developing countries (Zarfl et al., 2015). The percentage of newly constructed large dams that are significantly higher than 15 m has also increased since the beginning of this century (ICOLD, 2021a) (see Figure 4.2). In general, large dams were long considered a major driver to modernize countries by generating cheap energy, expanding irrigated agriculture, supplying water to urban areas, and controlling floods (Molle et al., 2009). The social and environmental consequences, though, have increasingly prompted widespread opposition to these large dam projects (Magilligan et al., 2017). Social and environmental impacts of dams, which mainly result from altered water and sediment fluxes, may include: loss of biodiversity (Ziv et al., 2012; Winemiller et al., 2016), coastal erosion (Kondolf, 1997), changes in food security (Richter et al., 2010; Ziv et al., 2012), displacement of residents (WCD, 2000; Gross, 2016), and loss of cultural sites (Anderson and Veilleux, 2016; Gross, 2016). In addition, large hydropower dams may not yield a net economic benefit, with actual costs being systematically higher than estimated costs (Ansar et al., 2014). Climate benefits might also be significantly lower than previously assumed due to the emission of GHG from the decay of submerged vegetation (e.g., Gross, 2016; Räsänen et al., 2018). Furthermore, transboundary conflicts might arise by the construction of dams in river basins that are shared by numerous countries (Kuenzer et al., 2013). Finally, the benefits and negative impacts of hydropower development are oftentimes unevenly distributed, with powerful elites benefitting, while the rural poor population is exposed to the impacts (Kuenzer et al., 2013).

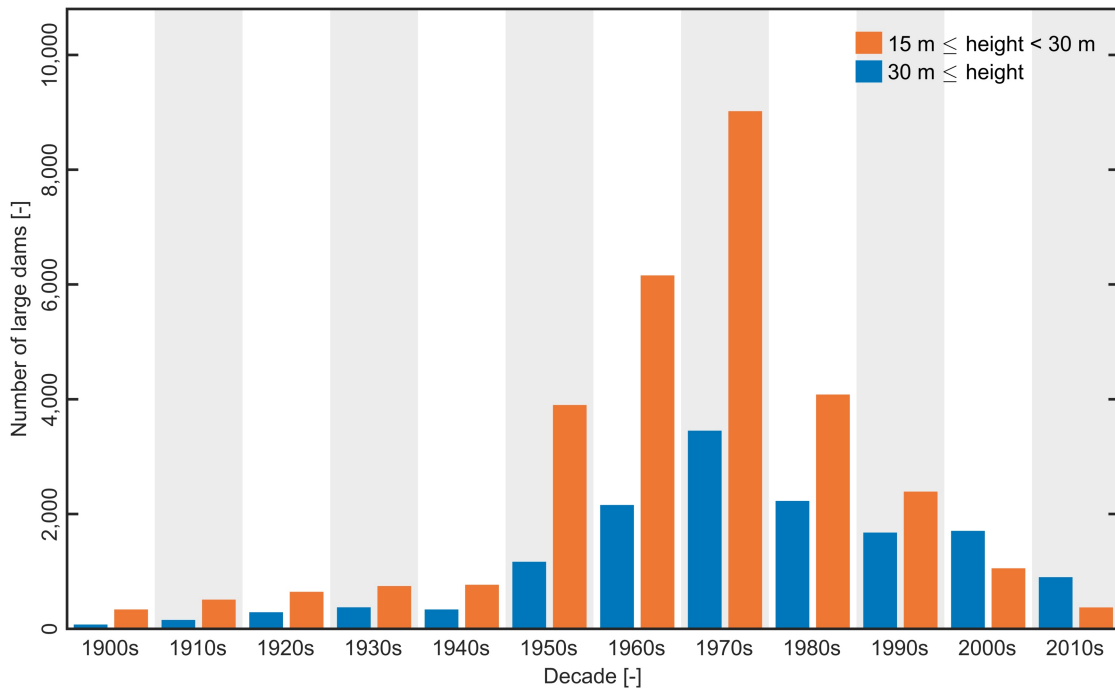


Figure 4.2: Construction of large dams by decade. Based on data from the World Register of Dams (ICOLD, 2021a).

Globally, around 48 % of river volume is currently at least moderately impacted by dams (i.e., more than a quarter of their main channel is fragmented or regulated by dams) (Grill et al., 2015). This number is projected to increase to 93 % if all dams currently under construction or planned are realized (Grill et al., 2015). In addition, the sediment trapping by reservoirs has led to a net reduction in the pre-human sediment flux to the oceans by around 1.4 Gt/yr, even though soil erosion has simultaneously increased the global sediment transport (Syvitski et al., 2005). At present, around 4 to 5 Gt/yr of sediment are trapped annually in reservoirs, representing more than a quarter of the global sediment flux (Vörösmarty et al., 2003). Assuming that around 0.8 % of global storage capacity is lost every year (Basson, 2008), the annual sediment trapping capacity of the world's reservoirs could even be significantly higher (Walling, 2009). In the future, the global amount of sediment being accumulated behind dams will only increase with the progression of hydropower expansion.

Prominent examples highlighting the outlined impacts of large dams are the Yellow River and the Mekong River. Known as one of the most-sediment-laden large rivers in the world, the Yellow River once delivered approx. 8 % of the global river sediment to the oceans (Milliman and Meade, 1983), but has reverted from a monsoon-driven to a heavily regulated system in recent decades (Yu et al., 2013). During the past 60 years, a stepwise

reduction in the Yellow River's water and sediment fluxes was observed that can mainly be attributed to the construction and operation of large dams along the river's upper and middle reaches (Yu et al., 2013). As part of China's Grain for Green project, soil conservation measures on the Chinese Loess Plateau have also contributed to the decrease in the river's sediment discharge (Chen et al., 2015). In relation to 1950s levels, modern-day (2000 to 2010) water and sediment fluxes to the sea have decreased by 70 and 90 %, respectively (Yu et al., 2013). Thus, today's sediment discharge resembles historical levels prior to the agricultural development of the Loess Plateau (Chen et al., 2015). Besides the significant decrease in water and sediment discharges, an observed decrease in SSCs and a coarsening of suspended sediments, as outlined in subchapter 3.1, can also be mainly attributed to the operation of large dams. Regarding the impact of large dams in the Yellow River Basin, the so-called water-sediment regulation scheme (WSRS) also has to be considered. The WSRS was implemented in 2002 after the completion of the Xiaolangdi Dam (see location in Figure 3.1B) to remove accumulated sediments from its reservoir and to scour the downstream riverbed, thus increasing the river's flood carrying capacity (Wang et al., 2017b). During the WSRS, which usually lasts around 20 days per year, approx. 30 % of the river's annual water discharge and 50 % of its annual sediment flux are delivered to the sea (Wang et al., 2017b). The severe environmental impacts of the operation of the WSRS include: increased fish mortality (Baoligao et al., 2016) and changes in nutrient fluxes impacting the coastal ecosystem (Liu, 2015). Although the design of the WSRS had no intention to stabilize the YRD, it initially provided sufficient sediment supply to nourish the delta (Wu et al., 2020). However, recent observations indicate that the YRD is presently facing an erosional stage, which is caused by a continuous decrease in reservoir capacity of the Xiaolangdi Dam and the armoring of the downstream riverbed (Wu et al., 2020).

Concentrating on the Mekong River, its hydropower potential was largely unused until 1993, when China completed the construction of the Manwan Dam on the Upper Mekong (Xue et al., 2011). While hydropower development is still ongoing on the Upper Mekong, the planning and construction of large hydropower dams has progressively expanded to the Lower Mekong and its tributary rivers (Kondolf et al., 2018). The construction of the Xayaburi Dam (see location in Figure 3.2B), the first on the mainstem of the Lower Mekong, has caused particular controversy. In 2010, the Laos government notified the intergovernmental Mekong River Commission (MRC) of its desire to build the dam, causing strong opposition from downstream riparian countries (Hensengerth, 2015). Even though a review by the MRC identified substantial problems with the design of the dam, Laos went on with the project largely unmodified (Hensengerth, 2015). Currently, at least 124 large dams (in operation, under construction, or at the planning stage) are located in the basin (Schmitt et al., 2019). As for the Yellow River, recent changes in discharge and sediment delivery to the VMD (see subchapter 3.2) can mainly be attributed to the operation of

existing upstream dams. Furthermore, Binh et al. (2020) showed that hydropower development is the main driver of riverbed incision in the VMD, being responsible for around 85 % of annual changes. As outlined in subchapter 4.1, this ongoing riverbed incision may trigger feedbacks (e.g., tidal amplification, increased salinity intrusion, increased import of marine sediments) that can severely alter an estuarine system. If all future dams on the river's mainstem and tributaries are constructed, monthly average flows during the dry season are projected to increase by up to 160 %, while wet season flows are projected to decrease by up to 24 % (Lauri et al., 2012). While the existing reservoirs on the Mekong River have the potential to trap around 40.2 Mt/yr of sediments annually, future sediment trapping could increase to around 97.6 Mt/yr if projected hydropower expansion is realized in all sub-basins (Kummu et al., 2010). Caused by the hydropower development, future sediment supply to the VMD might even decrease by up to 96 % (Kondolf et al., 2014; Manh et al., 2015), hence severely impacting a region that is already subject to re-treating coastlines (e.g., Anthony et al., 2015) and riverbank erosion (e.g., Jordan et al., 2019b). Assuming a decrease in sediment supply by 95 %, Jordan et al. (2020) also showed that hydropower dams will be the main driver of future erosion processes in the Tien River branch, followed by sand mining. As a result of the altered hydrological regime and sediment flux, there also will be less sediment-bound nutrients that are delivered to the river's floodplains, hence impacting agriculture and fisheries that provide food security to millions of people (Arias et al., 2014).

### 4.3 Climate change-induced alterations in hydrology

The hydrological response of rivers is mainly influenced by the spatial and temporal variability in precipitation and catchment characteristics. In meteorological terms, runoff is defined as the difference between precipitation and water loss, which is caused by evapotranspiration, water storage, and water consumption (Milliman and Farnsworth, 2011). In general, depending on the origin of the water, the hydrological regime of a river may be characterized as (i) glacial regime, (ii) nival regime, (iii) pluvial regime, or (iv) tropical regime (Zeiringer et al., 2018). At high altitudes, rivers mainly receive water from the melting of glaciers in summer (glacial regime). At lower elevations, seasonal peaks in spring are caused by snowmelt (nival regime), while floods caused by rainfall may occur at any time (pluvial regime). In tropical regions, the flow cycles are strongly linked to the dry and wet seasons (tropical regime). Several studies have quantified the annual freshwater fluxes of rivers to the global oceans between 29,485 and 44,290 km<sup>3</sup>/yr (e.g., Korzun et al., 1978; Vörösmarty et al., 2000; Oki et al., 2001). In addition, the world's rivers supply vast amounts of sediments to the coastal oceans annually. Multiple studies have quantified this annual sediment flux between around 16 to 19 Gt/yr (Milliman and Meade, 1983; Milliman and Farnsworth, 2011; Syvitski et al., 2005). Besides a river's hydrological

regime, the sediment erosion and subsequent transport in a river are mainly controlled by basin geometry, geology, vegetation cover, and anthropogenic activity (Milliman and Farnsworth, 2011). Hydro-morphodynamic processes, which involve the interactions between water and sediment in rivers, enable fluvial systems to absorb disturbances, such as climate change (Palmer et al., 2008).

Based on historical discharge data (1948 to 2004) for the world's largest rivers, statistically relevant changes could only be detected for about a third of the 200 investigated rivers (Dai et al., 2009). However, the assessment of observed trends may be challenging due to multiple drivers potentially being at play (Douville et al., 2021). Since there is medium confidence that global runoff increases with increasing temperatures (Douville et al., 2021), a future rise in freshwater fluxes to the coastal oceans is to be expected, concurrently also impacting the sediment supply (Best, 2019). According to Lehner et al. (2019), though, most regional runoff projections are associated with large uncertainties, which arise from how climate models partition precipitation into evapotranspiration and runoff as well as the sensitivity of this partitioning to global warming. Considering fluvial flood events, the AR6 suggests that there is medium confidence in projections at the global scale (Seneviratne et al., 2021). Multiple studies indicate that the frequency of extreme floods will increase in many river basins, with present-day 100-year floods occurring every 10 to 50 years in the future (e.g., Hirabayashi et al., 2013; Arnell and Gosling, 2016; Alfieri et al., 2017). As a result, a global warming scenario of 1.5 °C could expose twice as many people to river floods annually and lead to a significant increase in the yearly costs of flood related damage (+120 %) (Alfieri et al., 2017). Flood risks are projected to be particularly severe in Southeast Asia (see Figure 4.3), driven by socio-economic growth in addition to climate change (Winsemius et al., 2016). At the same time, extreme drought events are projected to occur more frequently in the future and increase in intensity (Seneviratne et al., 2021). Land irrigation may aggravate climate change-induced trends by depleting river discharges and increasing the vulnerability to droughts (Leng et al., 2015). Between 1980 and 2005, the global area of irrigated land increased by around 34 % (Siebert et al., 2015). Over roughly the same period (1981 to 2000), land irrigation (including extractions from reservoirs) led to a decrease in the annual global discharge by around 2.1 % (Biemans et al., 2011).

Focusing on the Yellow River, a recorded decrease in discharge since the 1950s can at least partly be attributed to climate change and a decreasing precipitation in the river's basin (Wang et al., 2017a). Additionally, around 30 % of the drastic decrease in the sediment load of the Yellow River since the 1950s is associated with climate change, while the remaining 70 % are caused by human activity (Wang et al., 2007). Considering future climate change-induced alterations in the hydrology of the Yellow River, some studies project an increase in discharge (e.g., Ji et al., 2021), while simulations by other authors indicate an opposing trend (e.g., Wang et al., 2017a). However, it is likely that regional

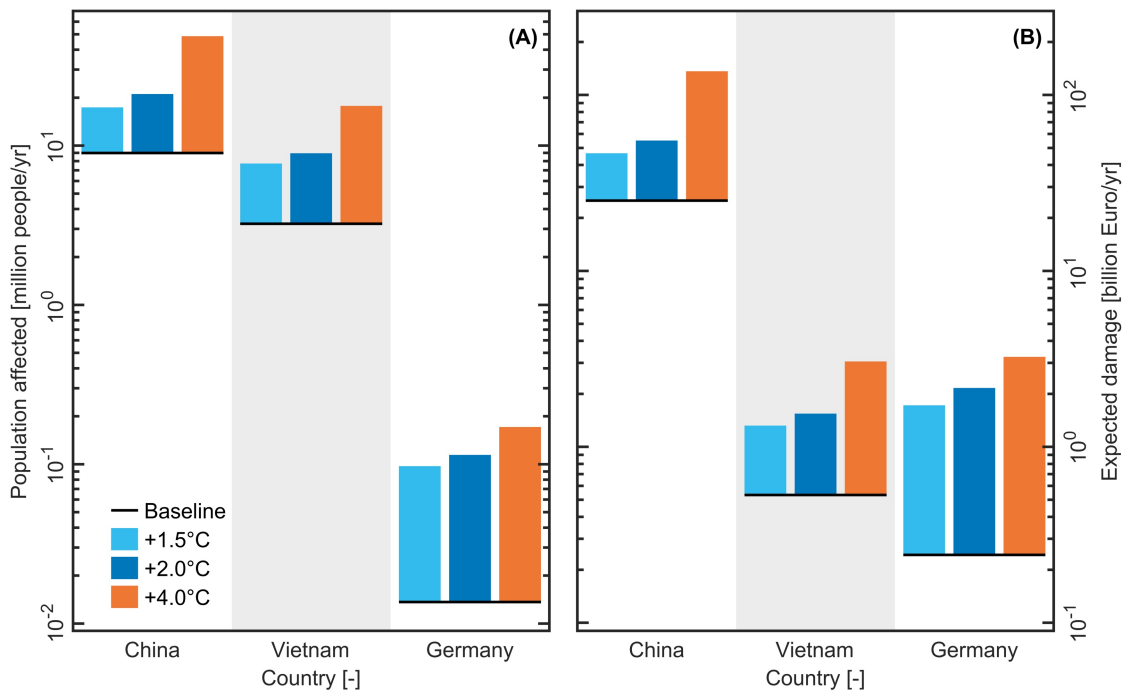


Figure 4.3: Projections for population affected and expected damage caused by river floods under different warming levels. (A) Projections for population affected by future river floods. (B) Projections for expected damage by future river floods. Based on data from Alfieri et al. (2017).

flood and drought events will aggravate in the future (Wang et al., 2017a). Considering a rise in temperature by 1.5 °C, for instance, the magnitude of 100-year flood events in the Yellow River may increase by 11 % (Huang et al., 2018).

Uncertainties, which are associated with future discharges under a warming climate, are also perfectly exemplified by the Mekong River, where the interaction of multiple processes makes it difficult to make reliable projections. According to Darby et al. (2016), around 63 % of the river's decline in suspended sediment load at Kratie over recent years (1981 to 2005) can be attributed to the eastwards shift in the tracks of cyclones. Furthermore, the river's water and sediment fluxes are significantly impacted by human interventions, such as sand mining (e.g., Jordan et al., 2019b; Hackney et al., 2020) (see subchapter 4.1) and the construction and operation of large hydropower dams (e.g., Konold et al., 2014; Räsänen et al., 2017) (see subchapter 4.2). While large uncertainties are associated with future precipitation in the Mekong River Basin, increased evapotranspiration and a shift to an earlier and less substantial snowmelt season are likely (Kingston et al., 2011). Even though global climate models (GCMs) might differ in the direction of monthly changes, river flow at Pakse (Laos) (see location in Figure 3.2B) is projected to increase from April to June while decreasing from July to August for a 2 °C global warming

(Kingston et al., 2011). Furthermore, by the end of the twenty-first century, the associated precipitation of tropical cyclones in the region is projected to increase by up to 53 %, while their tracks are expected to shift further eastwards (Redmond et al., 2015). Similar to the future discharge of the Mekong River, associated projections for the impact of climate change on the river's sediment transport also show high uncertainties. In comparison to the baseline period 2000 to 2010, changes in the annual sediment load at Kratie show a plausible range between -12 to +36 % for the future period 2050 to 2060 (Manh et al., 2015). However, the findings from a recent study also project that hydropower reservoirs will have a more substantial impact on the river's hydrology than climate change within the coming decades (Lauri et al., 2012). Using the upper bound of the future hydrograph at Kratie by Lauri et al. (2012) as input for a hydro-morphodynamic model, Jordan et al. (2020) also projected the morphological response of the Tien River branch to climate change. They showed that climate change will not amplify erosional trends in the Tien River, but rather lead to a local redistribution of sediments. Finally, Try et al. (2020) showed that the discharge of 100-year flood events in the Mekong River will increase by 33 % in the future (2051 to 2110), considering the Representative Concentration Pathway (RCP) 8.5 scenario.

Focusing on the German rivers Elbe, Weser, and Ems, historical trends since 1945 indicate increasing seasonal variability in discharge, i.e., increasing winter maxima and decreasing spring/summer minima, with climate change being the main driver of observed changes (Bormann, 2010). Using multi-model ensembles for assessing climate change-induced future runoff, Hattermann et al. (2015) were not able to identify specific trends for the Elbe, Weser, and Ems. In contrast, a continental scale study by Donnelly et al. (2017) projected a moderate increase in runoff for northern Germany while applying different levels of climate warming (+1.5° to +3.0 °C). They showed that runoff will mainly rise in winter and spring caused by increasing precipitation and decreasing evapotranspiration. Considering flood trends, Bormann et al. (2011) showed that maximum annual discharges in the Weser and Ems River exhibit a decreasing trend in recent decades, while non-uniform trends were found along the Elbe River. In relation to the period 1971 to 2000, annual flood discharges in the Elbe may rise by more than 25 % by the mid of the century (2031 to 2060), while increases between 10 to 25 % are to be expected in the Weser and Ems (85th percentile of RCP8.5) (Fritsch et al., 2021). In the future, most German rivers will also likely experience more extreme 50-year floods, while present-day 50-year droughts will become more frequent (Huang et al., 2015). Consequently, it is expected that flood-related damage in Germany will increase as a result of global warming (Hattermann et al., 2016). However, as outlined before, one must be careful with projections of future river hydrology, since large uncertainties are inherent to most studies.

## 4.4 Sea-level rise

When dealing with SLR, one must differentiate between relative sea-level rise (RSLR) and global mean sea-level rise (GMSLR). While GMSLR is used to assess global trends, RSLR is of great importance to coastal management and planning in order to be able to adapt to local-scale impacts (Huthnance et al., 2016). RSLR refers to changes in local mean sea-level relative to the local solid surface, hence being the difference between the geocentric sea-level change and vertical land movement (Gregory et al., 2019). Geocentric sea-level, which oftentimes is also referred to as absolute mean sea-level (AMSL) (Wahl et al., 2013), describes changes in local mean sea-level with respect to a reference ellipsoid, while vertical land movement accounts for variations in the height of the seafloor or the land surface (Gregory et al., 2019). GMSLR, which is defined as the increase in ocean volume divided by the ocean surface area, is essentially the global mean of RSLR (Gregory et al., 2019). GMSLR also is the sum of global mean thermosteric SLR and barystatic SLR (Gregory et al., 2019). Global mean thermosteric SLR refers to changes in global ocean volume that are caused by thermal expansion, i.e., the increase in seawater density with increasing temperature (Gregory et al., 2019). Barystatic SLR refers to changes in global ocean volume that are associated with the addition of water mass, which may originate from land area or the atmosphere, or the removal of water mass to be stored elsewhere (Gregory et al., 2019). According to the World Climate Research Programme (WCRP), thermal expansion has the largest contribution to GMSLR (42 %) from 1993 to present, followed by mass changes of glaciers (21 %) and contributions from the Greenland (15 %) and Antarctic ice-sheets (8 %) (WCRP Global Sea Level Budget Group, 2018). Since the early 1990s, satellite altimetry is used to record geocentric sea-level (Huthnance et al., 2016). In contrast, records of tide gauges, which directly measure RSLR, might date back several hundred years (Wahl et al., 2013). By removal of non-climatic contributions of SLR, such as glacial isostatic adjustment (i.e., movement of land once burdened by ice sheets) or human-driven subsidence (e.g., due to groundwater extraction), tide gauge records might also be used to analyze changes in AMSL (Huthnance et al., 2016). In order to gather information about sea-level changes at longer time scales, geological or archaeological proxies are needed (Rovere et al., 2016).

According to the AR6, the rate of GMSLR was of the order of 1.35 mm/yr for the period 1901 to 1990 and increased to 3.69 mm/yr during the past decade (2006 to 2018) (Fox-Kemper et al., 2021), thus updating previous trends from the IPCC Special Report on the Ocean and Cryosphere in a Changing Climate (SROCC) (Oppenheimer et al., 2019). The AR6 also includes recent findings from Dangendorf et al. (2017), who found smaller trends of GMSLR before 1990 than earlier estimates, hence also indicating that the overall acceleration of GMSLR in recent decades is larger than previously assumed. It is very likely that anthropogenic forcing is the dominant cause of the accelerated trend in GMSLR



since the 1970s (Bindoff et al., 2013). Since sea-level does not rise uniformly, regional-scale trends might also surpass global-scale trends (Fox-Kemper et al., 2021). Depending on the Shared Socioeconomic Pathway (SSP) and RCP scenario, the future GMSLR will likely be between 0.38 m (median of SSP1-1.9) and 0.77 m (median of SSP5-8.5) by the year 2100 in relation to 1995 to 2014 (Fox-Kemper et al., 2021) (see Figure 4.4). Regionally, future changes might differ from global trends by around  $\pm 20\%$  caused by ocean dynamics, climate variability, geodynamics (e.g., changes in Earth's gravity), and vertical land movements (Fox-Kemper et al., 2021). However, the outlined AR6 projections do not consider processes that cannot be projected skillfully with at least medium confidence (Fox-Kemper et al., 2021). Hence, higher projections also cannot be ruled out, when uncertain dynamics of the Greenland and Antarctic ice sheets are included (e.g., Kopp et al., 2017). Following the SSP5-8.5 scenario and also considering the potential ice sheet contributions, GMSLR by the year 2100 could be as high as 2.3 m (95th percentile) (Fox-Kemper et al., 2021). In the event of such a high-end projection, substantially more people may be exposed to rising sea-level than previously assumed, as indicated by recent high-accuracy digital elevation models (DEMs) (Kulp and Strauss, 2019; Minderhoud et al., 2019). Presently, around 110 million people inhabit land that is below high tide lines (Kulp and Strauss, 2019). Following a high-end projection by Kopp et al. (2017), the median estimate for people that may be exposed in 2100 is 340 million, thus increasing the global population permanently living below high tide lines by 230 million people (Kulp and Strauss, 2019). However, it must be noted that neither coastal defense strategies, nor socio-economic developments were considered by Kulp and Strauss (2019). Even when neglecting uncertain ice dynamics, the GMSLR will be between 1.7 to 6.8 m in 2300 if no effective mitigation measures are implemented to reduce GHG emissions (SSP5-8.5) (Fox-Kemper et al., 2021), hence impacting global populations even more.

Non-climatic anthropogenic drivers, such as socio-economic growth and human-induced land subsidence (e.g., due to groundwater exploitation), make low-lying coastal deltas particularly vulnerable to the threat of rising sea levels (Oppenheimer et al., 2019). For a total of 46 global deltas, Tessler et al. (2018) showed that the average rate of contemporary RSLR is of the order of 6.8 mm/yr, hence substantially surpassing recent trends of GMSLR. In the future, RSLR might increase by an additional 1 mm/yr in deltas that are impacted by the construction of new dams, while a further increase of around 2 mm/yr can be expected in deltas with infrastructure (e.g., flood protection or channelization) that prevents the inundation of floodplains (Tessler et al., 2018). Concentrating on the YRD, the recent rate of RSLR is of the order of 8 to 23 mm/yr (Syvitski et al., 2009). At local aquaculture facilities, the rate of RSLR is even an order of magnitude greater due to local subsidence that is as high as 250 mm/yr, which is likely caused by groundwater extraction (Higgins et al., 2013). Furthermore, the inconstant sediment discharge of the Yellow River (Wu et al., 2017) makes the YRD prone to coastal erosion resulting from future RSLR.

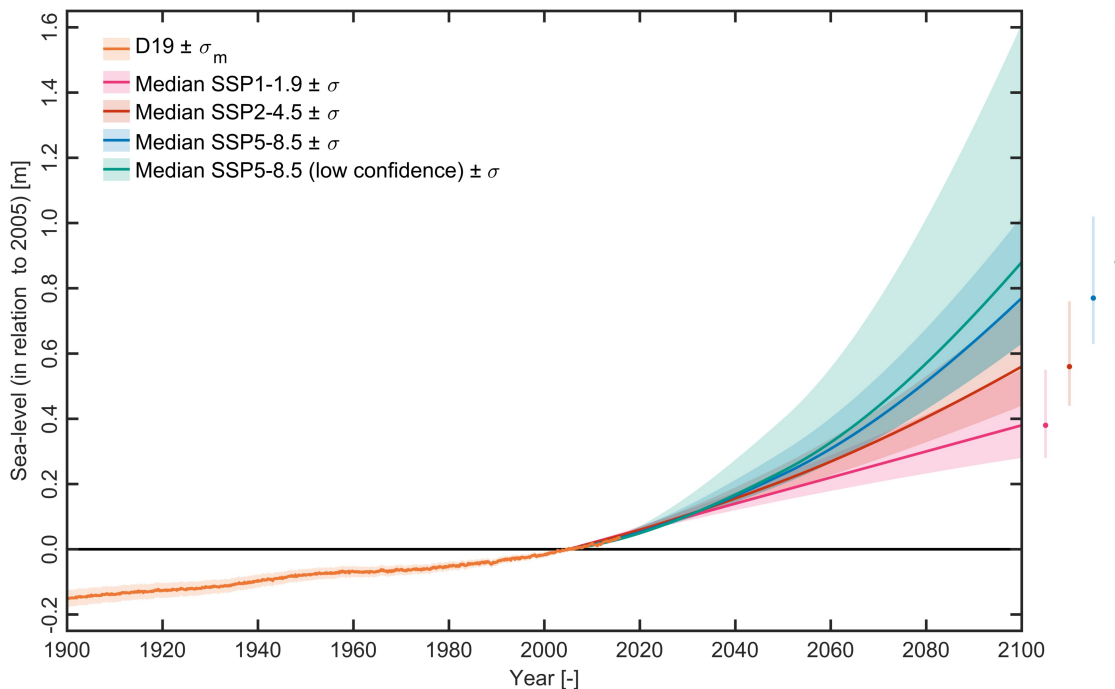


Figure 4.4: Twentieth century GMSLR and AR6 projections for future GMSLR.  $\sigma_m$  and  $\sigma$  are the standard error of the mean and the standard deviation, respectively. Twentieth century GMSLR, which is denoted as D19, is based on reconstruction data by Dangendorf et al. (2019), while shown projections are based on data by Fox-Kemper et al. (2021).

For the VMD, the present-day RSLR is around 6 mm/yr (Syvitski et al., 2009), since local rates of floodplain sedimentation (0.3 to 1.8 mm/yr) (Manh et al., 2014) are not able to counterbalance the impacts of land subsidence (locally up to 40 mm/yr) (Erban et al., 2014; Minderhoud et al., 2017) and GMSLR. In the case of a future RSLR of 1 m, 75 % of the delta area (home to around 12.3 million people) will fall below the sea-level due to the extremely low mean delta elevation (Minderhoud et al., 2019) (see subchapter 3.2). Rising sea-level will also aggravate salinity intrusion in large parts of the VMD, particularly during the dry season (Smajgl et al., 2015). The 4 g/L isohaline may intrude further upstream by 20 and 27 km in the Tien River and Hau River branches, respectively, if a future RSLR of 1 m is assumed (Toan, 2014). However, as shown by Jordan et al. (2020), SLR only has minimal impacts on future morphodynamic processes in the Tien River branch.

Similar to global trends, recent regional acceleration was also observed in tide gauge records along the coasts of the North Sea (Wahl et al., 2013). As shown by Wahl et al. (2013) for AMSL rise in the North Sea region from 1993 to 2009, the regional rate of  $4.0 \pm 1.5$  mm/yr is higher than the global rate of  $2.8 \pm 0.5$  mm/yr. Focusing on the German Bight, recent RSLR trends also highlight regional differences between the eastern and

southern German Bight (Wahl et al., 2011). Based on the analysis of tide gauge records for the period from 1971 to 2008, the rate of RSLR for the eastern German Bight was  $4.1 \pm 0.8$  mm/yr, while  $3.2 \pm 0.7$  mm/yr were observed in the southern German Bight (Wahl et al., 2011). Detailed regional projections for future sea-level changes in the North Sea exist for the United Kingdom (Lowe et al., 2009), the Netherlands (Katsman et al., 2011), and Norway (Simpson et al., 2012), but are missing for other countries. However, some global and regional studies also include detailed projections for locations along the coasts of the German Bight. Kopp et al. (2014) projected a RSLR of 0.81 m (median of RCP8.5) for Cuxhaven over the period 2000 to 2100. Similarly, the median projection of the RCP8.5 scenario by Grinsted et al. (2015) yields a RSLR of 0.80 m (2000 to 2100) for Hamburg. As shown by several studies concentrating on the North Sea, RSLR also has feedbacks on the regional hydro- and morphodynamic processes. Interactions between RSLR and tides (e.g., Pickering et al., 2012; Jordan et al., 2021), storm surges (Arns et al., 2015), waves (Arns et al., 2017), and coastal morphodynamics (e.g., Dissanayake et al., 2012; Becherer et al., 2018) are well-documented. The potential responses of tides and coastal morphodynamics to RSLR are summarized in more detail in subchapters 4.4.1 and 4.4.2, whereas the responses of storm surges and waves to RSLR are not addressed in this thesis.

Furthermore, it must be noted that hereinafter the more general term SLR is mostly used. Even though it is important to understand the difference between GMSLR and RSLR, these terms are only used in this thesis, where a clear distinction is suitable. For example, some regional studies on secondary impacts of rising sea-level might assume GMSLR for simplicity or due to a lack of up-to-date regional projections for RSLR.

#### 4.4.1 Response of tides to rising sea-level

Driven by astronomical variations in the orbits and relative positions of the Earth, Moon, and Sun, tides are one of the most persistent and dominant forces that shape our planet (Haigh et al., 2020). Tides are a main driver of hydro- and morphodynamic coastal processes while also impacting navigation to and from ports and the tidal renewable energy potential. The interplay between tidal currents and river discharge also drives unique estuarine processes, such as the formation of the estuarine circulation and the ETM (e.g., Burchard and Hetland, 2010; Burchard et al., 2018). In theory, the tidal water level  $\eta(t)$  at a location may be expressed as the sum of a finite number  $N$  of harmonic terms:

$$\eta(t) = A_0 + \sum_{n=1}^N A_n \cos(\omega_n t - \theta_n) \quad (4.4.1)$$

where  $A_0$  is the mean water level,  $A_n$  is the amplitude of a constituent  $n$ ,  $\omega_n$  is its angular speed, and  $\theta_n$  is its phase lag on the Equilibrium Tide at Greenwich (e.g., Pugh,

1987; Malcherek, 2010). The dominating component at many locations across the globe is the principal lunar semi-diurnal tide, which is abbreviated as M2. Other important astronomical constituents are the semi-diurnal constituent S2 and the diurnal constituents O1 and K1. The combination of the M2 and S2 constituents, for example, describes the spring-neap cycle, while diurnal inequalities in coastal water levels are formed by a combination of semi-diurnal and diurnal constituents (Malcherek, 2010). Non-linear effects due to the propagation of the tidal wave from the deep ocean into shallower waters also lead to the formation of non-astronomical constituents (Bosboom and Stive, 2021), which are called overtides (having periods that are integer fractions of an astronomical constituent) or compound tides (linear combinations of multiple astronomical constituents). By analyzing the phase differences between the M2 constituent and its overtide M4, the tidal asymmetry in an estuary may be analyzed (Friedrichs and Aubrey, 1988). Accordingly, estuaries may be classified as ebb-dominant if the indicator  $\sin(2\theta_{M2} - \theta_{M4})$  yields a negative value, while a positive value indicates flood dominance.

Studies have shown that tidal dynamics may significantly respond to rising sea-level, potentially also triggering feedbacks on associated coastal and estuarine processes (e.g., Wachler et al., 2020; Jordan et al., 2021). In general, the response of tides to SLR may be explained by two different mechanisms: (i) resonance and (ii) spatial re-organization of amphidromic points (Haigh et al., 2020). The first mechanism describes that the resonance frequency of an ocean basin or shelf sea can move closer to the frequency of the tidal forcing as the sea-level rises, resulting in an increase in tidal amplitudes (e.g., Green, 2010). The resonance frequency may also move away from the forcing frequency, hence leading to a reduction in tidal amplitudes. The second mechanism is associated with the theories of Taylor (1922), Hendershott and Speranza (1971), and Rienecker and Teubner (1980), which describe the migration of amphidromic points in a semi-enclosed basin in response to changes in energy dissipation (e.g., due to altered bottom friction). As a result of this spatial re-organization of amphidromes, tidal amplitudes may also change. Within estuaries, SLR will normally lead to an amplification of the tidal range, except for short estuaries with small tidal range at the mouth (Khojasteh et al., 2021). Besides SLR, other drivers, such as stratification or human activity (e.g., channel deepening or coastal protection strategies), may also alter tidal properties (Haigh et al., 2020). For a detailed list of potential drivers of tidal changes, the reader is referred to Haigh et al. (2020).

In general, alterations in tidal dynamics may be expressed in terms of tidal constituents or in terms of characteristic parameters, such as MHW, mean low water (MLW), or mean tidal range (MTR). Analyzing secular trends in tide gauge data, Mawdsley et al. (2015) found statistically significant changes in MTR for many locations around the world, but no correlation between MTR and SLR. However, the identification of drivers for observed trends can be challenging, since multiple small- and large-scale drivers may occur simultaneously (Haigh et al., 2020). In contrast to Mawdsley et al. (2015), some regional-scale

studies (e.g., Woodworth et al., 1991; Ray and Talke, 2019) were able to identify a relationship between observed trends in MTR and SLR. Concentrating on secular trends of the semi-diurnal constituent M2, several numerical studies also linked observed changes to rising sea-level (Müller et al., 2011; Schindelegger et al., 2018). Concentrating on the VMD, recent findings indicate that M2 amplitudes at the mouth are increasing by up to 2.0 mm/yr (Nhan, 2016). Also, observations over the past decade highlight that M2 amplitude changes in the distributary channels are an order of magnitude larger, with rates being as high as 2.0 cm/yr (Eslami et al., 2019). While offshore changes in M2 amplitudes are likely associated with SLR, observed trends in the estuarine distributaries are rather linked to ongoing channel incision (Nhan, 2016; Eslami et al., 2019). Focusing on the North Sea region, trends in MTR in the German Bight were documented as early as the 1970s. Analysis of the records of tide gauges showed a rise in MTR by around 3.5 mm/yr between 1934 to 1983 (Jensen, 1984), which was mainly caused by an increase in mean tidal high waters. In a more recent study concentrating on regional changes in MTR by Jänicke et al. (2021), a trend of  $-2.3$  mm/yr was observed at tide gauges in the United Kingdom from 1958 to 2014, while tidal range increased by up to 7.0 mm/yr in the German Bight during the same period. According to Jänicke et al. (2021), the documented changes along the British coast are primarily driven by an external signal from the North Atlantic of unknown origin, while the observed trend in the German Bight is mainly associated with changes of the vertical density structure of the North Sea.

Considering the response of tidal dynamics to future SLR, numerous numerical studies have projected the impacts on a global (e.g., Green, 2010; Pickering et al., 2017), regional (e.g., Pickering et al., 2012; Jordan et al., 2021), and local scale (Rasquin et al., 2020; Wachler et al., 2020) in recent years. Applying a global tide model, Pickering et al. (2017) showed that the response of tides is normally an order of magnitude higher in shelf seas than in the deep oceans. Assuming fixed coastlines and a uniform SLR of 2 m, Pickering et al. (2017) also demonstrated that the response of the dominant semi-diurnal constituent M2 may vary considerably between the 136 largest coastal cities. For this scenario, the M2 amplitude changes varied between  $-31$  and  $+35$  cm. Pickering et al. (2017) also highlighted that M2 amplitudes at approx. 10 % of the considered cities may change by more than  $\pm 10$  % of the imposed SLR.

Projections with a regional focus exist for many shelf seas, including the Bohai Sea. Since the YRD is located in the southwestern Bohai Sea, changes in the regional tidal dynamics will undoubtedly also have feedbacks on the dynamics of the Yellow River Estuary. Assuming fixed coastlines, Pelling et al. (2013b) showed that M2 amplitude changes in the Bohai Sea will be of the order of around  $-10$  and  $+10$  cm for a uniform SLR of 2 m. Furthermore, it was shown that recent coastline changes, resulting from morphological changes in the YRD and land reclamation projects, have made the regional tides more sensitive to future SLR.

For the VMD, regional studies projecting the response of future tidal dynamics to SLR are scarce. However, Nhan (2016) shows that the maximum tidal amplitudes will likely increase by around 5 and 25 cm on the west coast and east coast of the delta, respectively, when assuming a SLR of 0.75 m by the year 2100.

A particularly high number of regional projections exist for the northwest European shelf seas (NWES) or parts thereof. According to these studies, M2 amplitude changes in the North Sea may vary between  $-20$  and  $+30$  cm for a SLR of 2 m (Pickering et al., 2012; Ward et al., 2012; Pelling et al., 2013a; Jordan et al., 2021). Even though spatial patterns of M2 amplitude changes mostly agree between the applied numerical models, the results show significantly different responses of the tidal signal to SLR in the southeastern North Sea, where the German Bight is located. Early studies argued that these differences are caused by the way in which SLR is implemented in a model (Pelling et al., 2013a). While some models use the assumption of a fixed coastline (e.g., Pickering et al., 2012; Jordan et al., 2021), other models assume that coastlines will retreat in the future (Ward et al., 2012; Pelling et al., 2013a). However, a more recent explanation by Rasquin et al. (2020) pointed out that shallow areas of high energy dissipation, such as the Wadden Sea, are not well-resolved in most of the outlined models. Generally, the grid resolution of the pre-2020 models is insufficient to represent characteristic bathymetric features (e.g., intertidal flats, tidal inlets, and channels), thus potentially leading to imprecise results. In addition, several studies also highlight that potential bathymetric changes in the Wadden Sea need to be included in regional models in order to be able to make realistic projections of future tidal dynamics in the North Sea (Wachler et al., 2020; Jordan et al., 2021). By considering such morphological changes in the Wadden Sea while also applying locally-refined grid resolution, the study by Jordan et al. (2021) addresses the shortcomings of previous studies for the NWES. Accordingly, the results by Jordan et al. (2021) represent the most robust projection for M2 amplitude changes in the North Sea region to date. For some coastal areas, such as the North Frisian Wadden Sea, it is also shown that considerable uncertainties are associated with the response of the local tidal signal to SLR. Depending on the future morphological evolution of the Wadden Sea and the rate of SLR, the local amplitudes of the M2 amplitudes may rise or fall. Another key finding by Jordan et al. (2021), which is supported by a previous study from Wachler et al. (2020), indicates that the estuaries of the German rivers Elbe, Weser, and Ems will become more flood-dominant (or less ebb-dominant) if intertidal flats in the Wadden Sea are unable to keep up with SLR.

#### 4.4.2 Response of Wadden Sea tidal basins to rising sea-level

According to Dalrymple et al. (1992), intertidal flats are common in sediment-rich environments, where the river influence is small and tidal range is large in relation to the

significant wave height. A detailed review of available definitions is given by Amos (1995). Following a suggestion by Friedrichs (2011), intertidal flats may generally be defined by:

*"[Intertidal flats are] low bed slope environments, consisting of sediments in the absence of abundant tidal marsh or mangroves, and which are exposed subaerially between lowest and highest astronomical tide."*

Globally, the area of intertidal flats is around 128,000 km<sup>2</sup>, with most of the intertidal flats being located in Asia, followed by North and South America (Murray et al., 2019). During the last three decades, however, intertidal flats were lost at many locations due to reduced sediment supply from major rivers, increased coastal erosion, and SLR, as indicated by analysis of satellite imagery (Murray et al., 2019). Even though intertidal flats also exist in the YRD (Peying et al., 1999) or the VMD (Nittrouer et al., 2017), their spatial extent is small in relation to the Wadden Sea, which is the largest intertidal flat system in the world (CWSS, 2021b). Accordingly, many studies have focused on the historical and future evolution of tidal basins in the Wadden Sea, while comparable information for the Bohai Sea or the coasts of the VMD is scarce.

In general, sediment supply to the Wadden Sea tidal basins may be provided by ebb-tidal deltas, shorelines of barrier islands and the adjacent coast, and the seabed further offshore (Wang et al., 2018). Inside the tidal basins, sediment is also internally redistributed from the inlets/channels to the intertidal flats (Wang et al., 2018). Driving mechanisms that can lead to the import of sediment into the Wadden Sea are numerous. For instance, the sediment import may be driven by two processes called scour and settling lag (Van Straaten and Kuenen, 1957; Postma, 1961). The scour lag is caused by the difference between the velocity that is needed to erode a sediment particle and the velocity, which is necessary to keep the particle in suspension. In contrast, the settling lag describes the time lag between the moment a sediment particle in suspension starts sinking and the moment the particle touches the bed. More recently, density-driven flows, which are similar to the well-known estuarine circulation, were identified as a mechanism that may contribute to the accumulation of sediments in the Wadden Sea (Burchard et al., 2008; Flöser et al., 2011). These density-driven flows lead to a residual transport that is directed seaward in the higher part of water column and directed landward near the bed. In contrast, Stanev et al. (2007) suggested that a tidally-induced Stokes drift leads to a landward-directed residual transport near the surface, while the hypsometry (i.e., topographical characteristic of a tidal basin) is responsible for a seaward motion in the lower layer. In addition, Herrling and Winter (2015) argued that the effect of tide- and wind-driven residual fluxes on the water exchange between interconnected tidal basins, as well as between the North Sea and the Wadden Sea, also must be considered. Waves also play an important role in the sediment import into a tidal basin and the internal redistribution of sediments (e.g., Herrling and Winter, 2014; Hofstede, 2015). Finally, tidal asymmetry,

which is associated with the deformation of the tidal wave in shallow waters, might also lead to a net import of sediment into the Wadden Sea, even when there are no residual water fluxes through the tidal inlets (Friedrichs and Aubrey, 1988).

Generally, tidal basins strive to continuously maintain an equilibrium between their forcing conditions and their morphology (Wang et al., 2018). If the sea-level rises, the system will be permanently in a state that deviates from the equilibrium, and hence sediment import is induced in order to restore the equilibrium state (Van Goor et al., 2003). As long as the rate of SLR is below a critical limit, sediment import will be sufficient and the new dynamic equilibrium can be reached, while the system will eventually drown if the actual rate of SLR surpasses the critical limit (Van Goor et al., 2003). Even though tidal basins will strive to match the critical limit of SLR, in theory, the sediment import is limited by following factors: (i) accommodation space, (ii) sediment supply, and (iii) sediment transport capacity (Wang et al., 2018). A system is called accommodation-limited if the net accretion is only driven by the sediment demand in the basin. In the case that the sediment volume available for transport is insufficient to meet the demand, a system is called supply-limited. If the available sediment volume is sufficient, but the sediment transport capacity is too small to satisfy the demand, a system is called transport-limited. As indicated by numerical models (van der Wegen, 2013; Hofstede et al., 2018), tidal basins with relatively large tidal range may exhibit a higher critical limit, thus being more resilient against SLR than shallow basins with limited tidal forcing.

Recent observations for the Dutch Wadden Sea show that local tidal basins accumulated sediment at an average rate of around 4.0 mm/yr over the period 1935 to 2005 (Elias et al., 2012). However, this trend most likely is a response to the closure of the Zuiderzee rather than an adaptation to SLR (Elias et al., 2012). Analyzing DEMs from the period 1998 to 2016 for the German Wadden Sea, Benninghoff and Winter (2019) showed that local intertidal flats presently accumulate sediments at an average rate of 7.9 mm/yr, while the mean erosion of tidal channels is of the order of  $-20.0$  mm/yr. Hence, the accumulation of sediments in the local intertidal flats surpasses recent rates of observed SLR. As shown by Hofstede (2002), this internal sediment redistribution from the inlets/channels to the intertidal flats may indicate a response to recent SLR. Using an empirical model, Hofstede (2002) demonstrated that SLR and the associated increase in tidal prism will lead to enhanced erosion in the tidal channels and the subsequent deposition of eroded material on the intertidal flats during flood, driven by longer periods of tidal inundation.

Besides the analysis of historical trends, recent research has also shifted toward the response of Wadden Sea tidal basins to future rates of SLR. Focusing on a long-term morphological simulation (1990 to 2100) of the Ameland inlet/basin in the Dutch Wadden Sea, Dissanayake et al. (2012) demonstrated that the local intertidal flats will be stable under a low SLR of 0.2 m, while they will drown or may even completely disappear under a



SLR of 0.7 m. Since mud fractions were not considered, it has been argued that the numerical model yielded unrealistically low sediment deposition (Wang and van der Spek, 2015). Considering cohesive sediments in their process-based models, however, similar results were also shown by Becherer et al. (2018) and Hofstede et al. (2018) for selected tidal basins in the German Wadden Sea. Becherer et al. (2018) highlighted that the morphodynamic response of the Lister Tief tidal basin to the quickly changing hydrodynamic forcing, which is associated with future SLR, will not be fast enough to keep the system in dynamic equilibrium. Assuming a SLR of 1.13 m (2010 to 2100) and an increase in tidal range by up to 15 cm, it was shown that average sediment accumulation of just 6 cm in the back-barrier basin will not be able to compensate SLR, and hence intertidal flats will shrink by around 50 % until 2100. According to Becherer et al. (2018), even a more moderate SLR scenario (0.47 m) will lead to decreases in the area and volume of intertidal flats in the Lister Tief tidal basin after 2050. Hofstede et al. (2018) also showed that individual tidal basins in the North Frisian Wadden Sea may differ in their response to SLR. It was highlighted that the area and height of intertidal flats in the Lister Tief tidal basin is likely to decrease for a SLR of 6.0 to 7.0 mm/yr, whereas it would take more than a century for the Meldorf Bight tidal basin to disappear even for a SLR as high as 17 mm/yr. Similar results were also shown by Wang et al. (2018) for the Dutch Wadden Sea by application of a semi-empirical model. Following the RCP8.5 scenario, Wang et al. (2018) demonstrated that the critical limit for drowning will be surpassed for the tidal basins of Texel, Vlie, and Ameland by the year 2100, while the critical limit will not be exceeded by other tidal basins in the Dutch Wadden Sea until after 2100.

#### **Summary of chapter 4:**

- **Sand mining/dredging**

With an extraction rate of around 25 Gt/yr, gravel and sand are the most extracted materials in the world. However, these aggregates are extracted at a rate far exceeding the annual sediment supply by the world's rivers. According to projections, future extraction rates will further rise, almost doubling by the year 2060. Due to this increasing demand for sand, the focus has gradually shifted from terrestrial to riverine and marine sources. For the construction industry, riverine aggregates are usually preferred over marine aggregates due to easier access, low processing costs, and their high quality. Nevertheless, due to a lack of regulations, sand is extracted unsustainably or even illegally from many rivers in underdeveloped or developing countries. In contrast to most river basins, sand mining in the Mekong River is relatively well-documented. However, newest estimates indicate that previously reported volumes severely underestimated the actual sand extraction rates

- **Sand mining/dredging (continued)**

in the Mekong River. Since the supply of sand ( $6.2 \pm 2.0$  Mt/yr) is significantly smaller than the extracted amount of sand ( $\approx 134$  Mt/yr), negative impacts are to be expected. In general, the deepening of estuarine channels can cause a tidal amplification that may become so large that a tipping point is passed. As a result, a positive feedback loop might be established that ultimately turns an estuary into a hyper-turbid system, as exemplified by the Ems Estuary. Besides impacts on the hydrology, morphology, and sediment transport, sand mining from riverine sources may also impact biodiversity, water tables, and infrastructure.

- **Damming**

Socio-economic growth, climate change, and increasing energy demand have led to a recent boom in hydropower development, particularly in underdeveloped and developing countries. The benefits of large hydropower projects, however, are oftentimes accompanied by severe negative impacts on local communities and the environment. Generally, impacts may vary depending on the locations of dams in a river basin, their designs, and their operations. Presently, around 48% of global river volume is at least moderately fragmented or regulated by dams, while 4 to 5 Gt/yr of sediment are trapped annually in reservoirs. Examples from the Yellow River and Mekong River show how flows and sediment supply were severely altered by hydropower development in recent decades. Besides impacting water and sediment fluxes, large dams might lead to changes in river and coastal morphology, a loss of biodiversity, changes in food security, and the displacement of people. Due to different interests in river basins that are shared by numerous countries, transboundary conflicts may also arise from hydropower development. Globally, the future expansion of hydropower is projected to dramatically decrease the number of free-flowing large river systems, while significantly less sediment will be discharged into the coastal oceans. Similar to the Yellow River, the Mekong River may turn from a monsoon-driven regime to a heavily regulated system if hydropower expansion is realized in all sub-basins. As a result, the low-lying VMD could become even more vulnerable to erosion processes than today.

- **Climate change-induced alterations in hydrology**

A river's ability to adjust to climate change may substantially be limited by human-induced interventions, such as urbanization or dams. Future projections indicate that global freshwater and sediment fluxes will be altered under a warming climate, even though large uncertainties are inherent to many studies. Under a  $1.5^\circ\text{C}$  global warming, twice as many people as today will likely be exposed to river floods annually. For the same scenario, the yearly costs of damage are expected to increase by around 120%. Since the response of discharge to climate change is not

- **Climate change-induced alterations in hydrology (continued)**

simply a function of precipitation, impacts need to be investigated on the scale of individual river basins. Observed changes in the water and sediment fluxes of the Yellow River can at least partly be attributed to climate change. Projections for the future hydrological regime of the Yellow River show large uncertainties. However, regional flood and drought events will likely aggravate in the future. For the Mekong River, water and sediment fluxes will be altered due to changes in the volumes and timing of the monsoon-driven hydrological regime. In the region, the future intensities and tracks of tropical cyclones will also impact the river's discharge and suspended sediment load. Human interventions, such as damming and sand mining, will also amplify climate change-related impacts. Furthermore, the magnitude of extreme floods is projected to increase. Focusing on northern Germany, local rivers are likely to experience a moderate increase in runoff under a warmer climate, particularly in spring and winter. By the mid of this century (2031 to 2060), the annual flood discharges in the Elbe, Weser, and Ems may also increase between 10 and more than 25%. In general, the frequency of extreme floods and droughts is expected to increase in river basins across Germany.

- **Sea-level rise**

Recent rates of around 3.7 mm/yr (2006 to 2018) indicate a recent acceleration in GMSLR. The majority of present GMSLR can be explained by thermal expansion, followed by the contributions from glaciers, the Greenland ice sheet, and the Antarctic ice sheet. As highlighted by examples from the YRD, the VMD, and the German Bight, trends for RSLR can even surpass global trends. Differences between regional and global trends are driven by ocean dynamics, climate variability, geodynamics, and vertical land movements. Depending on which SSP and RCP scenario is followed, projections for future GMSLR by the year 2100 are between 0.38 and 0.77 m (in relation to 1995 to 2014). However, due to uncertainties in the dynamics of the Greenland and Antarctic ice sheets, projections with significantly higher GMSLR cannot be ruled out. For the majority of coastal locations, projections of RSLR will be within  $\pm 20\%$  of the projected GMSLR. Existing projections of RSLR for the German Bight are largely in agreement with global trends. Generally, RSLR may have severe consequences for coastal areas, e.g., flooding, coastal erosion, and salinity intrusion. Low-lying deltas, such as the YRD and VMD, are particularly vulnerable to coastal hazards that are associated with SLR.

- **Response of tides to rising sea-level**

Tides are one of the main drivers of hydro- and morphodynamic processes in coastal waters and estuaries. Increasing water depths due to SLR can lead to the re-organization of amphidromes or might change the resonance properties of ocean basins or shelf seas. As a result, tidal properties may be altered in response to SLR. Globally, trends can be observed in M2 amplitudes or in the MTR of historical

- **Response of tides to rising sea-level (continued)**

water level records. While these trends can be attributed to SLR at some locations, other superimposed processes (e.g., stratification or ongoing incision of estuarine channels) were also identified as possible driving mechanisms elsewhere. Global projections show that the response of tides to future SLR will be an order of magnitude larger in shelf seas than in the deep oceans. Locally, M2 amplitude changes may even exceed  $\pm 10\%$  of the imposed SLR. Projections with a regional focus exist for many shelf seas and coastal areas, such as the Bohai Sea, the VMD, and the North Sea. As exemplified by the North Sea, regional projections may vary considerably between studies. Hence, in order to make reliable projections, a sufficiently fine resolution of bathymetric features is needed in shallow areas of high energy dissipation (e.g., the Wadden Sea). Additionally, potential bathymetric changes, which may be triggered by SLR, should also be included in projections of future tides. While addressing these issues, new results shows that the response of M2 amplitudes in the German Bight is highly dependent on the rate of cumulative vertical accretion in the Wadden Sea, in addition to the rate of SLR. Furthermore, tidal asymmetry in the estuaries of the rivers Elbe, Weser, and Ems will be significantly altered if intertidal flats are unable to keep up with rising sea-level.

- **Response of Wadden Sea tidal basins to rising sea-level**

The Wadden Sea, which is the largest intertidal flat system in the world, is of high ecological and socio-economic value. Main morphological elements of the Wadden Sea tidal inlet/basin systems are the ebb-tidal deltas, inlets/channels, and intertidal flats. Ebb-tidal deltas, shorelines of barrier islands and the adjacent coast, and the seabed further offshore may act as a source of sediment import into the basins. Numerous driving mechanisms (e.g., settling and scour lag, estuarine circulation) may contribute to the sediment import. In general, tidal basins strive to maintain an equilibrium between their morphology and the forcing conditions. If the sea-level rises, the sediment demand of tidal basins increases in order to restore the equilibrium. If SLR surpasses a critical rate, i.e., the sediment demand exceeds the sediment volume available for transport or the transport capacity is too small, the system will eventually drown. Presently, the rate of sediment accumulation in the Wadden Sea tidal basins surpasses the local rates of SLR. As indicated by several studies, though, the intertidal flats in the tidal basins may not be able to keep up with future acceleration in SLR. However, individual tidal basins may respond differently to SLR, with some being more resilient against SLR than others.

## 5 Applied methods

In this chapter, the principles of hydroacoustics in general - and the bottom mapping via MBES in particular - are briefly presented. During two field surveys in 2018, bottom mapping was used to create high-resolution bathymetric maps of a section of the Tien River branch in the VMD. Afterwards, these maps were used by Jordan et al. (2019b) to make estimations of local sand mining volumes and bed load transport rates. Furthermore, the maps were also used by Jordan et al. (2020) as input for the set-up of a hydro-morphodynamic model, which concentrates on the surveyed section of the Tien River. The software suite Delft3D, which was used by Jordan et al. (2020) and Jordan et al. (2021) to perform numerical simulations, is also briefly described in this chapter. Using a thoroughly calibrated and validated model of the Tien River, Jordan et al. (2020) projected the impacts of human activity and global changes on local morphodynamics. Furthermore, a calibrated and validated model of North Sea tidal dynamics was used by Jordan et al. (2021) to investigate the responses of regional tides to SLR and morphological changes in the Wadden Sea.

### 5.1 Bottom mapping

In contrast to physical or numerical modeling, in-situ measurements concentrate on the acquisition of data by application of instrumentation directly at a site of interest. A powerful method to measure in-situ data in coastal environments is hydroacoustics, which uses the propagation of sound in water. For example, acoustic Doppler current profilers (ADCPs) are used to measure current velocities. ADCPs use the Doppler effect, which is responsible for the frequency shift between a transmitted acoustic signal and the echoes from suspended particles in the water column. Since the suspended particles (e.g., sediments or air bubbles) are motionless in relation to the surrounding water, the motion of these particles is equivalent with the motion of the water. Furthermore, echosounders may be used to measure the water depths in a river or an ocean. Echosounders transmit an acoustic signal and listen to the echo that is reflected from the riverbed or seafloor. Knowing the speed of sound in water, the time between the transmitted signal and the return of the echo is used to calculate the water depth. Even though ADCPs were also used by Jordan et al. (2019b) to measure current velocities along selected transects in the Tien River branch, their study mainly focused on the analysis of high-resolution bathymetric datasets, which were measured via MBES. While the following paragraph gives a short description of bottom mapping by means of MBES, the reader may refer to Lurton (2002) or Bjørnø (2017) for more in-depth information.

Nowadays, MBESs are widely-used for bottom mapping of rivers, coastal regions, or even deep oceans. In general, a MBES can be considered an extension of the singlebeam

echosounder (SBES). As the name suggests, a SBES emits a single beam and makes one depth measurement with each acoustic pulse. Hence, they are only able to cover a small area of the bathymetry underneath a ship. While SBESs are in use since the 1920s, MBESs became publicly available in the late 1970s (e.g., Renard and Allenou, 1979; Farr, 1980). In contrast to the SBES, the MBES is able to make numerous simultaneous depth measurements by transmitting and receiving a fan of hundreds of beams perpendicular to the ship track. For example, the fan, which is commonly referred to as swath, can cover a width of 7.5 times the water depth when operating with a swath angle of  $150^\circ$  (Lurton, 2002). Furthermore, the angle of individual beams is narrow (usually  $< 1^\circ$ ) in comparison to the SBES. Accordingly, the MBES has the advantage of collecting higher-resolution data in a shorter amount of time. Typically, a MBES consists of a projector unit, a receiver unit, a linking unit, and a processor unit. In addition, several auxiliary sensors are needed to ensure high-quality measurements. A sound velocity probe (SVP) is needed to gain knowledge about the local sound velocity, which is needed to correctly process transmitted and received signals. Since ship movement cannot be avoided during a survey, a motion sensor is also needed as input in order to apply corrections for characteristic ship movements, such as pitch, roll, heave, and yaw. Finally, the use of a global navigation satellite system (GNSS) is imperative for accurately referencing the geographical position of a survey vessel. After a survey, bathymetric datasets need to be post-processed to remove erroneous data points. Afterwards, bathymetric maps may be used for further analysis. By applying median filtering, for example, smaller-scale features may be separated from the surrounding bathymetry (e.g., Wessel, 1998; Kim and Wessel, 2008). By using the bedform translation method (Nittrouer et al., 2008), it is also possible to estimate rates of bed load transport from a sequence of bathymetric maps if bedforms are present on a riverbed. For a surveyed section of the Tien River, the median filtering technique and the bedform translation method were applied by Jordan et al. (2019b) to estimate sand mining volumes and bed load transport rates. Accordingly, the reader is referred to Jordan et al. (2019b) or the references therein for more details on these methods.

## 5.2 Hydro-morphodynamic modeling

Even though they might have high computational demands, numerical models are powerful tools to analyze processes in coastal environments, such as flows, waves, sediment transport, and morphodynamics (Roelvink and Reniers, 2011). Typically, numerical modeling involves the selection of an appropriate set of equations to simulate the coastal processes that are studied and the application of suitable techniques in order to solve the equations. Boundary and initial conditions must also be provided as model input so that a solution can be found. In addition, numerical models should be verified, val-

idated, and calibrated. Following Roache (1997), the verification may be described as *"solving the equations right"*, while the validation implies *"solving the right equations"*. Commonly used numerical software tools are usually thoroughly tested, hence ensuring that the equations are correctly solved. To validate a numerical model, a user may show that a simulation is able to accurately reproduce observational data. During the calibration procedure, different sets of parameters are tested to find the optimum values that are in good agreement with observations. Generally, numerical models may be classified according to their spatial dimensions as (i) one-dimensional, (ii) two-dimensional, or (iii) three-dimensional. Usually, the complexity of the processes at hand determines whether a 1D-, 2D-, or 3D-model should be applied. A numerical model may also be classified on the basis of the characteristic spatial and temporal scales of a system/feature that is studied. Considering the morphological evolution of estuaries, for example, typical dimensions are tens to hundreds of kilometers, while significant changes normally take place within years to millennia (e.g., Bosboom and Stive, 2021). When dealing with such long-term morphodynamics, one must also differentiate between process-based and behavior-based models, as noted by Sutherland (2019). Behavior-based models are developed to simulate known behaviors while neglecting the underlying physics. In contrast, process-based models are mainly based on physical laws, even though they might apply the behavior-based approach to small-scale processes. Finally, models can be distinguished based on the numerical methods that are used to solve the model equations (e.g., finite differences, finite volumes, or finite elements).

In general, numerous numerical software suites (e.g., Delft3D, Telemac, Mike3, SCHISM) are suitable for the simulation of hydro- and morphodynamic processes in coastal environments (Roelvink and Reniers, 2011). Among available options, the widely-applied Delft3D software was selected by Jordan et al. (2020) and Jordan et al. (2021) to set up, calibrate, and validate their depth-averaged numerical models. The process-based model Delft3D can generally be described as a software suite for multi-dimensional computations for coastal, river, and estuarine areas. The software suite is composed of several modules, which interact with one another, enabling simulations of flows, waves, sediment transports, and morphological developments. The Delft3D-FLOW and Delft3D-MOR modules (see Figure 5.1), which are essential for hydro- and morphodynamic simulations, are briefly presented in the following paragraphs, as described in the manual (Deltares, 2020). For more details regarding the formulations and implementation of Delft3D, the reader is also referred to Lesser et al. (2004) and to the manual (Deltares, 2020).

Delft3D-FLOW is a hydrodynamic module, which can be used in depth-integrated (2D) or three-dimensional mode. The Delft3D-FLOW module calculates non-steady flows and salt/heat transport. Accordingly, the main set of equations consists of the horizontal equations of motion, the continuity equation, and transport equations for conservative constituents. Those equations are solved on a regular or a curvilinear grid while using

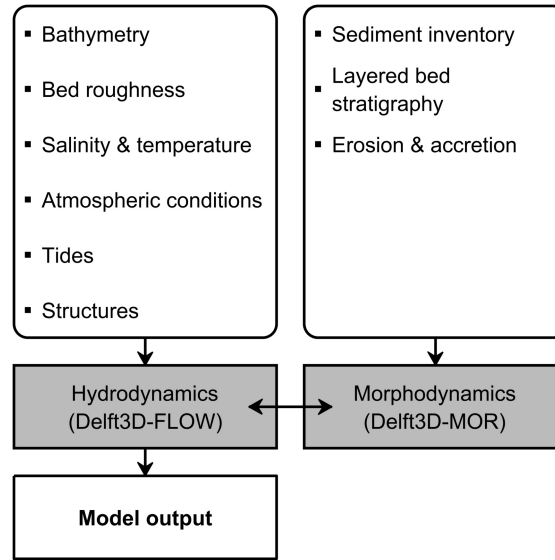


Figure 5.1: Conceptual flow chart of Delft3D-FLOW and Delft3D-MOR with related inputs and interactions. Adapted from Lojek (2019).

a finite-difference scheme. Considering supported coordinate systems, spherical coordinates are typically used for large area models (e.g., regional models), while cartesian coordinates may be applied to models with a smaller spatial scale. To ensure a stable solution, the Courant-Friedrichs-Lewy (CFL) number needs to be considered ( $CFL \leq 10$ ) (Deltares, 2020), which is defined by:

$$CFL = \frac{(\Delta t \sqrt{gH})}{\{\Delta x, \Delta y\}} \quad (5.2.1)$$

where  $\Delta t$  is the time step in seconds and  $\{\Delta x, \Delta y\}$  is the minimum grid spacing in horizontal direction. Bed roughness coefficients, which are one of the main variables for the calibration of numerical models, may generally be computed according to Manning, White-Colebrook, or Chézy. If information about sediment characteristics in the bed is available, bed roughness predictors (e.g., van Rijn, 2007) may also be applied. Hydrodynamic forcing along the boundaries can be provided in different forms, including astronomical constituents or time-series of observations. Furthermore, spatially and temporally varying atmospheric boundary conditions might be implemented in the model. Finally, the Delft3D-FLOW module contains several other important physical phenomena, such as the effect of Earth's rotation (Coriolis force), barotropic and baroclinic effects, turbulence closure models, and the drying and flooding of intertidal flats.

The Delft3D-MOR module, which is forced by flow fields originating from the Delft3D-FLOW module, is used for morphodynamic simulations. Using Delft3D-MOR, multiple



non-cohesive (sand) as well as cohesive sediment fractions may be considered in a model. The sediment inventory in the bed can be implemented as one well-mixed layer or as a stratified bed layer model, i.e., an active transport layer on top of a limited number of buffering underlayers. For cohesive sediment transport, the well-known Partheniades-Krone formulations are used (Partheniades, 1965; Krone, 1962). For the transport of non-cohesive sediments, the approach by van Rijn et al. (2001) is typically followed. However, numerous other transport formulas can be selected (e.g., Engelund and Hansen, 1967; van Rijn, 2007), which consider the bed load and/or suspended transport of non-cohesive sediments. Computed bed shear stresses from the Delft3D-FLOW module are used to determine the magnitude and direction of the sediment transport. Resulting from the erosion and sedimentation of available sediments, the feedback of bed level changes to the Delft3D-FLOW module ultimately enables full morphodynamic simulations. Finally, a morphological acceleration factor  $f_{MORFAC}$  (Roelvink, 2006) can be applied for simulations of long-term morphodynamic development.

#### Summary of chapter 5:

- **Bottom mapping**

Hydroacoustics provide a powerful tool to perform in-situ measurements in coastal environments. For example, MBESs can be used to measure water depths in rivers, coastal waters, or deep oceans. Jordan et al. (2019b) used bottom mapping by means of a MBES to calculate sand mining volumes and to estimate bed load transport rates for a surveyed section of the Tien River. Collected bathymetric datasets were also used by Jordan et al. (2020) for the set-up of a numerical model of local hydro- and morphodynamics. By transmitting and receiving a fan of hundreds of beams perpendicular to a ship track, a MBES makes simultaneous depth measurements that cover a wide area underneath the ship. Using input from auxiliary sensors, a MBES enables highly accurate and geo-referenced bottom mapping in a relatively short amount of time. After post-processing, quality-checked datasets may be used for further analysis (e.g., median filtering technique or bedform translation method) that concentrate on specific bathymetric features.

- **Hydro-morphodynamic modeling**

Numerical models are powerful tools, which may be used to analyze phenomena in coastal environments. The process-based numerical software tool Delft3D was used in depth-averaged mode by Jordan et al. (2020) to investigate the future mor-



- **Hydro-morphodynamic modeling (continued)**

phodynamics of the Tien River branch in the VMD. A depth-averaged Delft3D model of North Sea tides was also applied by Jordan et al. (2021) to project the response of regional tidal properties to SLR and bathymetric changes in the Wadden Sea. In general, Delft3D uses the modules FLOW and MOR, which interact with one another, to simulate hydro- and morphodynamic processes. Using horizontal equations for motion, the continuity equation, and transport equations for conservative constituents, the Delft3D-FLOW module calculates non-steady flows and salt/heat transport. Using input from Delft3D-FLOW, the MOR module calculates bed level changes based on well-known formulas for the transport of non-cohesive (sand) and cohesive sediments.

## 6 Publications

In this chapter, a brief overview of the published papers in this thesis is given. This chapter contains an adapted version of the abstract and conclusions for each paper, complemented by a selection of the main figures. All considered papers are published under an open access license and are thus freely available for everyone. A link to these articles is given by their digital object identifier (DOI).

The first publication focuses on the present-day amount of sand extraction in the VMD, which was estimated based on datasets that were obtained during two field surveys in 2018. Acquired high-resolution bathymetries enabled the most precise estimation of sand mining volumes for the surveyed Tien River section to date. Besides highlighting discrepancies between official statistics and actual extraction volumes, the results also uncovered the unsustainable nature of the local sand mining. Focusing on the projected responses of morphodynamic processes in the VMD to the main drivers of regional changes, the second publication is directly linked to the first publication. Datasets that were acquired during the field surveys were used to set up and validate a hydro-morphodynamic model of the Tien River. Furthermore, the insights from the first publication helped to develop scenarios that were used to assess the future impacts of sand mining on the morphology of the VMD. To address shortcomings of previous studies, damming, climate change-induced alterations in hydrology, and SLR were considered as the main drivers of future developments in the VMD, besides sand mining. For the future period 2050 to 2060, the results projected that morphological changes in the VMD are mainly impacted by damming, followed by increasing sand mining activity. In contrast to the other publications, the third publication focuses on the tidal response of the North Sea and the adjacent estuaries in the German Bight to SLR. Since the VMD and the estuaries in the German Bight differ considerably in terms of the drivers of future changes, only SLR was considered as a driver impacting the future tidal dynamics in the region. By combining different rates of SLR with numerous rates of vertical accretion in local intertidal areas, the impact of potential bathymetric changes in the Wadden Sea was included in investigated projections. The results showed that tidal asymmetries in the German estuaries will be increased if a SLR without vertical accretion in the intertidal flats is assumed. If intertidal flats keep up with the sea-level, though, tidal asymmetries will remain comparable to present-day conditions.

## 6.1 Sand mining in the Mekong Delta revisited – current scales of local sediment deficits

Jordan, C., Tiede, J., Lojek, O., Visscher, J., Apel, H., Nguyen, H. Q., et al. (2019b). Sand mining in the Mekong Delta revisited – current scales of local sediment deficits. *Scientific Reports* 9:17823. doi: 10.1038/s41598-019-53804-z

### 6.1.1 Abstract

The delta of the Mekong River in Vietnam has been heavily impacted by anthropogenic interventions in recent years, such as upstream dam construction and sand mining within the main and distributary channels, leading to riverbank and coastal erosion. Intensive bathymetric surveys, conducted within the Tien River branch during the dry and wet season of 2018, reveal a high magnitude of sand mining activity. For the year 2018, an analysis of bathymetric maps and the local refilling processes leads to an estimated sand extraction volume of  $4.64 \pm 0.31 \text{ Mm}^3/\text{yr}$  in the study area, which covered around 20 km. Reported statistics of sand mining for all of the Mekong's channels within the delta, which have a cumulative length of several hundred kilometers, are  $17.77 \text{ Mm}^3/\text{yr}$  for this period. Results from this study highlight that these statistics are likely too conservative. It is also shown that natural sediment supplies from the upper reaches of the Mekong are insufficient to compensate for the loss of extracted bed aggregates, illustrating the non-sustainable nature of the local sand mining practices.

### 6.1.2 Conclusion and Outlook

Generally, extraction pits due to sand mining act as a sediment sink for river aggregates. If sediment transport rates are too small to compensate for sediment losses due to mining activity, the relation between sediment supply and transport capacity becomes distorted. The consequent sediment starvation within the water acts as a trigger for erosion processes. As shown here, the anthropogenic-induced imbalance between sediment supply (see Figure 6.1) and sand mining activity (see Figure 6.2) can be substantial within the VMD. Resulting incision of river channels and bank erosion, which have previously already been reported for the Mekong River (Brunier et al., 2014; Kummur et al., 2008; Miyazawa et al., 2008), are strikingly exposed for a 20 km stretch of the Tien River (see Figure 6.3), which was investigated in this study. Even though it seems impossible to quantify the detailed impact of sand mining on the local morphological processes, it is indisputable that sand mining is an important cause for the changing environment within the VMD and a trigger for erosion processes.

On a large scale, the reduction of downstream sediment supply, resulting from the cumu-



lative impacts of sand mining, dam construction, and changes in the local cyclone activity (Darby et al., 2016), put the delta's future stability into question. The manifold consequences, including bank erosion (Kummu et al., 2008; Miyazawa et al., 2008), recessing coastlines (Anthony et al., 2015; Li et al., 2017; Luijendijk et al., 2018), increasing salinity intrusion (Dyer, 1997), and a loss of mangrove forests (Phan et al., 2015), will likely only accelerate if current sand mining practices are maintained in the future. To ensure sustainable development within the delta region, the overarching objective must be the implementation and enforcement of regulations that mitigate the net loss of sediments due to sand mining. In particular, local sand mining practices should be monitored and controlled in more detail to prevent informal activities. Reliable data is of particular importance to understand the relations between the sand mining and the triggered processes. Accordingly, continuous measurements and numerical models should also be used to reduce existing uncertainties and provide more insight into the links between the underlying hydro- and morphological processes. These models could also project the impacts of possible future scenarios for the local extraction of bed aggregates.

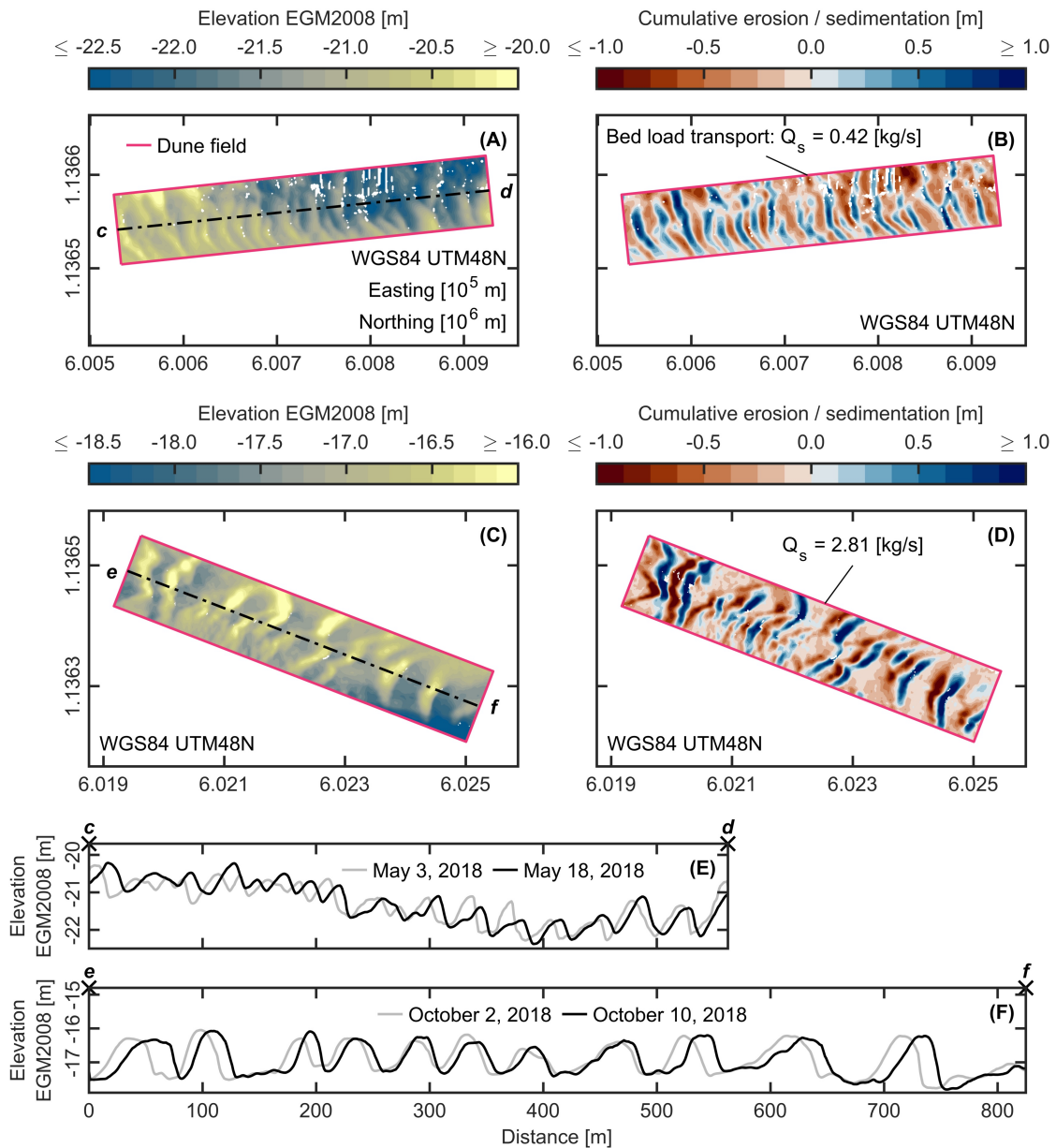


Figure 6.1: Bathymetric changes and associated bed load transport rates within dune fields DF01 (wet season) and DF02 (dry season). **(A)** Bathymetric map of dune field DF02 on May 3, 2018. **(B)** Cumulative erosion (red) and sedimentation (blue) within dune field DF02 from May 3 to 18, 2018. **(C)** Bathymetric map of dune field DF01 on October 2, 2018. **(D)** Cumulative erosion (red) and sedimentation (blue) within dune field DF01 from October 2 to 10, 2018. **(E)** Migration of dunes along cross-section c-d (see panel (A)) during the dry season 2018. **(F)** Migration of dunes along cross-section e-f (see panel (C)) during the wet season 2018. See Figure 1 in Jordan et al. (2019b) for positions of dune fields DF01 and DF02 in the Tien River branch. Adapted from Jordan et al. (2019b).

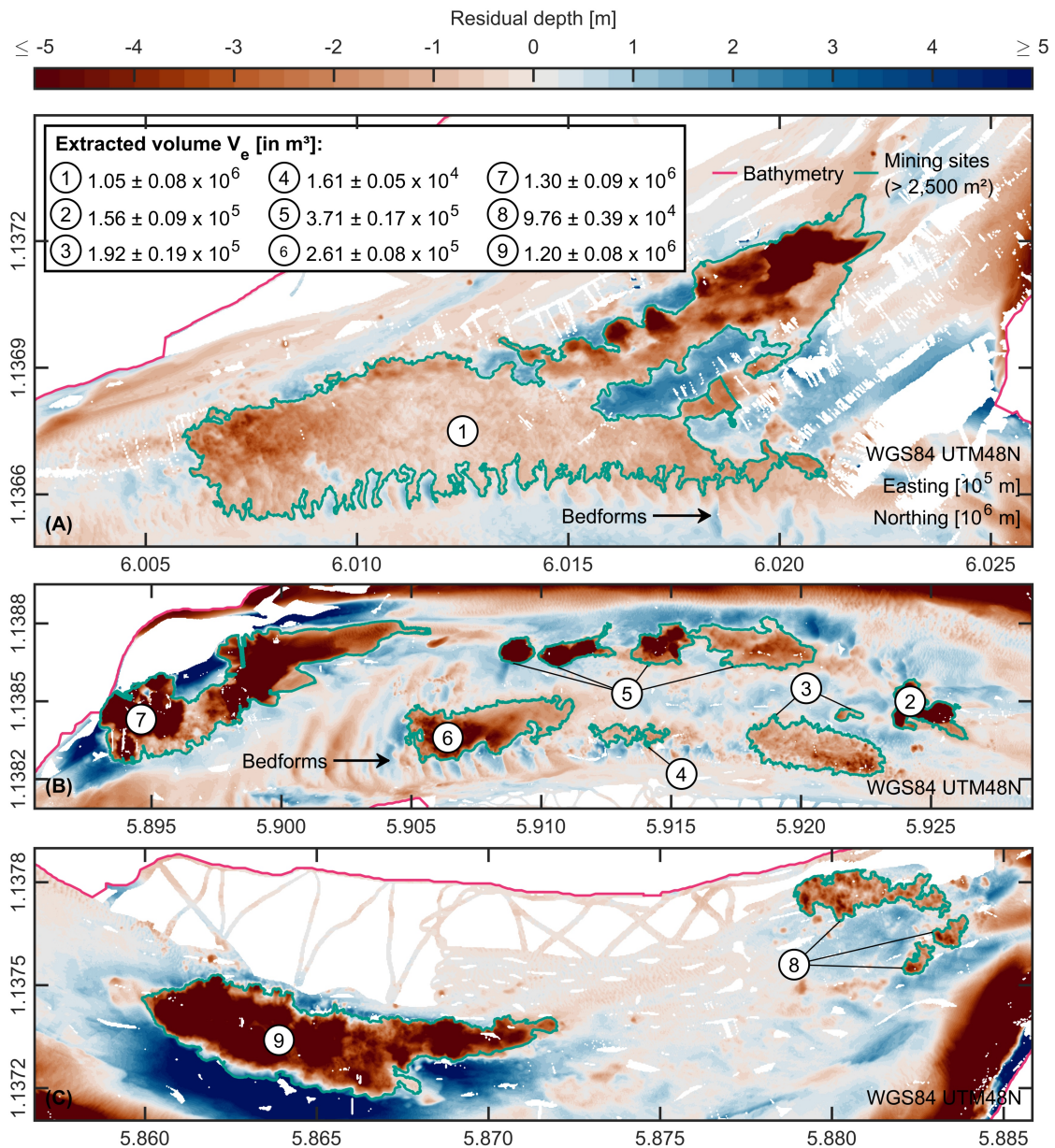


Figure 6.2: Detailed map of sand mining sites detected during the dry season 2018 and associated extraction volumes. (A) Residual bathymetry with mining sites between river kilometer marker (RKM) -3 to -1. (B) Residual bathymetry with mining sites between RKM 8 to 11. (C) Residual bathymetry with mining sites between RKM 12 to 15. Red color indicates areas below the median, while blue color indicates areas above the median. Shown residual bathymetries are based on an exemplary filter width of 500 m. Note that this filter width does not necessarily reflect the optimal diameter for each mining site, according to the optimal robust separator (ORS) algorithm by Kim and Wessel (2008). See Figure 1 in Jordan et al. (2019b) for locations of the RKM. Adapted from Jordan et al. (2019b).

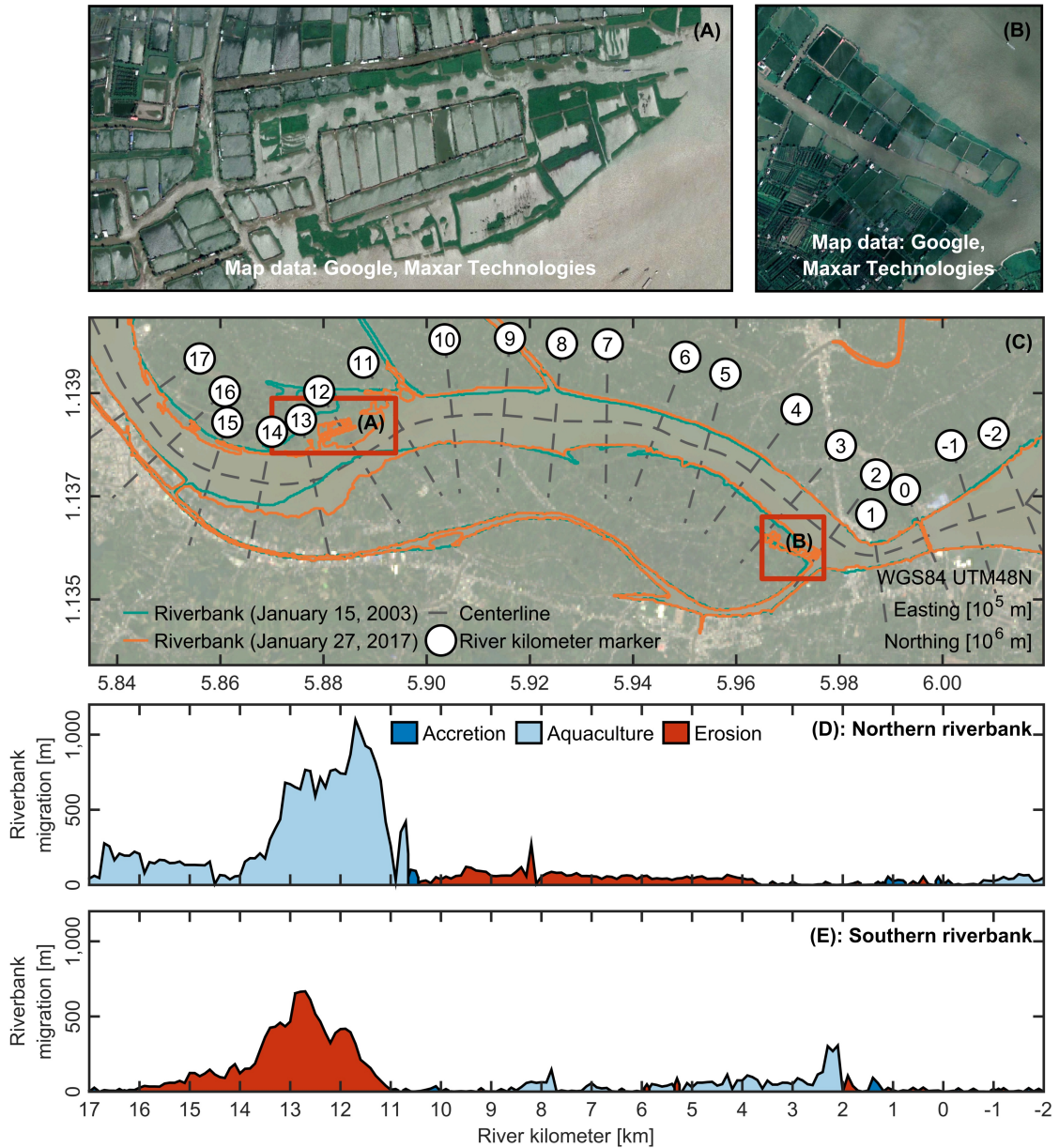


Figure 6.3: Changes in riverbank positions in the study area between January 2003 and January 2017. **(A, B)** Aquaculture infrastructure built between January 2003 and January 2017. **(C)** Map with locations of riverbanks for January 15, 2003, and January 29, 2017. Riverbanks were extracted from historical Landsat imagery using the modified normalized difference water index (MNDWI) (Xu, 2006). Landsat-8 image from January 29, 2017, was used as background image. **(D)** Accretion and erosion along the northern riverbank (RKM -2 to 17) between January 2003 and January 2017. **(E)** Accretion and erosion along the southern riverbank (RKM -2 to 17) between January 2003 and January 2017. Accretion corresponding to locations of aquaculture infrastructure was highlighted separately. Satellite images shown in **(A)** and **(B)** were provided by Google Earth (<https://earth.google.com/web>) and are based on data from Maxar Technologies for December 22, 2017. Landsat images courtesy of the USGS, downloaded from the USGS EROS Center (<https://earthexplorer.usgs.gov/>). Adapted from Jordan et al. (2019b).



## 6.2 Impacts of Human Activity and Global Changes on Future Morphodynamics within the Tien River, Vietnamese Mekong Delta

Jordan, C., Visscher, J., Dung, N. V., Apel, H., and Schlurmann, T. (2020). Impacts of Human Activity and Global Changes on Future Morphodynamics within the Tien River, Vietnamese Mekong Delta. *Water* 12:2204. doi: 10.3390/w12082204

### 6.2.1 Abstract

The hydro- and morphodynamic processes within the Vietnamese Mekong Delta are heavily impacted by human activity, which in turn affects the livelihood of millions of people. The main drivers that could impact future developments within the delta are local drivers like hydropower development and sand mining, but also global challenges like climate change and relative sea-level rise. Within this study, a hydro-morphodynamic model was developed, which focused on a stretch of the Tien River and was nested into a well-calibrated model of the delta's hydrodynamics. Multiple scenarios were developed in order to assess the projected impacts of the different drivers on the river's morphodynamics. Simulations were carried out for a baseline scenario (2000 to 2010) and a set of plausible scenarios for a future period (2050 to 2060). The results for the baseline scenario indicate that the Tien River is already subject to substantial erosion under present-day conditions. For the future period, hydropower development has the highest impact on the local erosion and deposition budget, thus amplifying erosion processes, followed by an increase in sand mining activity and climate change-related variations in discharge. The results also indicate that relative sea-level rise only has a minimal impact on the local morphodynamics of this river stretch, while erosional trends are slowed by a complete prohibition of sand mining activity. In the future, an unfavorable combination of drivers could increase the local imbalance between erosion and deposition by up to 89 %, while the bed level could be incised by an additional 146 %.

### 6.2.2 Conclusions and Outlook

Based on in-situ data, which was measured during the 2018 dry and wet seasons, a hydro-morphodynamic model was set up and validated, focusing on a stretch of the Tien River within the VMD. The model was nested into a well-calibrated hydrodynamic model of the whole VMD (Manh et al., 2014, 2015) in order to generate boundary forcing for plausible future developments within the delta region. Mainly focusing on the upper bound of possible changes, the impacts of hydropower development, sand mining activity, climate change-related variations in discharge, and RSLR on the local morphodynamics were analyzed. The main findings are as follows:

- The study area must already be characterized as an erosional environment under present-day conditions (see Figure 6.4), as indicated by the local imbalance between erosion and deposition and mean bed level changes.
- Based on tendencies for additional bed level incision (see Figure 6.5) and the local imbalance between erosion and deposition (see Figure 6.6), hydropower development has the highest impact of all investigated drivers, followed by an increase in sand mining activity and a climate change-related increase in riverine discharge. A complete prohibition of local sand mining activity can counter the impact of other drivers on the local morphological processes, while the overall impact of RSLR is almost negligible.
- Nonlinear processes, which are caused by the interaction of multiple drivers, will likely lead to negative feedback effects on the evolution of the local bathymetry, thus amplifying prevailing erosional trends. The combination of hydropower development, increased sand mining, and RSLR will lead to the largest imbalance in the local erosion and deposition budget ( $R_{ero/dep, DM+S} = 2.97$ ) (see Figure 6.6). In relation to the baseline scenario, bed level incision is likely to be amplified by up to 146% caused by the cumulative impacts of hydropower development, increased sand mining activity, and a climate change-related increase in discharge (see Figure 6.5).

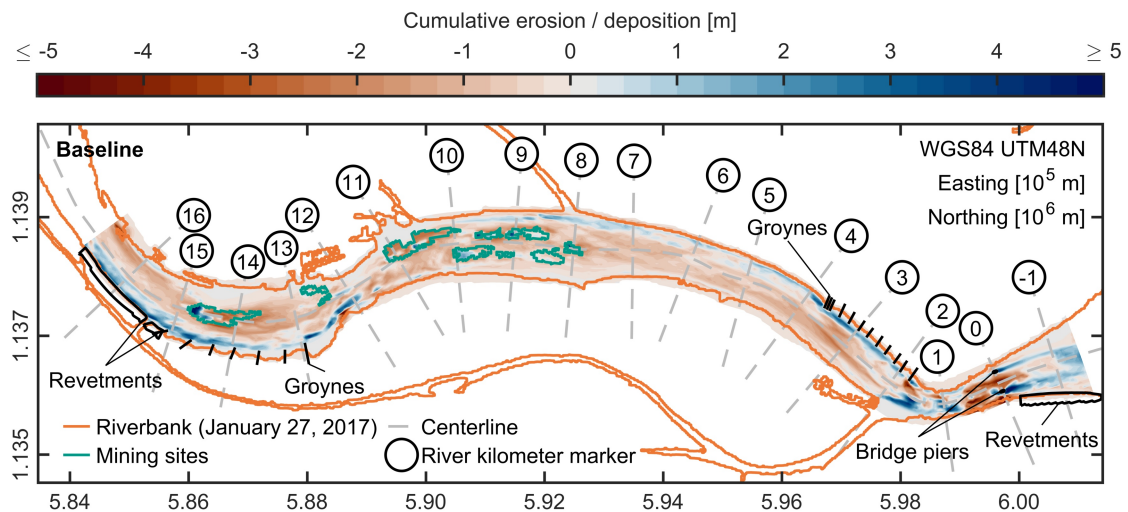


Figure 6.4: Pattern of cumulative erosion (red) and deposition (blue) at the end of the baseline scenario, including positions of riverbanks, RKM, implemented sand mining sites and hydraulic structures. Riverbanks were extracted from historical Landsat imagery using the MNDWI (Xu, 2006). Landsat images courtesy of the USGS, downloaded from the USGS EROS Centre (<https://earthexplorer.usgs.gov>). Sand mining sites were separated from the surrounding bathymetry using the approach described in Jordan et al. (2019b). Adapted from Jordan et al. (2020).

The results highlight the need for a more sustainable future development of the VMD. Strategic hydropower planning on a basin-wide scale is needed to identify scenarios that minimize the negative impacts of hydropower (Schmitt et al., 2019). Furthermore, it is imperative to implement a management plan for local and basin-wide sand mining activity (Jordan et al., 2019b; Hackney et al., 2020). To prevent unsustainable or even informal practices, sand mining should be monitored closely. A complete prohibition of sand mining activity could mitigate the local net loss of sediments and therefore counter the impact of other drivers that amplify erosion processes.

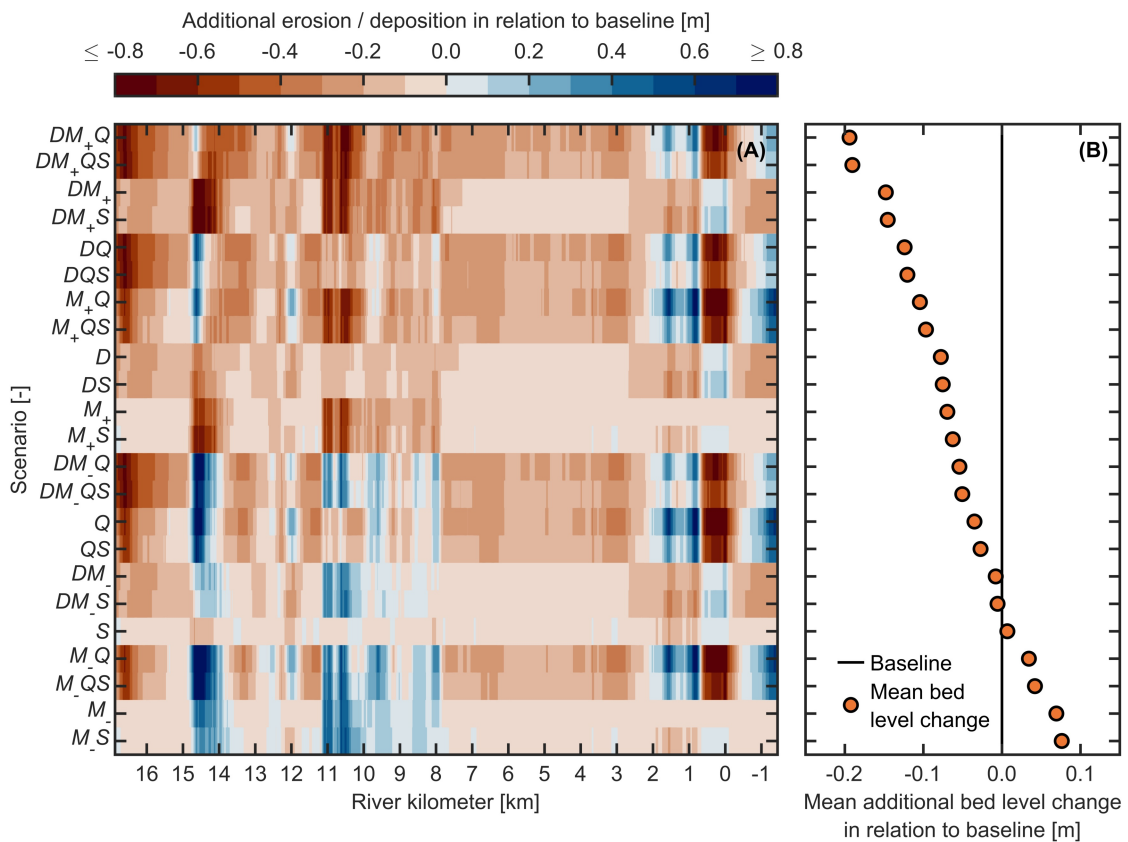


Figure 6.5: Mean bed level changes in relation to the baseline scenario. (A) Cross-sectional averages of bed level changes along the RKM system (see Figure 6.4), indicating river sections of additional erosion (red) and deposition (blue) in relation to the baseline scenario. (B) Domain-wide averages of bed level changes in relation to the baseline scenario. Scenarios were sorted according to impact (from most additional deposition (bottom) to most additional erosion (top)). The notation of the scenarios is a combination of the individual driver notations listed in Table 6.2.1. Adapted from Jordan et al. (2020).

Table 6.2.1: Notations used by Jordan et al. (2020) for single drivers and associated changes in discharge ( $Q_{BC}$ ), sediment concentrations ( $SSC_{sBC}$ ), and sand extraction volume ( $V_{Extr.}$ ). Discharges and sediment concentrations represent mean values along the model's boundaries over the duration of the simulation period. Percentages indicate changes in relation to the baseline scenario.

Driver	Notation	$Q_{BC}$	$SSC_{sBC}$	$V_{Extr.}$
Baseline	-	12,577 m <sup>3</sup> /s	0.149 kg/m <sup>3</sup>	3.59 Mm <sup>3</sup> /yr
Hydropower dams	D	-8 %	-95 %	0 %
Increase in sand mining	M <sub>+</sub>	0 %	0 %	+100 %
Decrease in sand mining	M <sub>-</sub>	0 %	0 %	-100 %
Climate change	Q	+22 %	+12 %	0 %
RSLR	S	-5 %	-2 %	0 %

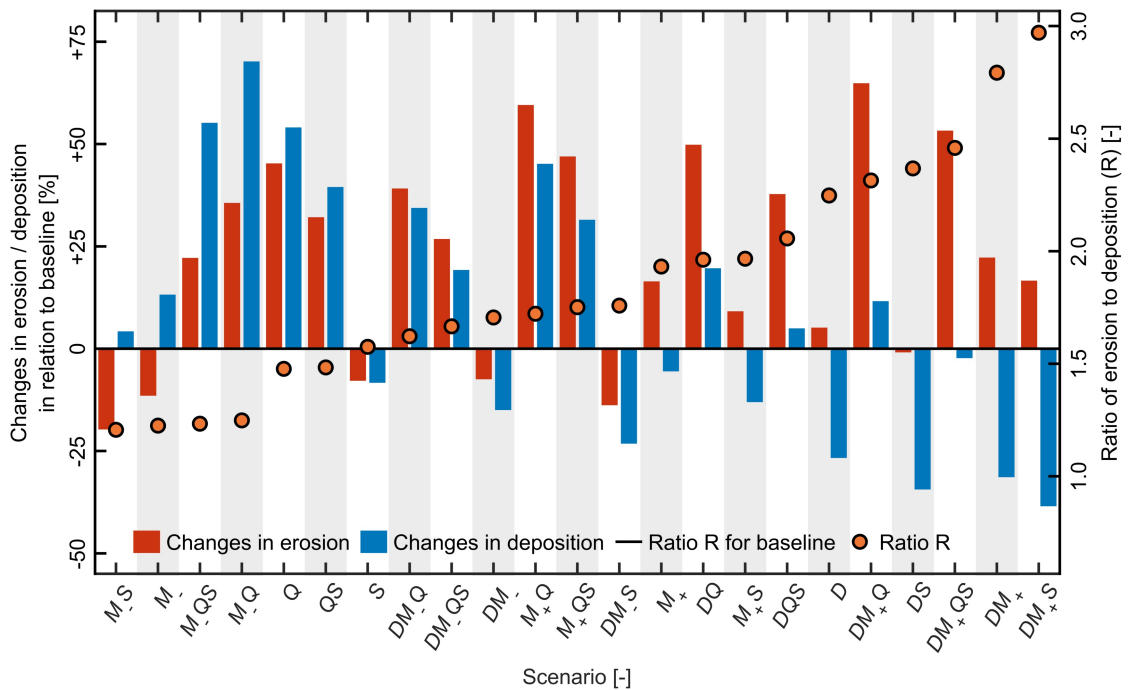


Figure 6.6: Domain-wide changes in total erosion and deposition volumes in relation to the baseline scenario as well as ratios between erosion and deposition volumes. Scenarios were sorted according to impact (from lowest imbalance (left) to highest imbalance (right) between erosion and deposition volumes). The notation of the scenarios is a combination of the individual driver notations listed in Table 6.2.1. Adapted from Jordan et al. (2020).

### 6.3 Projected Responses of Tidal Dynamics in the North Sea to Sea-Level Rise and Morphological Changes in the Wadden Sea

Jordan, C., Visscher, J., and Schlurmann, T. (2021). Projected Responses of Tidal Dynamics in the North Sea to Sea-Level Rise and Morphological Changes in the Wadden Sea. *Frontiers in Marine Science* 8:685758. doi: 10.3389/fmars.2021.685758

#### 6.3.1 Abstract

This study explores the projected responses of tidal dynamics in the North Sea induced by the interplay between plausible projections of SLR and morphological changes in the Wadden Sea. This is done in order to gain insight into the causal relationships between physical drivers and hydro-morphodynamic processes. To achieve this goal, a hydronumerical model of the NWES was set up and validated. By implementing a plausible set of projections for global SLR (SLR<sub>RCP8.5</sub> of 0.8 m and SLR<sub>high-end</sub> of 2.0 m) by the end of this century and beyond, the model was run to assess the responses of the regional tidal dynamics. In addition, for each considered SLR, various projections for cumulative rates of vertical accretion were applied to the intertidal flats in the Wadden Sea (ranging from 0 to 100% of projected SLR). Independent of the rate of vertical accretion, the spatial pattern of M2 amplitude changes remains relatively stable throughout most of the model domain for a SLR of 0.8 m. However, the model shows a substantial sensitivity toward the different rates of vertical accretion along the coasts of the Wadden Sea, but also in remote regions like the Skagerrak. If no vertical accretion is assumed in the intertidal flats of the Wadden Sea, the German Bight and the Danish west coast are subject to decreases in M2 amplitudes. In contrast, those regions experience increases in M2 amplitudes if the local intertidal flats are able to keep up with the projected SLR of 0.8 m. Between the different scenarios, the North Frisian Wadden Sea shows the largest differences in M2 amplitudes, locally varying by up to 14 cm. For a SLR of 2.0 m, the M2 amplitude changes are even more amplified. Again, the differences between the various rates of vertical accretion are largest in the North Frisian Wadden Sea (> 20 cm). The local distortion of the tidal wave is also significantly different between the scenarios. In the case of no vertical accretion, tidal asymmetry in the German estuaries increases, leading to a potentially enhanced sediment import. The presented results have strong implications for local coastal protection strategies and navigation in adjacent estuaries.

#### 6.3.2 Summary and Outlook

The knowledge of future North Sea tidal dynamics has wide-ranging implications for the regional environment and economy, including impacts on sediment transport, coastal habitats, maritime navigation, and the offshore wind energy industry. Covering the

NWES, a hydronumerical model was set up within this study to investigate the responses of regional tidal dynamics to the combined impact of SLR and the morphological evolution of intertidal flats in the Wadden Sea. Focusing on the North Sea region, the thoroughly validated model reproduces the present-day tidal dynamics with good accuracy. In order to correctly represent characteristic bathymetric features in shallow coastal areas (e.g., tidal channels and intertidal flats), a fine resolution ( $\approx 250 \times 250$  m) was applied for the Wadden Sea. Though our results agree with previous studies for most of the North Sea region, our estimated responses of M2 tidal amplitudes to SLR reveal some discrepancies along the Wadden Sea coast. Due to coarse model resolution, earlier projections were unable to correctly reproduce the responses of current velocities in the Wadden Sea to SLR (Rasquin et al., 2020). Accordingly, our results presumably represent the first robust projection for the impacts of SLR on the M2 tide for the entire Wadden Sea region.

Due to uncertainties in the projections of SLR, it is still slightly unknown how intertidal flats will cope with future accelerated SLR. Though it seems plausible that the availability of sediment from internal and external sources will lead to local accretion, it is unclear to which degree the intertidal flats will be able to counterbalance the impacts of SLR. However, as shown in this study, the future morphological evolution of the Wadden Sea will play an important role regarding the responses of the regional tidal dynamics to SLR. Starting at Den Helder and extending to the Skagerrak, the coasts of the Netherlands, Germany, and Denmark are particularly sensitive toward the combined impact of SLR and morphological changes in the Wadden Sea (see Figure 6.7). Depending on the rate of vertical accretion in the local intertidal flats, M2 amplitude changes can even vary in their sign. In the case of no vertical accretion, amplitude decreases are to be expected in the German Bight (see Figure 6.8B) and along the Danish coast. With increasing rates of vertical accretion, increases in M2 amplitudes become more pronounced, while areas with amplitude decreases begin to diminish (see Figure 6.8C-E). The largest amplitude increases occur in the case that intertidal flats are able to keep up with SLR (see Figure 6.8F). Between the applied rates of vertical accretion, the M2 amplitude changes can locally vary by more than 10 cm for a SLR of 0.8 m. For a SLR of 2.0 m, these differences can even surpass 20 cm. Besides M2 amplitude changes, which mainly impact the height of tidal high and low water levels, we also briefly assessed possible alterations in tidal asymmetries. Increases in flood dominance (and decreases in ebb dominance) are to be expected in the case of no vertical accretion in the intertidal areas of the Wadden Sea (see Figure 6.9).

### **Implications for Coastal Protection Strategies**

Design heights in coastal protection usually consider the superimposed impacts of tides, surges, waves, and SLR. As shown in our study, large uncertainties are inherent to the

local responses of tidal dynamics to the combined impacts of SLR and morphological changes in the Wadden Sea. For numerous regions (e.g., North Frisian Wadden Sea, Danish west coast), it is highly uncertain whether tidal amplitudes will be amplified or attenuated by SLR, depending on the various scenarios of possible morphological changes in the Wadden Sea. Dealing with large uncertainties in future SLR, Oppenheimer et al. (2019) proposed that flexible responses and adjusted decisions are needed in coastal management. We suggest that this adaptation pathway approach (e.g., Haasnoot et al., 2013, 2019) should also be applied in order to cope with the presented uncertainties in future tidal dynamics.

### **Implications for Sediment Transport in Estuaries**

Generally, large tidal amplitudes and shallow channels enhance flood dominance, while ebb dominance is enhanced by a large intertidal storage volume in comparison to the channel volume (Bosboom and Stive, 2021). If intertidal storage is lost due to SLR and lacking vertical accretion in the Wadden Sea, flood dominance will accordingly be enhanced (and ebb dominance be decreased). Since tidal asymmetry in estuaries controls the residual sediment transport, enhanced flood dominance will lead to more sediment being imported into the Ems, Weser, and Elbe estuaries. As identified by Winterwerp and Wang (2013), positive feedbacks between increased tidal asymmetry, increased sediment import, and reduced hydraulic drag might even bring an estuary into a hyper-turbid state. To cope with such possible regime shifts in the German estuaries, awareness must be raised and new strategies are required to improve the estuarine water quality and to safeguard operations of local critical infrastructure, e.g., waterways and ports. Accordingly, the design of resilient pathways for local port operations and waterways management should be studied in greater detail in the future.

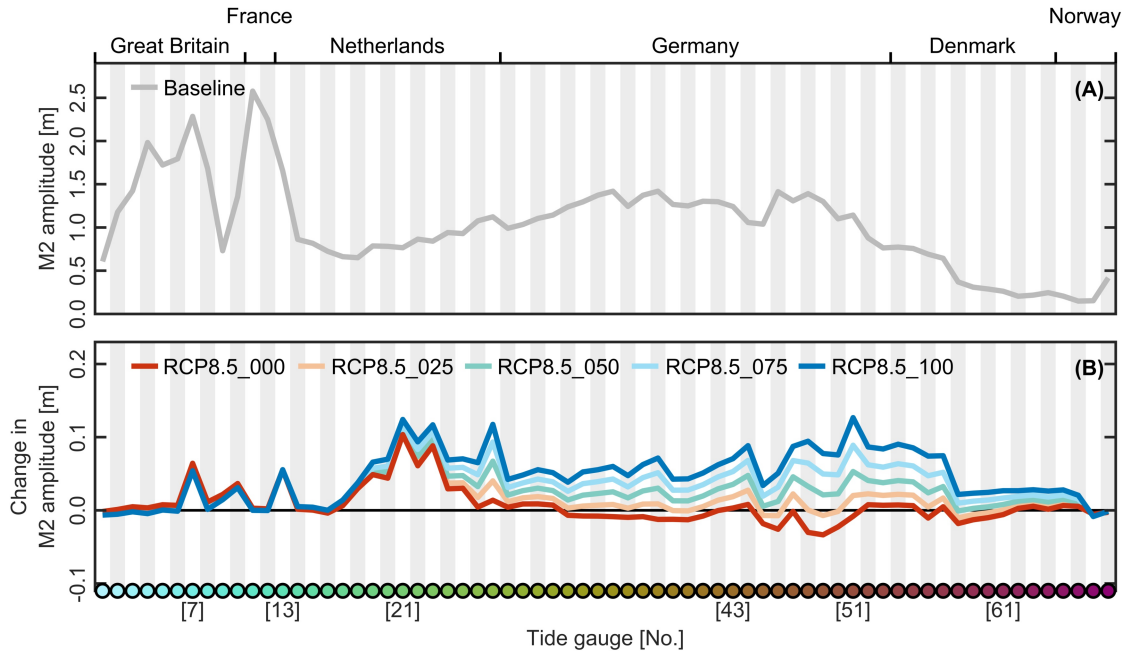


Figure 6.7: M2 amplitudes as a function of available tide gauge stations resulting from the combinations of 0.8 m SLR projection and various cumulative rates of vertical accretion. (A) M2 amplitudes for the baseline scenario, according to the 3-month period from September 1 to December 1, 2012. (B) Relative changes in M2 amplitudes resulting from 0.8 m SLR and various cumulative rates of vertical accretion. The color codes and locations of tide gauge stations are shown in Figure 1 of Jordan et al. (2021). Shown numbers indicate exemplary tide gauge stations that are highlighted in more detail in Figure 2 of Jordan et al. (2021). Notations for scenarios are summarized in Table 6.3.1. Adapted from Jordan et al. (2021).

Table 6.3.1: Notations of selected scenarios investigated by Jordan et al. (2021) as well as associated values of SLR and cumulative rates of vertical accretion.

Notation	Projected SLR by the year 2100	Cumulative rates of vertical accretion in the intertidal flats of the Wadden Sea
Baseline	0.0 m	0.0 m (-)
RCP8.5_000	0.8 m	0.0 m (= 0 % of projected SLR)
RCP8.5_025	0.8 m	0.2 m (= 25 % of projected SLR)
RCP8.5_050	0.8 m	0.4 m (= 50 % of projected SLR)
RCP8.5_075	0.8 m	0.6 m (= 75 % of projected SLR)
RCP8.5_100	0.8 m	0.8 m (= 100 % of projected SLR)



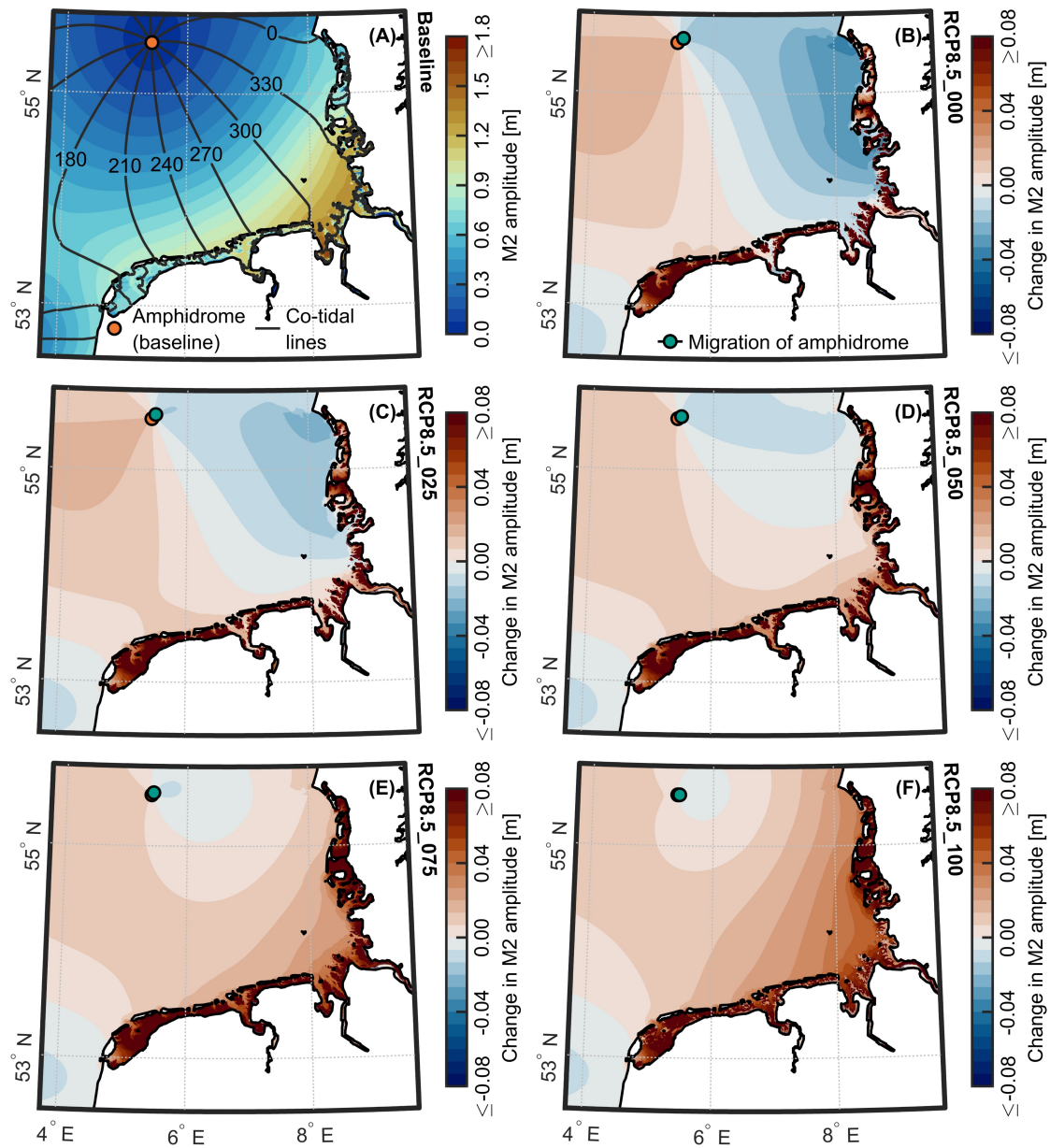


Figure 6.8: M2 amplitudes for the Wadden Sea resulting from the combinations of 0.8 m SLR projection and various cumulative rates of vertical accretion. (A) Map of M2 amplitudes for the Wadden Sea for the baseline scenario, according to the 3-month period from September 1 to December 1, 2012. Relative changes in M2 amplitudes for scenarios (B) RCP8.5\_000, (C) RCP8.5\_025, (D) RCP8.5\_050, (E) RCP8.5\_075, and (F) RCP8.5\_100. Green dots indicate movements of amphidromic points in relation to the baseline scenario (orange dots). Notations for scenarios are summarized in Table 6.3.1. Adapted from Jordan et al. (2021).

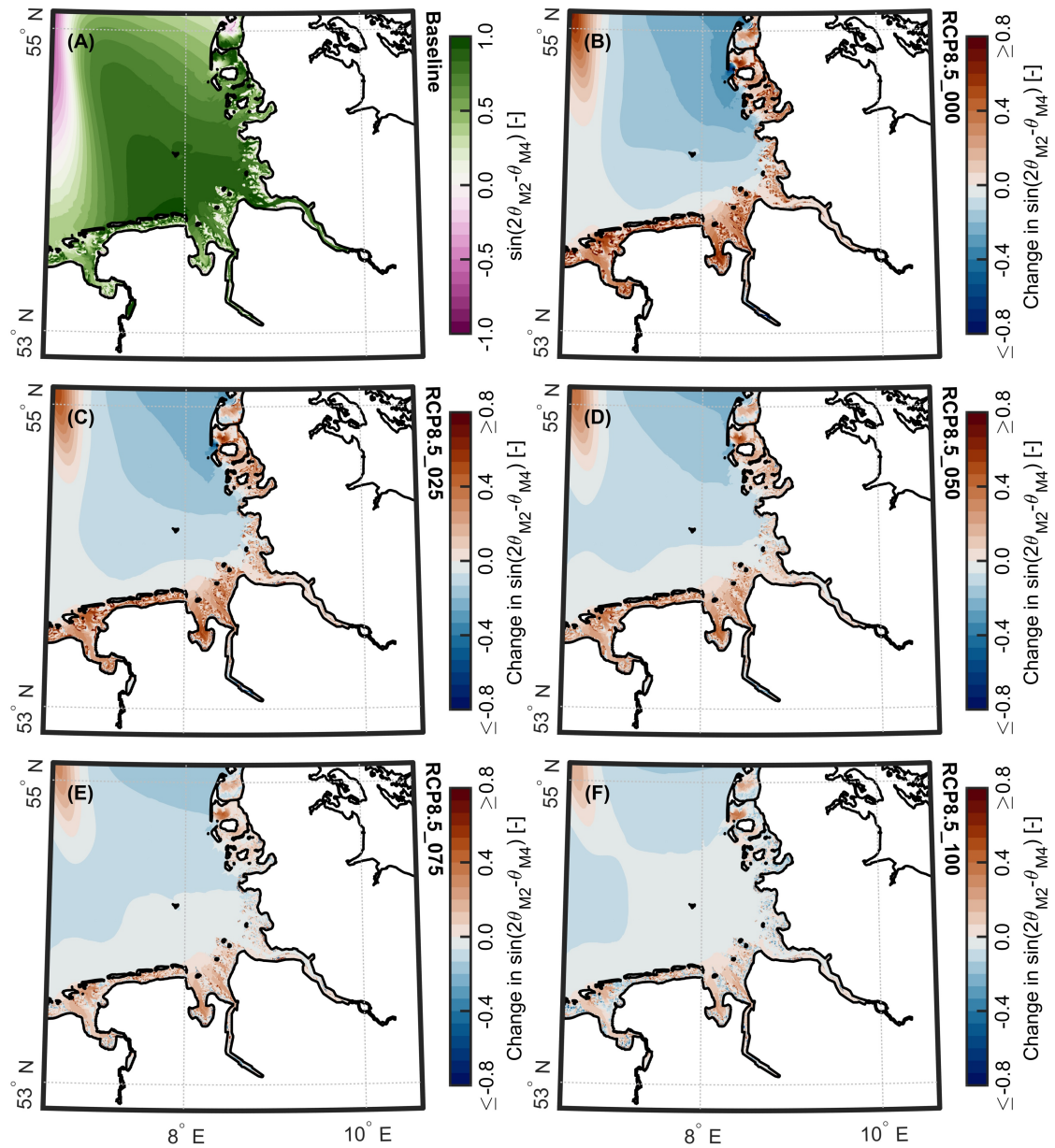


Figure 6.9: Flood and ebb dominance for the German Bight resulting from the combinations of 0.8 m SLR projection and various cumulative rates of vertical accretion. **(A)** Map of flood and ebb dominance for the German Bight for the baseline scenario, according to the 3-month period from September 1 to December 1, 2012. Relative changes in flood and ebb dominance for scenarios **(B)** RCP8.5\_000, **(C)** RCP8.5\_025, **(D)** RCP8.5\_050, **(E)** RCP8.5\_075, and **(F)** RCP8.5\_100. In panel **(A)**, values  $> 0$  indicate flood dominance, with values  $< 0$  signaling ebb dominance. In panels **(B)** to **(F)**, values  $> 0$  indicate increases in flood dominance or decreases in ebb dominance, while values  $< 0$  signal increased ebb dominance or decreased flood dominance. Notations for scenarios are summarized in Table 6.3.1. Adapted from Jordan et al. (2021).

## 7 Summary and Outlook

### 7.1 Summary

In order to conserve important ecosystem services of estuaries and to enhance estuarine contributions to achieving the UN SDGs, negative impacts of human activity and global warming need to be minimized. To achieve this goal, new insights into the response of estuarine environments to drivers of contemporary and future changes were provided in this thesis. The major contemporary and future drivers on estuaries that were discussed in this thesis are: sand mining/dredging, damming, climate change-induced alterations in hydrology, and SLR. The YRD, the VMD, as well as the German estuaries Elbe, Weser, and Ems were used as examples to demonstrate how these systems are impacted by human activity and climate change, at present and in the future. Considering sand mining, the focus has continuously shifted from terrestrial to riverine and marine sources due to a growing demand for sand, which is mainly driven by the economic growth and urbanization in Asian developing countries. Though estimates for sand mining volumes are lacking for many of the world's large rivers, several studies exist for the Mekong (e.g., Bravard et al., 2013; Jordan et al., 2019b; Hackney et al., 2020). Yet, recent findings indicate that early estimates of sand mining volumes vastly underestimated the actual amount of sand extraction (e.g., Jordan et al., 2019b). According to estimates for the year 2020, the combined sand extraction in the Lower Mekong (Cambodia) and VMD was around 134 Mt/yr (Hackney et al., 2021; Gruel et al., Preprint), which represents an increase by around 190% in relation to estimates for the year 2011 (Bravard et al., 2013). This also highlights a significant deficit in the local sand budget, since the sand flux that is entering the delta is just around  $6.2 \pm 2.0$  Mt/yr (Hackney et al., 2020). Like in most rivers in North America and Europe, sand extraction for industrial use is not practiced in the Elbe, Weser, and Ems. However, estuarine channels in the Elbe, Weser, and Ems were continuously deepened to ensure safe navigation (Boehlich and Strotmann, 2008; Lange et al., 2008; Krebs and Weilbeer, 2008). Besides sand mining/dredging, many of the world's rivers are significantly fragmented or regulated by dams. Estimates indicate that 4 to 5 Gt/yr of sediments are trapped in reservoirs annually, representing more than a quarter of the global annual sediment flux (Vörösmarty et al., 2003). On the Yellow River, for instance, the construction and operation of large dams along the river's upper and middle reaches have significantly altered the water and sediment fluxes. In contrast to 1950s levels, freshwater discharge and sediment load reaching the delta have decreased by 70 and 90%, respectively (Yu et al., 2013). At the Mekong, hydropower expansion is still ongoing, with many large dams being planned or under construction. If all large dams are realized, the characteristic monsoon-driven regime of the river will be significantly altered (Lauri et al., 2012), while the sediment flux reaching the delta could be reduced by up to 96% (Kondolf et al., 2014; Manh et al., 2015). Since global runoff increases with global warming, climate

change-induced alterations in hydrology are also to be expected. However, due to large uncertainties in global and regional climate models, it is rather difficult to project changes on the scale of individual river basins. Nevertheless, it is likely that extreme flood and drought events will increase in magnitude and occur more frequently in the future (e.g., Huang et al., 2015; Wang et al., 2017a). Concentrating on SLR, the newest projections indicate that GMSLR will be between 0.38 and 0.77 m (medians of SSP1-1.9 and SSP5-8.5) by the end of this century in relation to 1995 to 2014 (Fox-Kemper et al., 2021). Due to human-induced land subsidence, future RSLR in the low-lying YRD and VMD may exceed global trends (e.g., Higgins et al., 2013; Erban et al., 2014). While observed trends in the North Sea basin surpass recent rates of GMSLR (Wahl et al., 2013), regional projections of future RSLR (e.g., Grinsted et al., 2015) are largely in agreement with global projections. SLR may also alter tidal properties due to changes in the resonance frequency of an ocean basin/shelf sea or by spatial re-organization of amphidromic systems (Haigh et al., 2020). In areas, where extended intertidal flat systems are present, e.g., in the Wadden Sea, there may also be feedbacks between SLR, morphological evolution of intertidal areas, and tidal properties (Wachler et al., 2020; Jordan et al., 2021).

Since the interaction of freshwater fluxes and ocean tides is the main driver of the estuarine circulation, it is obvious that dam- or climate change-induced alterations in freshwater fluxes and SLR-induced changes in tides will alter estuarine mixing processes. Depending on the magnitude of changes, estuaries may become more susceptible to salinity intrusion (e.g., Smajgl et al., 2015), while the vertical structure in salinity might also be altered. Furthermore, if intertidal areas in an estuary are drowned by SLR, the system will become more flood-dominant (Wachler et al., 2020; Jordan et al., 2021), hence favoring the import of marine sediments. In addition, if the cumulative impacts of damming and unsustainable sand extraction lead to channel incision or estuarine channels are deliberately deepened, the impacts on estuarine environments can be aggravated. In general, deepening of channels leads to tidal amplification that can turn an estuary into a hyper-synchronous state. If tidal amplification becomes so large that a tipping point is passed, a positive feedback loop may occur between tidal amplification, flood dominance, import of fine sediments, and reduction in hydraulic drag (Winterwerp and Wang, 2013). As a consequence, an estuary might turn into a hyper-turbid state (Winterwerp and Wang, 2013). As observed for the Ems Estuary in recent decades, the ETM may move further upstream as a result, while substantially increased SSCs can lead to the formation of thick fluid mud layers (de Jonge et al., 2014). Other major impacts of global warming and human activity on estuarine systems may include: loss of biodiversity, increased riverbank/coastal erosion, increased fluvial/coastal flooding, and changes in food security.

Focusing on the main objectives of this thesis, three articles were published that address the impact of direct human activity and climate change on estuarine environments. The first publication dealt with sand mining activity in the Tien River branch in the VMD

(see subchapter 6.1). In contrast to previous studies that only relied on low-resolution ADCP measurements (e.g., Brunier et al., 2014) or questionnaires (Bravard et al., 2013) to estimate the intensity of sand extraction in the VMD, a MBES was employed to acquire high-resolution bathymetric datasets during two in-situ campaigns in 2018, thus greatly improving the monitoring/assessment of present-day conditions in the Tien River branch. Ideally, the monitoring of present-day conditions should cover the whole VMD. However, this was unfeasible within the scope of this study due to the time-consuming nature of MBES measurements. As demonstrated by Hackney et al. (2021) and Gruel et al. (Preprint), the analysis of high-resolution satellite imagery may be used in the future to complement MBES measurements, thus ensuring that impacts are monitored on different spatial scales. The main findings of Jordan et al. (2019b) can be summarized as follows:

- (i) By analyzing high-resolution bathymetric maps for a 20 km stretch of the Tien River, local sand mining volumes were estimated to be around  $4.64 \pm 0.31 \text{ Mm}^3/\text{yr}$ .
- (ii) Discrepancies between official statistics and own estimates were identified, indicating the presence of illegal sand extraction, i.e., extraction without valid licenses or the violation of license regulations.
- (iii) The unsustainable nature of the local sand mining was highlighted by comparing own estimates of sand extraction to previously reported values of sand transport for the whole Tien River branch ( $\approx 3.8 \text{ Mt/yr}$ ) by Stephens et al. (2017). With sand extraction substantially larger than the natural sand supply, a deficit is present in the local sand budget.
- (iv) By assessing satellite images of the surveyed section of the Tien River branch, areas of severe riverbank erosion were identified. It is likely that the observed riverbank erosion is directly linked to the unsustainable sand mining activity, identified in the published paper.

The second publication also focused on the surveyed section of the Tien River branch (see subchapter 6.2). For this section, a hydro-morphodynamic model was set up and validated, which was afterwards used for scenario simulations. Nested into a large-scale model of the whole VMD (Manh et al., 2014, 2015), the response of local morphodynamic processes to the main drivers of future changes in the VMD was assessed. For each driver, a plausible scenario for the future period 2050 to 2060 was considered<sup>5</sup>. Using a relatively high resolution of  $\approx 25 \times 50 \text{ m}$  for the Tien River branch, it was unfeasible to investigate multiple future scenarios for each driver. Nevertheless, the combination of individual drivers (hydropower development, sand mining, climate change-induced alterations in

---

<sup>5</sup>For sand mining, two different scenarios were considered: (i) a doubling of present-day extraction rates and (ii) a complete prohibition of sand mining activity.

hydrology, and RSLR) led to a total of 23 future scenarios, which were compared to a baseline scenario (2000 to 2010). Due to the application of such a diverse set of future scenarios, previously unaddressed local impacts of climate change and human activity were assessed. In contrast, earlier studies only concentrated on the future water and sediment fluxes (e.g., Lauri et al., 2012; Kondolf et al., 2014) or salinity intrusion (Smajgl et al., 2015). A previous study, which focused on the response of the Mekong River's morphology to intensified human activity (Tu et al., 2019), did neither consider climate change nor SLR as potential drivers for future changes. The main findings of Jordan et al. (2020) are:

- (i) For the baseline period, the investigated river section is already subject to substantial erosion, as shown by a channel incision of  $-0.13$  m over the course of a single wet season.
- (ii) Hydropower development was identified as the main driver for future erosion in the Tien River, followed by sand mining. Climate change-induced alterations in hydrology will not necessarily amplify erosional trends in the Tien River, but rather lead to a local redistribution of sediments, while the impact of RSLR is only minimal.
- (iii) The complete prohibition of sand mining activity could help to counterbalance the negative impacts of other drivers.
- (iv) Nonlinear processes, which are a result of the interaction of multiple drivers, are projected to amplify erosion processes. For instance, the largest channel incision will occur if future hydropower development coincides with increased sand mining activity and climate change-related alterations in hydrology.

The third publication concentrated on the response of tidal dynamics in the North Sea to SLR, including potential implications for the estuaries of the German rivers Elbe, Weser, and Ems (see subchapter 6.3). By considering bathymetric changes in the Wadden Sea and using a sufficient resolution to resolve intertidal flats, tidal inlets, and channels, relevant processes were addressed that were not included in earlier regional projections (e.g., Pickering et al., 2012; Ward et al., 2012; Pelling et al., 2013a). Additionally, two rates of SLR were combined with five different rates for cumulative vertical accretion in the intertidal flats of the Wadden Sea. Since long-term morphological simulations are computationally demanding, the different rates of vertical accretion were uniformly applied to the regional intertidal areas in order to mimic different plausible scenarios for the future morphological evolution of the Wadden Sea. Transient effects, such as regional variations in the morphological response of intertidal areas to SLR, are thus not covered by the model. In reality, future changes in regional tidal dynamics (e.g., current velocities and M2 amplitudes) will likely exhibit a more complex spatial pattern than shown here. Nevertheless, the investigated scenarios cover the broadest range of plausible projections for future North Sea tidal dynamics to date. By comparing the different scenarios, the un-

certainties in projecting future North Sea tides also become apparent. The main findings of Jordan et al. (2021) can be summarized as follows:

- (i) The response of the constituent M2 is non-linear between a SLR of 0.8 and 2.0 m.
- (ii) Most areas in the North Sea basin show no sensitivity toward the different rates of vertical accretion in the Wadden Sea. For a considered SLR, magnitudes and spatial patterns of M2 amplitude changes remain similar in these regions, irrespective of the morphological evolution of intertidal areas in the Wadden Sea.
- (iii) Along the coasts of the Wadden Sea, but also in remote regions like the Skagerrak, results vary considerably between the different scenarios. In some areas, such as the North Frisian Wadden Sea, the results of M2 amplitude changes can even vary in their sign, depending on the rate of vertical accretion in the Wadden Sea.
- (iv) In the Wadden Sea, the distortion of the tidal wave is also substantially different between the scenarios. If intertidal areas are not able to keep up with SLR, flood dominance will be enhanced (or ebb dominance will be reduced) in the estuaries of the German rivers Elbe, Weser, and Ems. If intertidal flats fully rise with the sea-level, patterns of flood and ebb dominance remain relatively stable in relation to present-day conditions.

## 7.2 Outlook

### 7.2.1 Future research regarding numerical models

In the future, the validated numerical models by Jordan et al. (2020) and Jordan et al. (2021) may be used for further studies. For instance, if new information becomes available regarding global warming and future human activity, model projections can be updated without much effort. Since spatially-varying wind and pressure fields are already included in the hydrodynamic model by Jordan et al. (2021), it may also be used to investigate storm surge impacts. Additional processes may also be implemented in the model, such as wind waves or morphodynamics. Furthermore, more detailed models of the Elbe Estuary, Weser Estuary, Ems Estuary, or individual Wadden Sea tidal basins can be nested into the regional model. Such models could be used to investigate the impact of contemporary and future drivers on the German estuaries in even more detail. Nested models could also be used to assess sediment management strategies (e.g., dredging, nourishment) or identify sediment transport patterns.

## 7.2.2 Potential adaptation strategies

In order to stop the unsustainable extraction of sand and minimize its impacts, a global agenda is needed. As suggested by Bendixen et al. (2019a), such an agenda should include the following components: (i) extraction of sand from sustainable sources, (ii) replacing sand with alternative materials, (iii) reusing of sand-based materials, (iv) reduction of concrete required in new structures, (v) multilateral frameworks for regulation and control of sand extraction, (vi) raising awareness for the issue of sand mining, and (vii) monitoring of global sand extraction activity and sharing of existing data. Sand that is extracted from rivers may be replaced by sand from Greenland in the future, when an abundance of sand will become available due to the melting of the Greenland ice sheet (Bendixen et al., 2019b). Additionally, the extraction of sand that is trapped in reservoirs could make downstream mining less attractive (Bendixen et al., 2019a). While finding suitable substitutes for sand in concrete is still an ongoing field of research, some promising alternatives include: fly ash, copper slag, or even recycled plastic (Koehnken and Rintoul, 2018). Reusing sand-based materials, such as demolition waste, could also minimize the demand for new sand sources. Furthermore, the application of 3D-printing technologies in the construction sector (e.g., Hager et al., 2016) should also help to significantly reduce the consumption of sand. Since current legal frameworks are not sufficient to prevent unsustainable sand extraction, existing standards need to be strengthened, while good-practice guidelines should also be established (UNEP, 2019). In accordance with the principles of raising awareness and sharing existing data, the findings by Jordan et al. (2019b), for example, were published under an open access license. Relevant datasets were also made available via the data repository PANGAEA (<https://www.pangaea.de/>) (Jordan et al., 2019a).

Regarding hydropower expansion, basin-scale strategic planning is needed to minimize the impacts of dam development (Schmitt et al., 2018, 2019). By identifying alternative dam locations and optimizing the sequence of dam construction, the cumulative sediment trapping can be significantly reduced while achieving the same level of power generation (Schmitt et al., 2018, 2019). For example, an optimal development sequence for the Mekong River would only prioritize dam construction in parts of the Upper Mekong that are already disconnected from the delta (Schmitt et al., 2019). An optimal development sequence for the Lower Mekong, where most of the river's future hydropower expansion is planned, should only concentrate on a limited number of mainstem dams with marginal sediment trapping while prioritizing dam construction on tributaries upstream and downstream of existing dams (Schmitt et al., 2019). Since large dams are oftentimes unsuitable for common sediment management options, such as flushing, they might also be replaced by a cascade of smaller dams, thus enabling improved sediment passage (Wild et al., 2016). Using dam designs, which incorporate bottom and mid-level outlets, could also



create flexibility for sediment passage (Kondolf et al., 2018). In addition, fish passage technologies (e.g., fishways, locks, and lifts) might help to mitigate the impacts of dams on fish populations (Dugan et al., 2010). However, fish passages might be unable to cope with the diversity of migrating fish in tropical rivers, such as the Mekong (Dugan et al., 2010). In transboundary river basins, multi-national cooperation is also needed for concerted dam operation, which is imperative for effective sediment and fish passage (Kondolf et al., 2018). Besides the environmental impacts, the social aspects of hydropower development must also be taken into consideration more (Siciliano et al., 2015). Finally, existing regulatory guidelines and standards that ensure best practices for dam development must be promoted more prominently. Following many recommendations by the World Commission on Dams (WCD) (WCD, 2000), the Hydropower Sustainability Assessment Protocol (HSAP) (IHA, 2010) was designed as a practical tool to evaluate the social and environmental aspects of hydropower dams during the planning, construction, and operation stages (Skinner and Haas, 2014). The majority of new hydropower dams, however, still are only subject to national standards (Skinner and Haas, 2014).

As outlined for the YRD, the VMD, and the German Bight, climate change is one of the major future challenges to coastal communities. Besides mitigation efforts to contain global warming, associated risks and possible response options need to be thoroughly assessed. Assessments must include possible changes in vulnerability and exposure (e.g., due to socio-economic growth), in addition to the hazards from future climate change (Nicholls et al., 2021). The robustness of present assessments also has to be critically reviewed by coastal planners, when new information becomes available (Nicholls et al., 2021). Furthermore, proactive adaptation strategies, such as the adaptation pathways approach (e.g., Haasnoot et al., 2013, 2019), are needed to cope with the large uncertainties that are inherent in projections of future runoff, SLR, tidal dynamics, and coastal morphodynamics. Based on a sequence of linked actions, adaptation pathways use a flexible stepwise approach (Haasnoot et al., 2019). Usually starting with a low-regret action when uncertainty is high, subsequent monitoring ensures that tipping points are identified, which signal that a switch to another action is imperative to achieve the overall objective (Haasnoot et al., 2019). In general, responses can be divided into the categories: protection, accommodation, retreat, advance, and ecosystem-based adaptation (Oppenheimer et al., 2019). While protection and accommodation are commonly used options, there is comparatively little experience with retreat and ecosystem-based adaptation (Nicholls et al., 2021). However, as recommended by the IPCC, all options are needed to respond to future climate change (Oppenheimer et al., 2019). As suggested by David (2021), adaptation strategies also must become more flexible to support communities to cope with climate change. Using the VMD as an example, dike construction could be postponed by raising buildings (Radhakrishnan et al., 2018). In addition, the restoration of mangroves could help to reduce flood risks (Gijsman et al., 2021), while salt-tolerant rice crops should



be adopted to ensure food production (Paik et al., 2020). Finally, no-build zones may be considered as an option of planned retreat (Haasnoot et al., 2019). Focusing on coastal protection in the German Bight, ecosystem-based adaptation may be used to complement the existing infrastructure (David, 2021). Furthermore, flexible climate profiles, which include a reserve for future construction, should be considered when reinforcing dike infrastructure (Hofstede et al., 2019). To increase the resilience of the Wadden Sea against SLR, the amount and location of sand nourishments may also need future adjustment to ensure sufficient sediment supply (Hofstede, 2015; Wang et al., 2018). Other options may include: the enlargement of tidal basins by means of dike relocation or the expansion of brushwood groin fields to prevent erosion (Hofstede, 2015). By retaining water during flood and strengthening the ebb flow, flood retention basins may be used to counterbalance the increasing flood dominance in the German estuaries (Donner et al., 2012). Other options that were recently explored for the Ems, such as a controlled storm surge barrier operation (Oberrecht and Wurpts, 2014), cannot easily be transferred to other estuaries (e.g., the Elbe Estuary and Weser Estuary).

## References

- Agardy, T., Alder, J., Dayton, P., Curran, S., Kitchingman, A., Wilson, M., et al. (2005). Coastal Systems. In *Ecosystems and Human Well-being: Current State and Trends, Volume 1*, eds. R. Hassan, R. Scholes, and N. Ash (Washington: Island Press). 513–549.
- Alferi, L., Bisselink, B., Dottori, F., Naumann, G., de Roo, A., Salamon, P., et al. (2017). Global projections of river flood risk in a warmer world. *Earth's Future* 5, 171–182, doi:10.1002/2016EF000485
- Amos, C. L. (1995). Siliciclastic Tidal Flats. In *Geomorphology and Sedimentology of Estuaries*, ed. G. M. E. Perillo (Amsterdam: Elsevier), Developments in Sedimentology 53. 273–306, doi:10.1016/S0070-4571(05)80030-5
- Anderson, E. P. and Veilleux, J. C. (2016). Cultural costs of tropical dams. *Science* 352, 159, doi:10.1126/science.352.6282.159
- Ansar, A., Flyvbjerg, B., Budzier, A., and Lunn, D. (2014). Should we build more large dams? The actual costs of hydropower megaproject development. *Energy Policy* 69, 43–56, doi:10.1016/j.enpol.2013.10.069
- Anthony, E. J., Brunier, G., Besset, M., Goichot, M., Dussouillez, P., and Nguyen, V. L. (2015). Linking rapid erosion of the Mekong River delta to human activities. *Scientific Reports* 5:14745, doi:10.1038/srep14745
- Arias, M. E., Cochrane, T. A., Kumm, M., Lauri, H., Holtgrieve, G. W., Koponen, J., et al. (2014). Impacts of hydropower and climate change on drivers of ecological productivity of Southeast Asia's most important wetland. *Ecological Modelling* 272, 252–263, doi:10.1016/j.ecolmodel.2013.10.015
- Arnell, N. W. and Gosling, S. N. (2016). The impacts of climate change on river flood risk at the global scale. *Climatic Change* 134, 387–401, doi:10.1007/s10584-014-1084-5
- Arns, A., Dangendorf, S., Jensen, J., Talke, S., Bender, J., and Pattiaratchi, C. (2017). Sea-level rise induced amplification of coastal protection design heights. *Scientific Reports* 7:40171, doi:10.1038/srep40171
- Arns, A., Wahl, T., Dangendorf, S., and Jensen, J. (2015). The impact of sea level rise on storm surge water levels in the northern part of the German Bight. *Coastal Engineering* 96, 118–131, doi:10.1016/j.coastaleng.2014.12.002
- Ashworth, P. J., Best, J. L., and Parsons, D. R. (2015). Preface. In *Fluvial-Tidal Sedimentology*, eds. P. J. Ashworth, J. L. Best, and D. R. Parsons (Amsterdam: Elsevier), Developments in Sedimentology 68. xxi–xxii, doi:10.1016/B978-0-444-63529-7.09985-5
- Baoligao, B., Xu, F., Chen, X., Wang, X., and Chen, W. (2016). Acute impacts of reservoir sediment flushing on fishes in the Yellow River. *Journal of Hydro-environment Research* 13, 26–35, doi:10.1016/j.jher.2015.11.003
- Barbier, E. B., Hacker, S. D., Kennedy, C., Koch, E. W., Stier, A. C., and Silliman, B. R. (2011). The value of estuarine and coastal ecosystem services. *Ecological Monographs* 81, 169–193, doi:10.1890/10-1510.1

- Basson, G. (2008). *Reservoir sedimentation – an overview of global sedimentation rates, sediment yield and sediment deposition prediction* (Bern: The International Workshop on Erosion, Transport and Deposition of Sediments).
- Becherer, J., Hofstede, J., Gräwe, U., Purkiani, K., Schulz, E., and Burchard, H. (2018). The Wadden Sea in transition - consequences of sea level rise. *Ocean Dynamics* 68, 131–151, doi:10.1007/s10236-017-1117-5
- Behre, K.-E. (2003). Eine neue Meeresspiegelkurve für die südliche Nordsee. Transgressionen und Regressionen in den letzten 10.000 Jahren. *Probleme der Küstenforschung im südlichen Nordseegebiet* 28, 9–63.
- Bendixen, M., Best, J., Hackney, C., and Iversen, L. L. (2019a). Time is running out for sand. *Nature* 571, 29–31, doi:10.1038/d41586-019-02042-4
- Bendixen, M., Overeem, I., Rosing, M. T., Bjørk, A. A., Kjær, K. H., Kroon, A., et al. (2019b). Promises and perils of sand exploitation in Greenland. *Nature Sustainability* 2, 98–104, doi:10.1038/s41893-018-0218-6
- Benninghoff, M. and Winter, C. (2019). Recent morphologic evolution of the German Wadden Sea. *Scientific Reports* 9:9293, doi:10.1038/s41598-019-45683-1
- Bernauer, D. and Jansen, W. (2006). Recent invasions of alien macroinvertebrates and loss of native species in the upper Rhine River, Germany. *Aquatic Invasions* 1, 55–71, doi:10.3391/ai.2006.1.2.2
- Best, J. (2019). Anthropogenic stresses on the world's big rivers. *Nature Geoscience* 12, 7–21, doi:10.1038/s41561-018-0262-x
- BfG (2008). *WSV Sedimentmanagement Tideelbe, Strategien und Potenziale – eine Systemstudie. Ökologische Auswirkungen der Umlagerung von Wedeler Baggergut* (Koblenz: German Federal Institute of Hydrology (German: Bundesanstalt für Gewässerkunde) (BfG)).
- Bi, N., Wang, H., and Yang, Z. (2014). Recent changes in the erosion–accretion patterns of the active Huanghe (Yellow River) delta lobe caused by human activities. *Continental Shelf Research* 90, 70–78, doi:10.1016/j.csr.2014.02.014
- Biemans, H., Haddeland, I., Kabat, P., Ludwig, F., Hutjes, R. W. A., Heinke, J., et al. (2011). Impact of reservoirs on river discharge and irrigation water supply during the 20th century. *Water Resources Research* 47:W03509, doi:10.1029/2009WR008929
- Bindoff, N. L., Stott, P. A., AchutaRao, K. M., Allen, M. R., Gillett, N., Gutzler, D., et al. (2013). Detection and Attribution of Climate Change: from Global to Regional. In *Climate Change 2013: The Physical Science Basis. Contribution of Working Group I to the Fifth Assessment Report of the Intergovernmental Panel on Climate Change*, eds. T. F. Stocker, D. Qin, G.-K. Plattner, M. Tignor, S. K. Allen, J. Boschung, et al. (Cambridge: Cambridge University Press). 867–952.
- Binh, D. V., Kantoush, S., and Sumi, T. (2020). Changes to long-term discharge and sediment loads in the Vietnamese Mekong Delta caused by upstream dams. *Geomorphology* 353:107011, doi:10.1016/j.geomorph.2019.107011
- Bisht, A. (2021). Conceptualizing sand extractivism: Deconstructing an emerging resource frontier. *The Extractive Industries and Society* 8:100904, doi:10.1016/j.exis.2021.100904

- Bjørnø, L. (2017). *Applied Underwater Acoustics* (Amsterdam: Elsevier).
- Boehlich, M. J. and Strotmann, T. (2008). The Elbe Estuary. *Die Küste* 74, 288–306.
- Bormann, H. (2010). Runoff regime changes in German rivers due to climate change. *Erdkunde* 64, 257–279, doi:10.3112/erdkunde.2010.03.04
- Bormann, H., Pinter, N., and Elfert, S. (2011). Hydrological signatures of flood trends on German rivers: Flood frequencies, flood heights and specific stages. *Journal of Hydrology* 404, 50–66, doi:10.1016/j.jhydrol.2011.04.019
- Bosboom, J. and Stive, M. J. F. (2021). *Coastal Dynamics* (Delft: Delft University of Technology), doi:10.5074/T.2021.001
- Bravard, J.-P., Goichot, M., and Gaillot, S. (2013). Geography of Sand and Gravel Mining in the Lower Mekong River. *EchoGéo* 26:13659, doi:10.4000/echogeo.13659
- Brunier, G., Anthony, E. J., Goichot, M., Provansal, M., and Dussouillez, P. (2014). Recent morphological changes in the Mekong and Bassac river channels, Mekong delta: The marked impact of river-bed mining and implications for delta destabilisation. *Geomorphology* 224, 177–191, doi:10.1016/j.geomorph.2014.07.009
- Bungenstock, F. and Schäfer, A. (2009). The Holocene relative sea-level curve for the tidal basin of the barrier island Langeoog, German Bight, Southern North Sea. *Global and Planetary Change* 66, 34–51, doi:10.1016/j.gloplacha.2008.07.007
- Burchard, H. and Baumert, H. (1998). The Formation of Estuarine Turbidity Maxima Due to Density Effects in the Salt Wedge. A Hydrodynamic Process Study. *Journal of Physical Oceanography* 28, 309–321, doi:10.1175/1520-0485(1998)028<0309:TFOETM>2.0.CO;2
- Burchard, H., Flöser, G., Staneva, J. V., Badewien, T. H., and Riethmüller, R. (2008). Impact of Density Gradients on Net Sediment Transport into the Wadden Sea. *Journal of Physical Oceanography* 38, 566–587, doi:10.1175/2007JPO3796.1
- Burchard, H. and Hetland, R. D. (2010). Quantifying the Contributions of Tidal Straining and Gravitational Circulation to Residual Circulation in Periodically Stratified Tidal Estuaries. *Journal of Physical Oceanography* 40, 1243–1262, doi:10.1175/2010JPO4270.1
- Burchard, H., Schuttelaars, H. M., and Ralston, D. K. (2018). Sediment Trapping in Estuaries. *Annual Review of Marine Science* 10, 371–395, doi:10.1146/annurev-marine-010816-060535
- Cameron, W. M. and Pritchard, D. W. (1963). Estuaries. In *The Sea, Volume 2: The Composition of Sea-Water; Comparative and Descriptive Oceanography*, ed. M. N. Hill (New York: John Wiley & Sons). 306–324.
- Campbell, I. C. (2012). Biodiversity of the Mekong Delta. In *The Mekong Delta System. Interdisciplinary Analyses of a River Delta*, eds. F. G. Renaud and C. Kuenzer (Dordrecht: Springer), Springer Environmental Science and Engineering. 293–313, doi:10.1007/978-94-007-3962-8\_11
- Chen, X., Chen, S., Dong, P., and Li, X. (2008). Temporal and spatial evolution of the coastal profiles along the Yellow River Delta over last three decades. *GeoJournal* 71, 185–199, doi:10.1007/s10708-008-9155-7
- Chen, Y., Syvitski, J. P. M., Gao, S., Overeem, I., and Kettner, A. J. (2012). Socio-economic Impacts on Flooding: A 4000-Year History of the Yellow River, China. *AMBIO* 41, 682–698,



- doi:10.1007/s13280-012-0290-5
- Chen, Y., Wang, K., Lin, Y., Shi, W., Song, Y., and He, X. (2015). Balancing green and grain trade. *Nature Geoscience* 8, 739–741, doi:10.1038/ngeo2544
- Costanza, R., d'Arge, R., de Groot, R., Farber, S., Grasso, M., Hannon, B., et al. (1997). The value of the world's ecosystem services and natural capital. *Nature* 387, 253–260, doi:10.1038/387253a0
- CWSS (2021a). *Convention and nomination*. Common Wadden Sea Secretariat (CWSS). Available online at: <https://waddensea-worldheritage.org/convention-and-nomination> (accessed July 26, 2021).
- CWSS (2021b). *One Wadden Sea. One Global Heritage*. CWSS. Available online at: <https://www.waddensea-worldheritage.org/one-wadden-sea-one-global-heritage> (accessed July 26, 2021).
- Dai, A., Qian, T., Trenberth, K. E., and Milliman, J. D. (2009). Changes in Continental Freshwater Discharge from 1948 to 2004. *Journal of Climate* 22, 2773–2792, doi:10.1175/2008JCLI2592.1
- Dalrymple, R. W., Zaitlin, B. A., and Boyd, R. (1992). Estuarine facies models; conceptual basis and stratigraphic implications. *Journal of Sedimentary Research* 62, 1130–1146, doi:10.1306/D4267A69-2B26-11D7-8648000102C1865D
- Dangendorf, S., Hay, C., Calafat, F. M., Marcos, M., Piecuch, C. G., Berk, K., et al. (2019). Persistent acceleration in global sea-level rise since the 1960s. *Nature Climate Change* 9, 705–710, doi:10.1038/s41558-019-0531-8
- Dangendorf, S., Marcos, M., Wöppelmann, G., Conrad, C. P., Frederikse, T., and Riva, R. (2017). Reassessment of 20th century global mean sea level rise. *Proceedings of the National Academy of Sciences of the United States of America* 114, 5946–5951, doi:10.1073/pnas.1616007114
- Darby, S. E., Hackney, C. R., Leyland, J., Kumm, M., Lauri, H., Parsons, D. R., et al. (2016). Fluvial sediment supply to a mega-delta reduced by shifting tropical-cyclone activity. *Nature* 539, 276–279, doi:10.1038/nature19809
- David, C. G. (2021). *From coastal protection to "low-regret" coastal adaptation. Changing perspectives on impacts and risk assessment when dealing with sea level rise (PhD thesis)* (Hannover: Gottfried Wilhelm Leibniz Universität Hannover).
- Davies, J. L. (1964). A morphogenic approach to world shorelines. *Zeitschrift für Geomorphologie* 8, 127–142, doi:10.1127/zfg/mortensen/8/1964/127
- de Jonge, V. N., Schuttelaars, H. M., van Beusekom, J. E. E., Talke, S. A., and de Swart, H. E. (2014). The influence of channel deepening on estuarine turbidity levels and dynamics, as exemplified by the Ems estuary. *Estuarine, Coastal and Shelf Science* 139, 46–59, doi:10.1016/j.ecss.2013.12.030
- Dee, D. P., Uppala, S. M., Simmons, A. J., Berrisford, P., Poli, P., Kobayashi, S., et al. (2011). The ERA-Interim reanalysis: configuration and performance of the data assimilation system. *Quarterly Journal of the Royal Meteorological Society* 137, 553–597, doi:10.1002/qj.828
- Deltares (2020). *Delft3D-FLOW. Simulation of multi-dimensional hydrodynamic flows and transport phenomena, including sediments. User Manual. Hydro-Morphodynamics* (Delft: Deltares).
- Dissanayake, D. M. P. K., Ranasinghe, R., and Roelvink, J. A. (2012). The morphological response of large tidal inlet/basin systems to relative sea level rise. *Climatic Change* 113, 253–276,

- doi:10.1007/s10584-012-0402-z
- Donnelly, C., Greuell, W., Andersson, J., Gerten, D., Pisacane, G., Roudier, P., et al. (2017). Impacts of climate change on European hydrology at 1.5, 2 and 3 degrees mean global warming above preindustrial level. *Climatic Change* 143, 13–26, doi:10.1007/s10584-017-1971-7
- Donner, M., Ladage, F., and Stoschek, O. (2012). *Impact and retention potential of tidal polders in an estuary with high suspended sediment concentrations* (Orlando: Proceedings of the 10th International Conference on Hydrosience and Engineering).
- Douville, H., Raghavan, K., Renwick, J., Allan, R. P., Arias, P. A., Barlow, M., et al. (2021). Water Cycle Changes. In *Climate Change 2021: The Physical Science Basis. Contribution of Working Group I to the Sixth Assessment Report of the Intergovernmental Panel on Climate Change*, eds. V. Masson-Delmotte, P. Zhai, A. Pirani, S. L. Connors, C. Péan, S. Berger, et al. (Cambridge: Cambridge University Press).
- Dugan, P. J., Barlow, C., Agostinho, A. A., Baran, E., Cada, G. F., Chen, D., et al. (2010). Fish Migration, Dams, and Loss of Ecosystem Services in the Mekong Basin. *AMBIO* 39, 344–348, doi:10.1007/s13280-010-0036-1
- Dyer, K. R. (1997). *Estuaries. A Physical Introduction, 2nd Edition* (Chichester: John Wiley & Sons).
- Eisma, D., Mook, W. G., and Laban, C. (1981). An Early Holocene Tidal Flat in the Southern Bight. In *Holocene Marine Sedimentation in the North Sea Basin*, eds. S.-D. Nio, R. T. E. Schüttenhelm, and T. C. E. Van Weering (Oxford: Blackwell Scientific Publications). 229–237, doi:10.1002/9781444303759.ch17
- Elias, E. P. L., van der Spek, A. J. F., Wang, Z. B., and de Ronde, J. (2012). Morphodynamic development and sediment budget of the Dutch Wadden Sea over the last century. *Netherlands Journal of Geosciences* 91, 293–310, doi:10.1017/S0016774600000457
- Engelund, F. and Hansen, E. (1967). *A monograph on sediment transport in alluvial streams* (Copenhagen: Technical University of Denmark).
- Erban, L. E., Gorelick, S. M., and Zebker, H. A. (2014). Groundwater extraction, land subsidence, and sea-level rise in the Mekong Delta, Vietnam. *Environmental Research Letters* 9:084010, doi:10.1088/1748-9326/9/8/084010
- Eslami, S., Hoekstra, P., Kernkamp, H. W. J., Trung, N. N., Duc, D. D., Nghia, H. N., et al. (2021). Dynamics of salt intrusion in the Mekong Delta: results of field observations and integrated coastal-inland modelling. *Earth Surface Dynamics* 9, 953–976, doi:10.5194/esurf-9-953-2021
- Eslami, S., Hoekstra, P., Trung, N. N., Kantoush, S. A., Doan, V. B., Do, D. D., et al. (2019). Tidal amplification and salt intrusion in the Mekong Delta driven by anthropogenic sediment starvation. *Scientific Reports* 9:18746, doi:10.1038/s41598-019-55018-9
- Fairbridge, R. W. (1980). The Estuary: Its Definition and Geodynamic Cycle. In *Chemistry and Biogeochemistry of Estuaries*, eds. E. Olausson and I. Cato (Chichester: John Wiley & Sons). 1–35.
- Farr, H. K. (1980). Multibeam bathymetric sonar: Sea beam and hydro chart. *Marine Geodesy* 4, 77–93, doi:10.1080/15210608009379375

- Fitch, S., Thomson, K., and Gaffney, V. (2005). Late Pleistocene and Holocene depositional systems and the palaeogeography of the Dogger Bank, North Sea. *Quaternary Research* 64, 185–196, doi:10.1016/j.yqres.2005.03.007
- Flöser, G., Burchard, H., and Riethmüller, R. (2011). Observational evidence for estuarine circulation in the German Wadden Sea. *Continental Shelf Research* 31, 1633–1639, doi:10.1016/j.csr.2011.03.014
- Fox-Kemper, B., Hewitt, H. T., Xiao, C., Aðalgeirsdóttir, G., Drijfhout, S. S., Edwards, T. L., et al. (2021). Ocean, Cryosphere and Sea Level Change. In *Climate Change 2021: The Physical Science Basis. Contribution of Working Group I to the Sixth Assessment Report of the Intergovernmental Panel on Climate Change*, eds. V. Masson-Delmotte, P. Zhai, A. Pirani, S. L. Connors, C. Péan, S. Berger, et al. (Cambridge: Cambridge University Press).
- Frei, C., Whitney, R., Schiffer, H.-W., Rose, K., Rieser, D. A., Al-Qahtani, A., et al. (2013). *World Energy Scenarios. Composing energy futures to 2050* (London: World Energy Council).
- Friedrichs, C. T. (2011). Tidal Flat Morphodynamics: A Synthesis. In *Treatise on Estuarine and Coastal Science. Volume 3: Estuarine and Coastal Geology and Geomorphology*, eds. B. W. Fleming and J. D. Hansom (London: Academic Press). 137–170, doi:10.1016/B978-0-12-374711-2.00307-7
- Friedrichs, C. T. and Aubrey, D. G. (1988). Non-linear tidal distortion in shallow well-mixed estuaries: a synthesis. *Estuarine, Coastal and Shelf Science* 27, 521–545, doi:10.1016/0272-7714(88)90082-0
- Fritsch, U., Zebisch, M., Voß, M., Linsenmeier, M., Kahlenborn, W., Porst, L., et al. (2021). *Klimawirkungs- und Risikoanalyse 2021 für Deutschland. Teilbericht 3: Risiken und Anpassung im Cluster Wasser* (Dessau-Roßlau: German Environment Agency (German: Umweltbundesamt) (UBA)).
- Galloway, W. E. (1975). Process Framework for Describing the Morphologic and Stratigraphic Evolution of Deltaic Depositional Systems. In *Deltas: Models for Exploration*, ed. M. L. Broussard (Houston: Houston Geological Society). 87–98.
- Gavriletea, M. D. (2017). Environmental Impacts of Sand Exploitation. Analysis of Sand Market. *Sustainability* 9:1118, doi:10.3390/su9071118
- GEBCO Compilation Group (2021). *GEBCO 2021 Grid*. Global Bathymetry Chart of the Oceans (GEBCO). doi: 10.5285/c6612cbe-50b3-0cff-e053-6c86abc09f8f (accessed September 26, 2021).
- Geyer, W. R. (1997). Influence of Wind on Dynamics and Flushing of Shallow Estuaries. *Estuarine, Coastal and Shelf Science* 44, 713–722, doi:10.1006/ecss.1996.0140
- Geyer, W. R. and MacCready, P. (2014). The Estuarine Circulation. *Annual Review of Fluid Mechanics* 46, 175–197, doi:10.1146/annurev-fluid-010313-141302
- Gijssman, R., Horstman, E. M., van der Wal, D., Friess, D. A., Swales, A., and Wijnberg, K. M. (2021). Nature-Based Engineering: A Review on Reducing Coastal Flood Risk With Mangroves. *Frontiers in Marine Science* 8:702412, doi:10.3389/fmars.2021.702412
- Grabemann, I. and Krause, G. (2001). On different time scales of suspended matter dynamics in the Weser estuary. *Estuaries* 24, 688–698, doi:10.2307/1352877



- Grabemann, I., Uncles, R. J., Krause, G., and Stephens, J. A. (1997). Behaviour of Turbidity Maxima in the Tamar (U.K.) and Weser (F.R.G.) Estuaries. *Estuarine, Coastal and Shelf Science* 45, 235–246, doi:10.1006/ecss.1996.0178
- Green, J. A. M. (2010). Ocean tides and resonance. *Ocean Dynamics* 60, 1243–1253, doi:10.1007/s10236-010-0331-1
- Gregory, J. M., Griffies, S. M., Hughes, C. W., Lowe, J. A., Church, J. A., Fukumori, I., et al. (2019). Concepts and Terminology for Sea Level: Mean, Variability and Change, Both Local and Global. *Surveys in Geophysics* 40, 1251–1289, doi:10.1007/s10712-019-09525-z
- Grill, G., Lehner, B., Lumsdon, A. E., MacDonald, G. K., Zarfl, C., and Reidy Liermann, C. (2015). An index-based framework for assessing patterns and trends in river fragmentation and flow regulation by global dams at multiple scales. *Environmental Research Letters* 10:015001, doi:10.1088/1748-9326/10/1/015001
- Grinsted, A., Jevrejeva, S., Riva, R. E. M., and Dahl-Jensen, D. (2015). Sea level rise projections for northern Europe under RCP8.5. *Climate Research* 64, 15–23, doi:10.3354/cr01309
- Gross, M. (2016). A global megadam mania. *Current Biology* 26, 779–782, doi:10.1016/j.cub.2016.08.050
- Gruel, C.-R., Park, E., Ho, H. L., Kantoush, S., Feng, L., Binh, D. V., et al. (Preprint). New systemically measured sand mining budget for the Mekong Delta reveals rising trends and significant volume underestimations. *EarthArXiv*, doi:10.31223/X5H61H
- GSO (2021). *Statistical Yearbook of Viet Nam 2020* (Hanoi: General Statistics Office of Vietnam (GSO)).
- Gugliotta, M., Saito, Y., Nguyen, V. L., Ta, T. K. O., Nakashima, R., Tamura, T., et al. (2017). Process regime, salinity, morphological, and sedimentary trends along the fluvial to marine transition zone of the mixed-energy Mekong River delta, Vietnam. *Continental Shelf Research* 147, 7–26, doi:10.1016/j.csr.2017.03.001
- Guilcher, A. (1958). *Coastal and Submarine Morphology* (London: Meuthen and Co.).
- Gundlach, J., Zorndt, A., van Prooijen, B. C., and Wang, Z. B. (2021). Two-Channel System Dynamics of the Outer Weser Estuary—A Modeling Study. *Journal of Marine Science and Engineering* 9:448, doi:10.3390/jmse9040448
- Haasnoot, M., Brown, S., Scussolini, P., Jimenez, J. A., Vafeidis, A. T., and Nicholls, R. J. (2019). Generic adaptation pathways for coastal archetypes under uncertain sea-level rise. *Environmental Research Communications* 1:071006, doi:10.1088/2515-7620/ab1871
- Haasnoot, M., Kwakkel, J. H., Walker, W. E., and ter Maat, J. (2013). Dynamic adaptive policy pathways: A method for crafting robust decisions for a deeply uncertain world. *Global Environmental Change* 23, 485–498, doi:10.1016/j.gloenvcha.2012.12.006
- Hackney, C. R., Darby, S. E., Parsons, D. R., Leyland, J., Best, J. L., Aalto, R., et al. (2020). River bank instability from unsustainable sand mining in the lower Mekong River. *Nature Sustainability* 3, 217–225, doi:10.1038/s41893-019-0455-3
- Hackney, C. R., Vasilopoulos, G., Heng, S., Darbari, V., Walker, S., and Parsons, D. R. (2021). Sand mining far outpaces natural supply in a large alluvial river. *Earth Surface Dynamics* 9,

- 1323–1334, doi:10.5194/esurf-9-1323-2021
- Hagen, R., Plüß, A., Ihde, R., Freund, J., Dreier, N., Nehlsen, E., et al. (2021). An integrated marine data collection for the German Bight – Part 2: Tides, salinity, and waves (1996–2015). *Earth System Science Data* 13, 2573–2594, doi:10.5194/essd-13-2573-2021
- Hager, I., Golonka, A., and Putanowicz, R. (2016). 3D Printing of Buildings and Building Components as the Future of Sustainable Construction? *Procedia Engineering* 151, 292–299, doi:10.1016/j.proeng.2016.07.357
- Haigh, I. D., Pickering, M. D., Green, J. A. M., Arbic, B. K., Arns, A., Dangendorf, S., et al. (2020). The Tides They Are A-Changin’: A Comprehensive Review of Past and Future Nonastronomical Changes in Tides, Their Driving Mechanisms, and Future Implications. *Reviews of Geophysics* 58:e2018RG000636, doi:10.1029/2018RG000636
- Hansen, D. V. and Rattray Jr., M. (1965). Gravitational Circulation in Straits and Estuaries. *Journal of Marine Research* 23, 104–122.
- Hansen, D. V. and Rattray Jr., M. (1966). New dimensions in estuary classification. *Limnology and Oceanography* 11, 319–326, doi:10.4319/lo.1966.11.3.0319
- Hattermann, F. F., Huang, S., Burghoff, O., Hoffmann, P., and Kundzewicz, Z. W. (2016). Brief Communication: An update of the article “Modelling flood damages under climate change conditions – a case study for Germany”. *Natural Hazards and Earth System Sciences* 16, 1617–1622, doi:10.5194/nhess-16-1617-2016
- Hattermann, F. F., Huang, S., and Koch, H. (2015). Climate change impacts on hydrology and water resources. *Meteorologische Zeitschrift* 24, 201–211, doi:10.1127/metz/2014/0575
- Hendershott, M. C. and Speranza, A. (1971). Co-oscillating tides in long, narrow bays; the Taylor problem revisited. *Deep Sea Research and Oceanographic Abstracts* 18, 959–980, doi:10.1016/0011-7471(71)90002-7
- Hensengerth, O. (2015). Where is the power? Transnational networks, authority and the dispute over the Xayaburi Dam on the Lower Mekong Mainstream. *Water International* 40, 911–928, doi:10.1080/02508060.2015.1088334
- Herrling, G. and Winter, C. (2014). Morphological and sedimentological response of a mixed-energy barrier island tidal inlet to storm and fair-weather conditions. *Earth Surface Dynamics* 2, 363–382, doi:10.5194/esurf-2-363-2014
- Herrling, G. and Winter, C. (2015). Tidally- and wind-driven residual circulation at the multiple-inlet system East Frisian Wadden Sea. *Continental Shelf Research* 106, 45–59, doi:10.1016/j.csr.2015.06.001
- Higgins, S., Overeem, I., Tanaka, A., and Syvitski, J. P. M. (2013). Land subsidence at aquaculture facilities in the Yellow River delta, China. *Geophysical Research Letters* 40, 3898–3902, doi:10.1002/grl.50758
- Hirabayashi, Y., Mahendran, R., Koirala, S., Konoshima, L., Yamazaki, D., Watanabe, S., et al. (2013). Global flood risk under climate change. *Nature Climate Change* 3, 816–821, doi:10.1038/nclimate1911
- Hofstede, J. (2002). Morphologic responses of Wadden Sea tidal basins to a rise in tidal water

- levels and tidal range. *Zeitschrift für Geomorphologie* 46, 93–108, doi:10.1127/zfg/46/2002/93
- Hofstede, J., Matelski, B., and Stock, M. (2019). Schleswig-Holsteins Klima-Anpassungsstrategie für das Wattenmeer 2100. *Die Küste* 87, 19–38, doi:10.18171/1.087102
- Hofstede, J. L. A. (2015). Theoretical considerations on how Wadden Sea tidal basins may react to accelerated sea level rise. *Zeitschrift für Geomorphologie* 59, 377–391, doi:10.1127/zfg/2014/0163
- Hofstede, J. L. A., Becherer, J., and Burchard, H. (2018). Are Wadden Sea tidal systems with a higher tidal range more resilient against sea level rise? *Journal of Coastal Conservation* 22, 71–78, doi:10.1007/s11852-016-0469-1
- Hori, K., Saito, Y., Zhao, Q., and Wang, P. (2002). Architecture and evolution of the tide-dominated Changjiang (Yangtze) River delta, China. *Sedimentary Geology* 146, 249–264, doi:10.1016/S0037-0738(01)00122-1
- Howarth, M. J. (1990). *Atlas of tidal elevations and currents around the British Isles. Offshore Technology Report OTH 89 293* (London: Department of Energy).
- HPA (2015). *Deutsches Gewässerkundliches Jahrbuch. Elbegebiet, Teil III. Untere Elbe ab der Havelmündung. 2013* (Hamburg: Freie und Hansestadt Hamburg, Hamburg Port Authority (HPA)).
- Huang, S., Krysanova, V., and Hattermann, F. (2015). Projections of climate change impacts on floods and droughts in Germany using an ensemble of climate change scenarios. *Regional Environmental Change* 15, 461–473, doi:10.1007/s10113-014-0606-z
- Huang, S., Kumar, R., Rakovec, O., Aich, V., Wang, X., Samaniego, L., et al. (2018). Multimodel assessment of flood characteristics in four large river basins at global warming of 1.5, 2.0 and 3.0 K above the pre-industrial level. *Environmental Research Letters* 13:124005, doi:10.1088/1748-9326/aae94b
- Huthnance, J., Weisse, R., Wahl, T., Thomas, H., Pietrzak, J., Souza, A. J., et al. (2016). Recent Change—North Sea. In *North Sea Region Climate Change Assessment*, eds. M. Quante and F. Colijn (Cham: Springer Open), Regional Climate Studies. 85–136, doi:10.1007/978-3-319-39745-0\_3
- Huthnance, J. M. (1991). Physical oceanography of the North Sea. *Ocean and Shoreline Management* 16, 199–231, doi:10.1016/0951-8312(91)90005-M
- ICES (1983). *Flushing times of the North Sea. Cooperative Research Report No. 123* (Copenhagen: International Council for the Exploration of the Sea (ICES)), doi:10.17895/ices.pub.5521
- ICOLD (2021a). *General Synthesis*. ICOLD. Available online at: [https://www.icold-cigb.org/article/GB/world\\_register/general\\_synthesis/general-synthesis](https://www.icold-cigb.org/article/GB/world_register/general_synthesis/general-synthesis) (accessed June 06, 2021).
- ICOLD (2021b). *Number of Dams by Country Members*. ICOLD. Available online at: [https://www.icold-cigb.org/article/GB/world\\_register/general\\_synthesis/number-of-dams-by-country-members](https://www.icold-cigb.org/article/GB/world_register/general_synthesis/number-of-dams-by-country-members) (accessed June 06, 2021).
- IHA (2010). *Hydropower Sustainability Assessment Protocol* (London: International Hydropower Association (IHA)).
- Jay, D. A. and Musiak, J. D. (1994). Particle trapping in estuarine tidal flows. *Journal of Geophys-*

- ical Research: Oceans* 99, 20445–20461, doi:10.1029/94JC00971
- Jensen, J. (1984). *Änderungen der mittleren Tidewasserstände an der Nordseeküste. Mitteilungen des Leichtweiß-Instituts für Wasserbau der Technischen Universität Braunschweig, Heft 83* (Braunschweig: Leichtweiß Institut für Wasserbau).
- Ji, G., Lai, Z., Xia, H., Liu, H., and Wang, Z. (2021). Future Runoff Variation and Flood Disaster Prediction of the Yellow River Basin Based on CA-Markov and SWAT. *Land* 10:421, doi:10.3390/land10040421
- Jordan, C., Lojek, O., Schlurmann, T., Wu, G., and Liang, B. (2016). *Field Measurements of Estuarine Circulation in the Yellow River (Huanghe) Estuary* (Qingdao: 8th Chinese-German Joint Symposium on Hydraulic and Ocean Engineering).
- Jordan, C., Tiede, J., Lojek, O., Visscher, J., Apel, H., Nguyen, H. Q., et al. (2019a). Digital elevation models showing sand mining activities within the Tien River branch, Vietnamese Mekong Delta. *PANGAEA*, doi:10.1594/PANGAEA.909665
- Jordan, C., Tiede, J., Lojek, O., Visscher, J., Apel, H., Nguyen, H. Q., et al. (2019b). Sand mining in the Mekong Delta revisited - current scales of local sediment deficits. *Scientific Reports* 9:17823, doi:10.1038/s41598-019-53804-z
- Jordan, C., Visscher, J., Dung, N. V., Apel, H., and Schlurmann, T. (2020). Impacts of Human Activity and Global Changes on Future Morphodynamics within the Tien River, Vietnamese Mekong Delta. *Water* 12:2204, doi:10.3390/w12082204
- Jordan, C., Visscher, J., and Schlurmann, T. (2021). Projected Responses of Tidal Dynamics in the North Sea to Sea-Level Rise and Morphological Changes in the Wadden Sea. *Frontiers in Marine Science* 8:685758, doi:10.3389/fmars.2021.685758
- Jänicke, L., Ebener, A., Dangendorf, S., Arns, A., Schindelegger, M., Niehüser, S., et al. (2021). Assessment of Tidal Range Changes in the North Sea From 1958 to 2014. *Journal of Geophysical Research: Oceans* 126:e2020JC016456, doi:10.1029/2020JC016456
- Kappenberg, J. and Fanger, H.-U. (2007). *Sedimenttransportgeschehen in der tidebeeinflussten Elbe, der Deutschen Bucht und in der Nordsee* (Geesthacht: GKSS-Forschungszentrum Geesthacht).
- Kappenberg, J. and Grabemann, I. (2001). Variability of the mixing zones and estuarine turbidity maxima in the Elbe and Weser estuaries. *Estuaries* 24, 699–706, doi:10.2307/1352878
- Katsman, C. A., Sterl, A., Beersma, J. J., van den Brink, H. W., Church, J. A., Hazeleger, W., et al. (2011). Exploring high-end scenarios for local sea level rise to develop flood protection strategies for a low-lying delta—the Netherlands as an example. *Climatic Change* 109, 617–645, doi:10.1007/s10584-011-0037-5
- Kausch, H. and Michaelis, W. (eds.) (1996). *Suspended Particulate Matter in Rivers and Estuaries. Proceedings of an International Symposium held at Reinbek near Hamburg, Germany*. Advances in Limnology 47 (Stuttgart: E. Schweizerbart'sche Verlagsbuchhandlung (Nägele u. Obermiller)).
- Kennish, M. J. (2017). Estuaries: Anthropogenic Impacts. In *Encyclopedia of Coastal Science*, eds. C. W. Finkl and C. Makowski (Cham: Springer), Encyclopedia of Earth Sciences Series.

- doi:10.1007/978-3-319-48657-4\_140-2
- Khojasteh, D., Chen, S., Felder, S., Heimhuber, V., and Glamore, W. (2021). Estuarine tidal range dynamics under rising sea levels. *PLoS ONE* 16:e0257538, doi:10.1371/journal.pone.0257538
- Kim, S.-S. and Wessel, P. (2008). Directional median filtering for regional-residual separation of bathymetry. *Geochemistry, Geophysics, Geosystems* 9:Q03005, doi:10.1029/2007GC001850
- Kingston, D. G., Thompson, J. R., and Kite, G. (2011). Uncertainty in climate change projections of discharge for the Mekong River Basin. *Hydrology and Earth System Sciences* 15, 1459–1471, doi:10.5194/hess-15-1459-2011
- Koehnken, L. and Rintoul, M. (2018). *Impacts of Sand Mining on Ecosystem Structure, Process and Biodiversity in Rivers* (Gland: World Wide Fund for Nature (WWF)).
- Kondolf, G. M. (1997). PROFILE: Hungry Water: Effects of Dams and Gravel Mining on River Channels. *Environmental Management* 21, 533–551, doi:10.1007/s002679900048
- Kondolf, G. M., Rubin, Z. K., and Minear, J. T. (2014). Dams on the Mekong: Cumulative sediment starvation. *Water Resources Research* 50, 5158–5169, doi:10.1002/2013WR014651
- Kondolf, G. M., Schmitt, R. J. P., Carling, P., Darby, S., Arias, M., Bizzi, S., et al. (2018). Changing sediment budget of the Mekong: Cumulative threats and management strategies for a large river basin. *Science of the Total Environment* 625, 114–134, doi:10.1016/j.scitotenv.2017.11.361
- Kopp, R. E., DeConto, R. M., Bader, D. A., Hay, C. C., Horton, R. M., Kulp, S., et al. (2017). Evolving Understanding of Antarctic Ice-Sheet Physics and Ambiguity in Probabilistic Sea-Level Projections. *Earth's Future* 5, 1217–1233, doi:10.1002/2017EF000663
- Kopp, R. E., Horton, R. M., Little, C. M., Mitrovica, J. X., Oppenheimer, M., Rasmussen, D. J., et al. (2014). Probabilistic 21st and 22nd century sea-level projections at a global network of tide-gauge sites. *Earth's Future* 2, 383–406, doi:10.1002/2014EF000239
- Korzun, V. I., Sokolow, A. A., Budyko, M. I., Voskresensky, K. P., Kalininin, G. P., Konoplyantsev, A. A., et al. (eds.) (1978). *World Water Balance and Water Resources of the Earth* (Paris: UNESCO).
- Krebs, M. and Weilbeer, H. (2008). Ems-Dollart Estuary. *Die Küste* 74, 252–262.
- Krone, R. B. (1962). *Flume studies of the transport of sediment in estuarial shoaling processes* (Berkeley: Hydraulic Engineering Laboratory, University of California).
- Kuenzer, C., Campbell, I., Roch, M., Leinenkugel, P., Tuan, V. Q., and Dech, S. (2013). Understanding the impact of hydropower developments in the context of upstream–downstream relations in the Mekong river basin. *Sustainability Science* 8, 565–584, doi:10.1007/s11625-012-0195-z
- Kuenzer, C., Heimhuber, V., Day, J., Varis, O., Bucx, T., Renaud, F., et al. (2020). Profiling resilience and adaptation in mega deltas: A comparative assessment of the Mekong, Yellow, Yangtze, and Rhine deltas. *Ocean & Coastal Management* 198:105362, doi:10.1016/j.ocecoaman.2020.105362
- Kuenzer, C., Ottinger, M., Liu, G., Sun, B., Baumhauer, R., and Dech, S. (2014). Earth observation-based coastal zone monitoring of the Yellow River Delta: Dynamics in China's second largest oil producing region over four decades. *Applied Geography* 55, 92–107, doi:10.1016/j.apgeog.2014.08.015

- Kulp, S. A. and Strauss, B. H. (2019). New elevation data triple estimates of global vulnerability to sea-level rise and coastal flooding. *Nature Communications* 10:4844, doi:10.1038/s41467-019-12808-z
- Kummu, M., Lu, X. X., Rasphone, A., Sarkkula, J., and Koponen, J. (2008). Riverbank changes along the Mekong River: Remote sensing detection in the Vientiane–Nong Khai area. *Quaternary International* 186, 100–112, doi:10.1016/j.quaint.2007.10.015
- Kummu, M., Lu, X. X., Wang, J. J., and Varis, O. (2010). Basin-wide sediment trapping efficiency of emerging reservoirs along the Mekong. *Geomorphology* 119, 181–197, doi:10.1016/j.geomorph.2010.03.018
- Lange, D., Müller, H., Piechotta, F., and Schubert, R. (2008). The Weser Estuary. *Die Küste* 74, 275–287.
- Latapie, A., Camenen, B., Rodrigues, S., Paquier, A., Bouchard, J. P., and Moatar, F. (2014). Assessing channel response of a long river influenced by human disturbance. *CATENA* 121, 1–12, doi:10.1016/j.catena.2014.04.017
- Lauri, H., de Moel, H., Ward, P. J., Räsänen, T. A., Keskinen, M., and Kummu, M. (2012). Future changes in Mekong River hydrology: impact of climate change and reservoir operation on discharge. *Hydrology and Earth System Sciences* 16, 4603–4619, doi:10.5194/hess-16-4603-2012
- Lebreton, L. C. M., van der Zwet, J., Damsteeg, J.-W., Slat, B., Andradý, A., and Reisser, J. (2017). River plastic emissions to the world's oceans. *Nature Communications* 8:15611, doi:10.1038/ncomms15611
- Lee, J. Y., Marotzke, J., Bala, G., Cao, L., Corti, S., Dunne, J. P., et al. (2021). Future Global Climate: Scenario-Based Projections and Near-Term Information. In *Climate Change 2021: The Physical Science Basis. Contribution of Working Group I to the Sixth Assessment Report of the Intergovernmental Panel on Climate Change*, eds. V. Masson-Delmotte, P. Zhai, A. Pirani, S. L. Connors, C. Péan, S. Berger, et al. (Cambridge: Cambridge University Press).
- Lehner, F., Wood, A. W., Vano, J. A., Lawrence, D. M., Clark, M. P., and Mankin, J. S. (2019). The potential to reduce uncertainty in regional runoff projections from climate models. *Nature Climate Change* 9, 926–933, doi:10.1038/s41558-019-0639-x
- Leng, G., Huang, M., Tang, Q., and Leung, L. R. (2015). A modeling study of irrigation effects on global surface water and groundwater resources under a changing climate. *Journal of Advances in Modeling Earth Systems* 7, 1285–1304, doi:10.1002/2015MS000437
- Lerczak, J. A. and Geyer, W. R. (2004). Modeling the Lateral Circulation in Straight, Stratified Estuaries. *Journal of Physical Oceanography* 34, 1410–1428, doi:10.1175/1520-0485(2004)034<1410:MTLCIS>2.0.CO;2
- Lesser, G. R., Roelvink, J. A., van Kester, J. A. T. M., and Stelling, G. S. (2004). Development and validation of a three-dimensional morphological model. *Coastal Engineering* 51, 883–915, doi:10.1016/j.coastaleng.2004.07.014
- Li, X., Liu, J. P., Saito, Y., and Nguyen, V. L. (2017). Recent evolution of the Mekong Delta and the impacts of dams. *Earth-Science Reviews* 175, 1–17, doi:10.1016/j.earscirev.2017.10.008
- Liu, G. H. and Drost, H. J. (1997). *Atlas of the Yellow River* (Beijing: The Publishing House of

- Surveying and Mapping).
- Liu, S., Lu, P., Liu, D., Jin, P., and Wang, W. (2009). Pinpointing the sources and measuring the lengths of the principal rivers of the world. *International Journal of Digital Earth* 2, 80–87, doi:10.1080/17538940902746082
- Liu, S. M. (2015). Response of nutrient transports to water–sediment regulation events in the Huanghe basin and its impact on the biogeochemistry of the Bohai. *Journal of Marine Systems* 141, 59–70, doi:10.1016/j.jmarsys.2014.08.008
- LLUR (2014). *Deutsches Gewässerkundliches Jahrbuch. Küstengebiet der Nordsee. 2013* (Flintbek: State Agency for Agriculture, the Environment and Rural Areas (German: Landesamt für Landwirtschaft, Umwelt und ländliche Räume) (LLUR)).
- Lojek, O. (2019). *Sensitivity analysis of single storm surges in the Jade-Weser Estuary (PhD thesis)* (Hannover: Gottfried Wilhelm Leibniz Universität Hannover), doi:10.15488/9331
- Lotze, H. K., Reise, K., Worm, B., van Beusekom, J., Busch, M., Ehlers, A., et al. (2005). Human transformations of the Wadden Sea ecosystem through time: a synthesis. *Helgoland Marine Research* 59, 84–95, doi:10.1007/s10152-004-0209-z
- Lowe, J. A., Howard, T. P., Pardaens, A., Tinker, J., Holt, J., Wakelin, S., et al. (2009). *UK Climate Projections science report: Marine and coastal projections* (Exeter: Met Office Hadley Centre).
- Lu, X. X., Zhang, S. R., Xie, S. P., and Ma, P. K. (2007). Rapid channel incision of the lower Pearl River (China) since the 1990s as a consequence of sediment depletion. *Hydrology and Earth System Sciences* 11, 1897–1906, doi:10.5194/hess-11-1897-2007
- Luijendijk, A., Hagenaars, G., Ranasinghe, R., Baart, F., Donchyts, G., and Aarninkhof, S. (2018). The State of the World's Beaches. *Scientific Reports* 8:6641, doi:10.1038/s41598-018-24630-6
- Lurton, X. (2002). *An Introduction to Underwater Acoustics. Principles and Applications*. Geophysical Sciences (Berlin: Springer).
- Magilligan, F. J., Sneddon, C. S., and Fox, C. A. (2017). The era of big dam building: It ain't over till it's over. In *The Politics of Fresh Water: Access, conflict and identity*, eds. C. M. Ashcraft and T. Mayer (Abingdon: Routledge). 78–97.
- Malcherek, A. (2010). *Gezeiten und Wellen. Die Hydromechanik der Küstengewässer* (Wiesbaden: Vieweg+Teubner), doi:10.1007/978-3-8348-9764-0
- Manh, N. V., Dung, N. V., Hung, N. N., Kummu, M., Merz, B., and Apel, H. (2015). Future sediment dynamics in the Mekong Delta floodplains: Impacts of hydropower development, climate change and sea level rise. *Global and Planetary Change* 127, 22–33, doi:10.1016/j.gloplacha.2015.01.001
- Manh, N. V., Dung, N. V., Hung, N. N., Merz, B., and Apel, H. (2014). Large-scale suspended sediment transport and sediment deposition in the Mekong Delta. *Hydrology and Earth System Sciences* 18, 3033–3053, doi:10.5194/hess-18-3033-2014
- Mawdsley, R. J., Haigh, I. D., and Wells, N. C. (2015). Global secular changes in different tidal high water, low water and range levels. *Earth's Future* 3, 66–81, doi:10.1002/2014EF000282
- Miatto, A., Schandl, H., Fishman, T., and Tanikawa, H. (2017). Global Patterns and Trends for Non-Metallic Minerals used for Construction. *Journal of Industrial Ecology* 21, 924–937,

- doi:10.1111/jiec.12471
- Milliman, J. D. and Farnsworth, K. L. (2011). *River Discharge to the Coastal Ocean. A Global Synthesis* (Cambridge: Cambridge University Press), doi:10.1017/CBO9780511781247
- Milliman, J. D. and Meade, R. H. (1983). World-Wide Delivery of River Sediment to the Oceans. *The Journal of Geology* 91, 1–21, doi:10.1086/628741
- Minderhoud, P. S. J., Coumou, L., Erkens, G., Middelkoop, H., and Stouthamer, E. (2019). Mekong delta much lower than previously assumed in sea-level rise impact assessments. *Nature Communications* 10:3847, doi:10.1038/s41467-019-11602-1
- Minderhoud, P. S. J., Erkens, G., Pham, V. H., Bui, V. T., Erban, L., Kooi, H., et al. (2017). Impacts of 25 years of groundwater extraction on subsidence in the Mekong delta, Vietnam. *Environmental Research Letters* 12:064006, doi:10.1088/1748-9326/aa7146
- Miyazawa, N., Sunada, K., and Sokhem, P. (2008). Bank erosion in the Mekong River Basin: Is bank erosion in my town caused by the activities of my neighbors? In *Modern myths of the Mekong. A critical review of water and development concepts, principles and policies*, eds. M. Kummu, M. Keskinen, and O. Varis (Helsinki: Helsinki University of Technology). 19–26.
- Molle, F., Mollinga, P. P., and Wester, P. (2009). Hydraulic Bureaucracies and the Hydraulic Mission: Flows of Water, Flows of Power. *Water Alternatives* 2, 328–349.
- MRC (2010). *State of the Basin Report 2010* (Vientiane: MRC).
- Murray, N. J., Phinn, S. R., DeWitt, M., Ferrari, R., Johnston, R., Lyons, M. B., et al. (2019). The global distribution and trajectory of tidal flats. *Nature* 565, 222–225, doi:10.1038/s41586-018-0805-8
- Müller, M., Arbic, B. K., and Mitrovica, J. X. (2011). Secular trends in ocean tides: Observations and model results. *Journal of Geophysical Research: Oceans* 116:C05013, doi:10.1029/2010JC006387
- Nhan, N. H. (2016). Tidal regime deformation by sea level rise along the coast of the Mekong Delta. *Estuarine, Coastal and Shelf Science* 183, 382–391, doi:10.1016/j.ecss.2016.07.004
- Nicholls, R. J., Hanson, S. E., Lowe, J. A., Slangen, A. B. A., Wahl, T., Hinkel, J., et al. (2021). Integrating new sea-level scenarios into coastal risk and adaptation assessments: An ongoing process. *WIREs Climate Change* 12:e706, doi:10.1002/wcc.706
- Nichols, M. M. and Biggs, R. B. (1985). Estuaries. In *Coastal Sedimentary Environments. Second Revised, Expanded Edition*, ed. R. A. Davis Jr. (New York: Springer). 77–186, doi:10.1007/978-1-4612-5078-4\_2
- Nittrouer, C. A., Mullarney, J. C., Allison, M. A., and Ogston, A. S. (2017). Introduction to the Special Issue on Sedimentary Processes Building a Tropical Delta Yesterday, Today, and Tomorrow: The Mekong System. *Oceanography* 30, 10–21, doi:10.5670/oceanog.2017.310
- Nittrouer, J. A., Allison, M. A., and Campanella, R. (2008). Bedform transport rates for the lowermost Mississippi River. *Journal of Geophysical Research: Earth Surface* 113:F03004, doi:10.1029/2007JF000795
- NLWKN (2015). *Deutsches Gewässerkundliches Jahrbuch. Weser- und Emsgebiet. 2013* (Norden: Lower Saxony Water Management, Coastal Protection and Nature Conservation Agency)



- (German: Niedersächsischer Landesbetrieb für Wasserwirtschaft, Küsten- und Naturschutz) (NLWKN)).
- Nowacki, D. J., Ogston, A. S., Nittrouer, C. A., Fricke, A. T., and Van, P. D. T. (2015). Sediment dynamics in the lower Mekong River: Transition from tidal river to estuary. *Journal of Geophysical Research: Oceans* 120, 6363–6383, doi:10.1002/2015JC010754
- Oberrecht, D. (2020). *Development of a numerical modeling approach for large-scale fluid mud flow in estuarine environments (PhD thesis)* (Hannover: Gottfried Wilhelm Leibniz Universität Hannover), doi:10.15488/10488
- Oberrecht, D. and Wurpts, A. (2014). Impact of Controlled Tidal Barrier Operation on Tidal Dynamics in the Ems Estuary. *Die Küste* 81, 427–433.
- OECD (2018). *Global Material Resources Outlook to 2060: Economic Drivers and Environmental Consequences* (Paris: OECD Publishing), doi:10.1787/9789264307452-en
- Oki, T., Agata, Y., Kanae, S., Saruhashi, T., Yang, D., and Musiake, K. (2001). Global assessment of current water resources using total runoff integrating pathways. *Hydrological Sciences Journal* 46, 983–995, doi:10.1080/02626660109492890
- Oppenheimer, M., Glavovic, B. C., Hinkel, J., van de Wal, R., Magnan, A. K., Abd-Elgawad, A., et al. (2019). Sea Level Rise and Implications for Low-Lying Islands, Coasts and Communities. In *IPCC Special Report on the Ocean and Cryosphere in a Changing Climate*, eds. H.-O. Pörtner, D. C. Roberts, V. Masson-Delmotte, P. Zhai, M. Tignor, E. Poloczanska, et al. (Cambridge: Cambridge University Press). 321–445.
- Paik, S., Le, D. T. P., Nhu, L. T., and Mills, B. F. (2020). Salt-tolerant rice variety adoption in the Mekong River Delta: Farmer adaptation to sea-level rise. *PLoS ONE* 15:e0229464, doi:10.1371/journal.pone.0229464
- Palmer, M. A., Reidy Liermann, C. A., Nilsson, C., Flörke, M., Alcamo, J., Lake, P. S., et al. (2008). Climate change and the world's river basins: anticipating management options. *Frontiers in Ecology and the Environment* 6, 81–89, doi:10.1890/060148
- Papenmeier, S., Schrottke, K., Bartholomä, A., and Flemming, B. W. (2013). Sedimentological and Rheological Properties of the Water–Solid Bed Interface in the Weser and Ems Estuaries, North Sea, Germany: Implications for Fluid Mud Classification. *Journal of Coastal Research* 29, 797–808, doi:10.2112/JCOASTRES-D-11-00144.1
- Partheniades, E. (1965). Erosion and Deposition of Cohesive Soils. *Journal of the Hydraulics Division* 91, 105–139, doi:10.1061/JYCEAJ.0001165
- Peduzzi, P. (2014). Sand, rarer than one thinks. *Environmental Development* 11, 208–218, doi:10.1016/j.envdev.2014.04.001
- Pein, J. U., Stanev, E. V., and Zhang, Y. J. (2014). The tidal asymmetries and residual flows in Ems Estuary. *Ocean Dynamics* 64, 1719–1741, doi:10.1007/s10236-014-0772-z
- Pelling, H. E., Green, J. A. M., and Ward, S. L. (2013a). Modelling tides and sea-level rise: To flood or not to flood. *Ocean Modelling* 63, 21–29, doi:10.1016/j.ocemod.2012.12.004
- Pelling, H. E., Uehara, K., and Green, J. A. M. (2013b). The impact of rapid coastline changes and sea level rise on the tides in the Bohai Sea, China. *Journal of Geophysical Research: Oceans*



- 118, 3462–3472, doi:10.1002/jgrc.20258
- Peying, L., Jun, Y., Lejun, L., and Mingzuo, F. (1999). Vulnerability assessment of the Yellow River Delta to predicted climate change and sea level rise. In *Vulnerability assessment of two major wetlands in the Asia-Pacific region to climate change and sea level rise. Supervising Scientist Report 149*, eds. R. A. Dam, C. M. Finlayson, and D. Watkins (Darwin: Supervising Scientist). 7–73.
- Phan, L. K., van Thiel de Vries, J. S. M., and Stive, M. J. F. (2015). Coastal Mangrove Squeeze in the Mekong Delta. *Journal of Coastal Research* 31, 233–243, doi:10.2112/JCOASTRES-D-14-00049.1
- Pickering, M. D., Horsburgh, K. J., Blundell, J. R., Hirschi, J. J.-M., Nicholls, R. J., Verlaan, M., et al. (2017). The impact of future sea-level rise on the global tides. *Continental Shelf Research* 142, 50–68, doi:10.1016/j.csr.2017.02.004
- Pickering, M. D., Wells, N. C., Horsburgh, K. J., and Green, J. A. M. (2012). The impact of future sea-level rise on the European Shelf tides. *Continental Shelf Research* 35, 1–15, doi:10.1016/j.csr.2011.11.011
- Postma, H. (1961). Transport and accumulation of suspended matter in the Dutch Wadden Sea. *Netherlands Journal of Sea Research* 1, 148–190, doi:10.1016/0077-7579(61)90004-7
- Pritchard, D. W. (1952). Estuarine Hydrography. *Advances in Geophysics* 1, 243–280, doi:10.1016/S0065-2687(08)60208-3
- Pritchard, D. W. (1955). Estuarine circulation patterns. *Proceedings of the American Society of Civil Engineers* 81, 1–11.
- Pugh, D. T. (1987). *Tides, Surges and Mean Sea-Level* (Chichester: John Wiley & Sons).
- Radhakrishnan, M., Nguyen, H. Q., Gersonius, B., Pathirana, A., Vinh, K. Q., Ashley, R. M., et al. (2018). Coping capacities for improving adaptation pathways for flood protection in Can Tho, Vietnam. *Climatic Change* 149, 29–41, doi:10.1007/s10584-017-1999-8
- Rasquin, C., Seiffert, R., Wachler, B., and Winkel, N. (2020). The significance of coastal bathymetry representation for modelling the tidal response to mean sea level rise in the German Bight. *Ocean Science* 16, 31–44, doi:10.5194/os-16-31-2020
- Ray, R. D. and Talke, S. A. (2019). Nineteenth-Century Tides in the Gulf of Maine and Implications for Secular Trends. *Journal of Geophysical Research: Oceans* 124, 7046–7067, doi:10.1029/2019JC015277
- Redmond, G., Hodges, K. I., Mcsweeney, C., Jones, R., and Hein, D. (2015). Projected changes in tropical cyclones over Vietnam and the South China Sea using a 25 km regional climate model perturbed physics ensemble. *Climate Dynamics* 45, 1983–2000, doi:10.1007/s00382-014-2450-8
- Renard, V. and Allenou, J.-P. (1979). Sea Beam, Multi-Beam Echo-Sounding in "Jean Charcot" - Description, Evaluation and First Results. *The International Hydrographic Review* 56, 35–67.
- Renaud, F. G. and Kuenzer, C. (2012). Introduction. In *The Mekong Delta System. Interdisciplinary Analyses of a River Delta*, eds. F. G. Renaud and C. Kuenzer (Dordrecht: Springer), Springer Environmental Science and Engineering. 3–5, doi:10.1007/978-94-007-3962-8
- Richter, B. D., Postel, S., Revenga, C., Scudder, T., Lehner, B., Churchill, A., et al. (2010). Lost in

- Development's Shadow: The Downstream Human Consequences of Dams. *Water Alternatives* 3, 14–42.
- Rienecker, M. M. and Teubner, M. D. (1980). A note on frictional effects in Taylor's problem. *Journal of Marine Research* 38, 183–191.
- Roache, P. J. (1997). Quantification of uncertainty in computational fluid dynamics. *Annual Review of Fluid Mechanics* 29, 123–160, doi:10.1146/annurev.fluid.29.1.123
- Roelvink, D. and Reniers, A. (2011). *A Guide to Modeling Coastal Morphology*. Advances in Coastal and Ocean Engineering: Volume 12 (Singapore: World Scientific), doi:10.1142/7712
- Roelvink, J. A. (2006). Coastal morphodynamic evolution techniques. *Coastal Engineering* 53, 277–287, doi:10.1016/j.coastaleng.2005.10.015
- Rolinski, S. and Eichweber, G. (2000). Deformations of the Tidal Wave in the Elbe Estuary and their Effect on Suspended Particulate Matter Dynamics. *Physics and Chemistry of the Earth, Part B: Hydrology, Oceans and Atmosphere* 25, 355–358, doi:10.1016/S1464-1909(00)00025-3
- Roos, P. C., Velema, J. J., Hulscher, S. J. M. H., and Stolk, A. (2011). An idealized model of tidal dynamics in the North Sea: resonance properties and response to large-scale changes. *Ocean Dynamics* 61, 2019–2035, doi:10.1007/s10236-011-0456-x
- Rovere, A., Stocchi, P., and Vacchi, M. (2016). Eustatic and Relative Sea Level Changes. *Current Climate Change Reports* 2, 221–231, doi:10.1007/s40641-016-0045-7
- Räsänen, T. A. and Kummu, M. (2013). Spatiotemporal influences of ENSO on precipitation and flood pulse in the Mekong River Basin. *Journal of Hydrology* 476, 154–168, doi:10.1016/j.jhydrol.2012.10.028
- Räsänen, T. A., Someth, P., Lauri, H., Koponen, J., Sarkkula, J., and Kummu, M. (2017). Observed river discharge changes due to hydropower operations in the Upper Mekong Basin. *Journal of Hydrology* 545, 28–41, doi:10.1016/j.jhydrol.2016.12.023
- Räsänen, T. A., Varis, O., Scherer, L., and Kummu, M. (2018). Greenhouse gas emissions of hydropower in the Mekong River Basin. *Environmental Research Letters* 13:034030, doi:10.1088/1748-9326/aaa817
- Schindelegger, M., Green, J. A. M., Wilmes, S.-B., and Haigh, I. D. (2018). Can We Model the Effect of Observed Sea Level Rise on Tides? *Journal of Geophysical Research: Oceans* 123, 4593–4609, doi:10.1029/2018JC013959
- Schmidt, C., Krauth, T., and Wagner, S. (2017). Export of Plastic Debris by Rivers into the Sea. *Environmental Science & Technology* 51, 12246–12253, doi:10.1021/acs.est.7b02368
- Schmitt, R. J. P., Bizzi, S., Castelletti, A., and Kondolf, G. M. (2018). Improved trade-offs of hydropower and sand connectivity by strategic dam planning in the Mekong. *Nature Sustainability* 1, 96–104, doi:10.1038/s41893-018-0022-3
- Schmitt, R. J. P., Bizzi, S., Castelletti, A., Opperman, J. J., and Kondolf, G. M. (2019). Planning dam portfolios for low sediment trapping shows limits for sustainable hydropower in the Mekong. *Science Advances* 5:eaaw2175, doi:10.1126/sciadv.aaw2175
- Schrottke, K., Becker, M., Bartholomä, A., Flemming, B. W., and Hebbeln, D. (2006). Fluid mud dynamics in the Weser estuary turbidity zone tracked by high-resolution side-scan sonar and

- parametric sub-bottom profiler. *Geo-Marine Letters* 26, 185–198, doi:10.1007/s00367-006-0027-1
- Schwarzer, K., Ricklefs, K., Bartholomä, A., and Zeiler, M. (2008). Geological Development of the North Sea and the Baltic Sea. *Die Küste* 74, 1–17.
- Seedorf, H. H. and Meyer, H.-H. (1992). *Landeskunde Niedersachsen. Band 1: Historische Grundlagen und naturräumliche Ausstattung* (Neumünster: Wachholtz Verlag).
- Seneviratne, S. I., Zhang, X., Adnan, M., Badi, W., Dereczynski, C., Di Luca, A., et al. (2021). Weather and Climate Extreme Events in a Changing Climate. In *Climate Change 2021: The Physical Science Basis. Contribution of Working Group I to the Sixth Assessment Report of the Intergovernmental Panel on Climate Change*, eds. V. Masson-Delmotte, P. Zhai, A. Pirani, S. L. Connors, C. Péan, S. Berger, et al. (Cambridge: Cambridge University Press).
- Siciliano, G., Urban, F., Kim, S., and Lonn, P. D. (2015). Hydropower, social priorities and the rural–urban development divide: The case of large dams in Cambodia. *Energy Policy* 86, 273–285, doi:10.1016/j.enpol.2015.07.009
- Siebert, S., Kummu, M., Porkka, M., Döll, P., Ramankutty, N., and Scanlon, B. R. (2015). A global data set of the extent of irrigated land from 1900 to 2005. *Hydrology and Earth System Sciences* 19, 1521–1545, doi:10.5194/hess-19-1521-2015
- Simpson, M., Breili, K., Kierulf, H. P., Lysaker, D., Ouassou, M., and Haug, E. (2012). *Estimates of Future Sea-Level Changes for Norway. Technical Report of the Norwegian Mapping Authority* (Hønefoss: Norwegian Mapping Authority).
- Skinner, J. and Haas, L. J. (2014). *Watered down? A review of social and environmental safeguards for large dam projects. Natural Resource Issues No. 28* (London: International Institute for Environment and Development (IIED)).
- Smajgl, A., Toan, T. Q., Nhan, D. K., Ward, J., Trung, N. H., Tri, L. Q., et al. (2015). Responding to rising sea levels in the Mekong Delta. *Nature Climate Change* 5, 167–174, doi:10.1038/nclimate2469
- Smith, D. E., Harrison, S., Firth, C. R., and Jordan, J. T. (2011). The early Holocene sea level rise. *Quaternary Science Reviews* 30, 1846–1860, doi:10.1016/j.quascirev.2011.04.019
- Speckhann, G. A., Kreibich, H., and Merz, B. (2021). Inventory of dams in Germany. *Earth System Science Data* 13, 731–740, doi:10.5194/essd-13-731-2021
- Stanev, E. V., Flemming, B. W., Bartholomä, A., Staneva, J. V., and Wolff, J.-O. (2007). Vertical circulation in shallow tidal inlets and back-barrier basins. *Continental Shelf Research* 27, 798–831, doi:10.1016/j.csr.2006.11.019
- Stephens, J. D., Allison, M. A., Di Leonardo, D. R., Weathers III, H. D., Ogston, A. S., McLachlan, R. L., et al. (2017). Sand dynamics in the Mekong River channel and export to the coastal ocean. *Continental Shelf Research* 147, 38–50, doi:10.1016/j.csr.2017.08.004
- Sturt, F., Garrow, D., and Bradley, S. (2013). New models of North West European Holocene palaeogeography and inundation. *Journal of Archaeological Science* 40, 3963–3976, doi:10.1016/j.jas.2013.05.023
- Sutherland, J. (2019). *Model types*. Available online at: [http://www.coastalwiki.org/wiki/Model\\_](http://www.coastalwiki.org/wiki/Model_)

- types (accessed August 04, 2021).
- Syvitski, J. P. M., Kettner, A. J., Overeem, I., Hutton, E. W. H., Hannon, M. T., Brakenridge, G. R., et al. (2009). Sinking deltas due to human activities. *Nature Geoscience* 2, 681–686, doi:10.1038/ngeo629
- Syvitski, J. P. M., Vörösmarty, C. J., Kettner, A. J., and Green, P. (2005). Impact of Humans on the Flux of Terrestrial Sediment to the Global Coastal Ocean. *Science* 308, 376–380, doi:10.1126/science.1109454
- Ta, T. K. O., Nguyen, V. L., Tateishi, M., Kobayashi, I., Tanabe, S., and Saito, Y. (2002). Holocene delta evolution and sediment discharge of the Mekong River, southern Vietnam. *Quaternary Science Reviews* 21, 1807–1819, doi:10.1016/S0277-3791(02)00007-0
- Taylor, G. I. (1922). Tidal Oscillations in Gulfs and Rectangular Basins. *Proceedings of the London Mathematical Society* s2-20, 148–181, doi:10.1112/plms/s2-20.1.148
- Tessler, Z. D., Vörösmarty, C. J., Overeem, I., and Syvitski, J. P. M. (2018). A model of water and sediment balance as determinants of relative sea level rise in contemporary and future deltas. *Geomorphology* 305, 209–220, doi:10.1016/j.geomorph.2017.09.040
- Toan, T. Q. (2014). Climate Change and Sea Level Rise in the Mekong Delta: Flood, Tidal Inundation, Salinity Intrusion, and Irrigation Adaptation Methods. In *Coastal Disasters and Climate Change in Vietnam. Engineering and Planning Perspectives*, eds. N. D. Thao, H. Takagi, and M. Esteban (Amsterdam: Elsevier). 199–218, doi:10.1016/B978-0-12-800007-6.00009-5
- Torres, A., Simoni, M. U., Keiding, J. K., Müller, D. B., zu Ermgassen, S. O. S. E., Liu, J., et al. (2021). Sustainability of the global sand system in the Anthropocene. *One Earth* 4, 639–650, doi:10.1016/j.oneear.2021.04.011
- Try, S., Tanaka, S., Tanaka, K., Sayama, T., Hu, M., Sok, T., et al. (2020). Projection of extreme flood inundation in the Mekong River basin under 4K increasing scenario using large ensemble climate data. *Hydrological Processes* 34, 4350–4364, doi:10.1002/hyp.13859
- Tu, L. X., Thanh, V. Q., Reynolds, J., Van, S. P., Anh, D. T., Dang, T. D., et al. (2019). Sediment transport and morphodynamical modeling on the estuaries and coastal zone of the Vietnamese Mekong Delta. *Continental Shelf Research* 186, 64–76, doi:10.1016/j.csr.2019.07.015
- UN (2015). *General Assembly Resolution A/RES/70/1. Transforming Our World, the 2030 Agenda for Sustainable Development* (New York: UN).
- UNEP (2019). *Sand and sustainability: Finding new solutions for environmental governance of global sand resources* (Geneva: GRID-Geneva, United Nations Environment Programme (UNEP)).
- UNEP-DHI and UNEP (2016). *Transboundary River Basins: Status and Trends* (Nairobi: UNEP).
- UNSD (2021). *UN Comtrade Database*. United Nations Statistics Division (UNSD). Available online at: <https://comtrade.un.org/data/> (accessed August 12, 2021).
- Valle-Levinson, A. (2010). Definition and classification of estuaries. In *Contemporary Issues in Estuarine Physics*, ed. A. Valle-Levinson (Cambridge: Cambridge University Press). 1–11, doi:10.1017/CBO9780511676567.002
- van der Spek, A. J. F. (1994). *Large-scale evolution of Holocene tidal basins in the Netherlands*

- (*PhD thesis*) (Utrecht: Universiteit Utrecht).
- van der Wegen, M. (2013). Numerical modeling of the impact of sea level rise on tidal basin morphodynamics. *Journal of Geophysical Research: Earth Surface* 118, 447–460, doi:10.1002/jgrf.20034
- Van Goor, M. A., Zitman, T. J., Wang, Z. B., and Stive, M. J. F. (2003). Impact of sea-level rise on the morphological equilibrium state of tidal inlets. *Marine Geology* 202, 211–227, doi:10.1016/S0025-3227(03)00262-7
- van Rijn, L. C. (2007). Unified View of Sediment Transport by Currents and Waves. I: Initiation of Motion, Bed Roughness, and Bed-Load Transport. *Journal of Hydraulic Engineering* 133, 649–667, doi:10.1061/(ASCE)0733-9429(2007)133:6(649)
- van Rijn, L. C., Roelvink, J. A., and ter Horst, W. (2001). *Approximation formulae for sand transport by currents and waves and implementation in DELFT-MOR* (Delft: Delft Hydraulics).
- Van Straaten, L. M. J. U. and Kuenen, P. H. (1957). Accumulation of fine grained sediments in the Dutch Wadden Sea. *Geologie en Mijnbouw* 19, 329–354.
- Vörösmarty, C. J., Green, P., Salisbury, J., and Lammers, R. B. (2000). Global Water Resources: Vulnerability from Climate Change and Population Growth. *Science* 289, 284–288, doi:10.1126/science.289.5477.284
- Vörösmarty, C. J., Meybeck, M., Fekete, B., Sharma, K., Green, P., and Syvitski, J. P. M. (2003). Anthropogenic sediment retention: major global impact from registered river impoundments. *Global and Planetary Change* 39, 169–190, doi:10.1016/S0921-8181(03)00023-7
- Wachler, B., Seiffert, R., Rasquin, C., and Kösters, F. (2020). Tidal response to sea level rise and bathymetric changes in the German Wadden Sea. *Ocean Dynamics* 70, 1033–1052, doi:10.1007/s10236-020-01383-3
- Wahl, T., Haigh, I. D., Woodworth, P. L., Albrecht, F., Dillingh, D., Jensen, J., et al. (2013). Observed mean sea level changes around the North Sea coastline from 1800 to present. *Earth-Science Reviews* 124, 51–67, doi:10.1016/j.earscirev.2013.05.003
- Wahl, T., Jensen, J., Frank, T., and Haigh, I. D. (2011). Improved estimates of mean sea level changes in the German Bight over the last 166 years. *Ocean Dynamics* 61, 701–715, doi:10.1007/s10236-011-0383-x
- Walling, D. E. (2009). *The Impact of Global Change on Erosion and Sediment Transport by Rivers: Current Progress and Future Challenges* (Paris: UNESCO).
- Wang, G., Zhang, J., Jin, J., Weinberg, J., Bao, Z., Liu, C., et al. (2017a). Impacts of climate change on water resources in the Yellow River basin and identification of global adaptation strategies. *Mitigation and Adaptation Strategies for Global Change* 22, 67–83, doi:10.1007/s11027-015-9664-x
- Wang, H., Bi, N., Saito, Y., Wang, Y., Sun, X., Zhang, J., et al. (2010a). Recent changes in sediment delivery by the Huanghe (Yellow River) to the sea: Causes and environmental implications in its estuary. *Journal of Hydrology* 391, 302–313, doi:10.1016/j.jhydrol.2010.07.030
- Wang, H., Bi, N., Wang, Y., Saito, Y., and Yang, Z. (2010b). Tide-modulated hyperpycnal flows off the Huanghe (Yellow River) mouth, China. *Earth Surface Processes and Landforms* 35, 1315–



- 1329, doi:10.1002/esp.2032
- Wang, H., Wu, X., Bi, N., Li, S., Yuan, P., Wang, A., et al. (2017b). Impacts of the dam-orientated water-sediment regulation scheme on the lower reaches and delta of the Yellow River (Huanghe): A review. *Global and Planetary Change* 157, 93–113, doi:10.1016/j.gloplacha.2017.08.005
- Wang, H., Yang, Z., Saito, Y., Liu, J. P., and Sun, X. (2006). Interannual and seasonal variation of the Huanghe (Yellow River) water discharge over the past 50 years: Connections to impacts from ENSO events and dams. *Global and Planetary Change* 50, 221–225, doi:10.1016/j.gloplacha.2006.01.005
- Wang, H., Yang, Z., Saito, Y., Liu, J. P., Sun, X., and Wang, Y. (2007). Stepwise decreases of the Huanghe (Yellow River) sediment load (1950–2005): Impacts of climate change and human activities. *Global and Planetary Change* 57, 331–354, doi:10.1016/j.gloplacha.2007.01.003
- Wang, Y., Wang, H., Bi, N., and Yang, Z. (2011). Numerical modeling of hyperpycnal flows in an idealized river mouth. *Estuarine, Coastal and Shelf Science* 93, 228–238, doi:10.1016/j.ecss.2011.02.011
- Wang, Z. B., Elias, E. P. L., van der Spek, A. J. F., and Lodder, Q. J. (2018). Sediment budget and morphological development of the Dutch Wadden Sea: impact of accelerated sea-level rise and subsidence until 2100. *Netherlands Journal of Geosciences* 97, 183–214, doi:10.1017/njg.2018.8
- Wang, Z. B. and van der Spek, A. (2015). *Importance of mud for morphological response of tidal basins to sea level rise* (San Diego: Proceedings of Coastal Sediments).
- Ward, S. L., Green, J. A. M., and Pelling, H. E. (2012). Tides, sea-level rise and tidal power extraction on the European shelf. *Ocean Dynamics* 62, 1153–1167, doi:10.1007/s10236-012-0552-6
- WCD (2000). *Dams and Development. A New Framework for Decision-Making. The Report of the World Commission on Dams* (London: Earthscan).
- WCRP Global Sea Level Budget Group (2018). Global sea-level budget 1993–present. *Earth System Science Data* 10, 1551–1590, doi:10.5194/essd-10-1551-2018
- Wessel, P. (1998). An Empirical Method for Optimal Robust Regional-Residual Separation of Geophysical Data. *Mathematical Geology* 30, 391–408, doi:10.1023/A:1021744224009
- Wild, T. B., Loucks, D. P., Annandale, G. W., and Kaini, P. (2016). Maintaining Sediment Flows through Hydropower Dams in the Mekong River Basin. *Journal of Water Resources Planning and Management* 142:05015004, doi:10.1061/(ASCE)WR.1943-5452.0000560
- Winemiller, K. O., McIntyre, P. B., Castello, L., Fluet-Chouinard, E., Giarrizzo, T., Nam, S., et al. (2016). Balancing hydropower and biodiversity in the Amazon, Congo, and Mekong. *Science* 351, 128–129, doi:10.1126/science.aac7082
- Winsemius, H. C., Aerts, J. C. J. H., van Beek, L. P. H., Bierkens, M. F. P., Bouwman, A., Jongman, B., et al. (2016). Global drivers of future river flood risk. *Nature Climate Change* 6, 381–385, doi:10.1038/nclimate2893
- Winterwerp, J. C. and Wang, Z. B. (2013). Man-induced regime shifts in small estuaries—I: theory. *Ocean Dynamics* 63, 1279–1292, doi:10.1007/s10236-013-0662-9
- Winterwerp, J. C., Wang, Z. B., van Braeckel, A., van Holland, G., and Kösters, F. (2013). Man-



- induced regime shifts in small estuaries—II: a comparison of rivers. *Ocean Dynamics* 63, 1293–1306, doi:10.1007/s10236-013-0663-8
- Wolanski, E., Huan, N. N., Dao, L. T., Nhan, N. H., and Thuy, N. N. (1996). Fine-sediment Dynamics in the Mekong River Estuary, Vietnam. *Estuarine, Coastal and Shelf Science* 43, 565–582, doi:10.1006/ecss.1996.0088
- Wolanski, E., Nhan, N. H., and Spagnol, S. (1998). Sediment Dynamics During Low Flow Conditions in the Mekong River Estuary, Vietnam. *Journal of Coastal Research* 14, 472–482.
- Wong, P. P., Losada, I. J., Gattuso, J.-P., Hinkel, J., Khattabi, A., McInnes, K. L., et al. (2014). Coastal systems and low-lying areas. In *Climate Change 2014: Impacts, Adaptation, and Vulnerability. Part A: Global and Sectoral Aspects. Contribution of Working Group II to the Fifth Assessment Report of the Intergovernmental Panel on Climate Change*, eds. C. B. Field, V. R. Barros, D. J. Dokken, K. J. Mach, M. D. Mastrandrea, T. E. Bilir, et al. (Cambridge: Cambridge University Press). 361–409.
- Woodworth, P. L., Shaw, S. M., and Blackman, D. L. (1991). Secular trends in mean tidal range around the British Isles and along the adjacent European coastline. *Geophysical Journal International* 104, 593–609, doi:10.1111/j.1365-246X.1991.tb05704.x
- Wright, L. D. (1985). River Deltas. In *Coastal Sedimentary Environments. Second Revised, Expanded Edition*, ed. R. A. Davis Jr. (New York: Springer). 1–76, doi:10.1007/978-1-4612-5078-4\_1
- Wright, L. D., Yang, Z.-S., Bornhold, B. D., Keller, G. H., Prior, D. B., and Wiseman Jr., W. J. (1986). Hyperpycnal plumes and plume fronts over the Huanghe (Yellow River) delta front. *Geo-Marine Letters* 6, 97–105, doi:10.1007/BF02281645
- WSV (2021). *Stammdaten für Weserwehr UW*. Federal Waterways and Shipping Administration (German: Wasserstraßen- und Schifffahrtsverwaltung des Bundes) (WSV). Available online at: <https://pegelonline.wsv.de/gast/stammdaten?pegelnr=4910040> (accessed August 03, 2021).
- Wu, X., Bi, N., Syvitski, J., Saito, Y., Xu, J., Nittrouer, J. A., et al. (2020). Can Reservoir Regulation Along the Yellow River Be a Sustainable Way to Save a Sinking Delta? *Earth's Future* 8:e2020EF001587, doi:10.1029/2020EF001587
- Wu, X., Bi, N., Xu, J., Nittrouer, J. A., Yang, Z., Saito, Y., et al. (2017). Stepwise morphological evolution of the active Yellow River (Huanghe) delta lobe (1976–2013): Dominant roles of riverine discharge and sediment grain size. *Geomorphology* 292, 115–127, doi:10.1016/j.geomorph.2017.04.042
- Xu, H. (2006). Modification of normalised difference water index (NDWI) to enhance open water features in remotely sensed imagery. *International Journal of Remote Sensing* 27, 3025–3033, doi:10.1080/01431160600589179
- Xue, Z., He, R., Liu, J. P., and Warner, J. C. (2012). Modeling transport and deposition of the Mekong River sediment. *Continental Shelf Research* 37, 66–78, doi:10.1016/j.csr.2012.02.010
- Xue, Z., Liu, J. P., and Ge, Q. (2011). Changes in hydrology and sediment delivery of the Mekong River in the last 50 years: connection to damming, monsoon, and ENSO. *Earth Surface Processes and Landforms* 36, 296–308, doi:10.1002/esp.2036



- Yang, Z., Ji, Y., Bi, N., Lei, K., and Wang, H. (2011). Sediment transport off the Huanghe (Yellow River) delta and in the adjacent Bohai Sea in winter and seasonal comparison. *Estuarine, Coastal and Shelf Science* 93, 173–181, doi:10.1016/j.ecss.2010.06.005
- Yu, Y., Wang, H., Shi, X., Ran, X., Cui, T., Qiao, S., et al. (2013). New discharge regime of the Huanghe (Yellow River): Causes and implications. *Continental Shelf Research* 69, 62–72, doi:10.1016/j.csr.2013.09.013
- Yuill, B. T., Gaweesh, A., Allison, M. A., and Meselhe, E. A. (2016). Morphodynamic evolution of a lower Mississippi River channel bar after sand mining. *Earth Surface Processes and Landforms* 41, 526–542, doi:10.1002/esp.3846
- Zarfl, C., Lumsdon, A. E., Berlekamp, J., Tydecks, L., and Tockner, K. (2015). A global boom in hydropower dam construction. *Aquatic Sciences* 77, 161–170, doi:10.1007/s00027-014-0377-0
- Zeiringer, B., Seliger, C., Greimel, F., and Schmutz, S. (2018). River Hydrology, Flow Alteration, and Environmental Flow. In *Riverine Ecosystem Management. Science for Governing Towards a Sustainable Future*, eds. S. Schmutz and J. Sendzimir (Cham: Springer Open), Aquatic Ecology Series. 67–90, doi:10.1007/978-3-319-73250-3
- Zhang, J., Huang, W. W., and Shi, M. C. (1990). Huanghe (Yellow River) and its estuary: Sediment origin, transport and deposition. *Journal of Hydrology* 120, 203–223, doi:10.1016/0022-1694(90)90150-V
- Zhou, L., Liu, J., Saito, Y., Zhang, Z., Chu, H., and Hu, G. (2014). Coastal erosion as a major sediment supplier to continental shelves: example from the abandoned Old Huanghe (Yellow River) delta. *Continental Shelf Research* 82, 43–59, doi:10.1016/j.csr.2014.03.015
- Ziv, G., Baran, E., Nam, S., Rodríguez-Iturbe, I., and Levin, S. A. (2012). Trading-off fish biodiversity, food security, and hydropower in the Mekong River Basin. *Proceedings of the National Academy of Sciences of the United States of America* 109, 5609–5614, doi:10.1073/pnas.1201423109



## A Appendix

### A.1 Curriculum Vitae

#### Personal Data

---

Name: Christian Jordan  
Date of Birth: May 12, 1985  
Place of Birth: Uslar, Germany  
Nationality: German

#### Work experience

---

**04/2014 - 12/2019** *Research associate*  
Ludwig-Franzius-Institute for Hydraulic, Estuarine and Coastal Engineering  
Leibniz University Hannover

**10/2013 - 12/2013** *Research assistant*  
Ludwig-Franzius-Institute for Hydraulic, Estuarine and Coastal Engineering  
Leibniz University Hannover

**04/2013 - 05/2013** *Student assistant*  
Ludwig-Franzius-Institute for Hydraulic, Estuarine and Coastal Engineering  
Leibniz University Hannover

#### Education

---

**11/2014 - today** *PhD student*  
Ludwig-Franzius-Institute for Hydraulic, Estuarine and Coastal Engineering  
Leibniz University Hannover

**10/2006 - 09/2013** University education in civil engineering  
Leibniz University Hannover  
Degree: Diploma

**10/2005 - 09/2006** University education in mathematics  
Georg August University of Göttingen  
Degree: -

**1997 - 2004** Gymnasium Uslar  
Graduated with Abitur (German qualification for higher education)

#### Awards

---

**09/2016** Best Paper Award for Youth Scholar at the 8th Chinese-German  
Joint Symposium on Hydraulic and Ocean Engineering

**09/2014** Award of the Gesellschaft der Förderer des Ludwig-Franzius-Instituts  
for diploma thesis